NMR in Biomedicine

Imaging of Cancer Lipid Metabolism in Response to Therapy

Journal:	*NMR in Biomedicine*
Manuscript ID	NBM-18-0160.R2
Wiley - Manuscript type:	Review Article
Date Submitted by the Author:	n/a
Complete List of Authors:	Arlauckas, Sean; Mass General Hospital Browning, Elizabeth; The University of Pennsylvania, Dept of Radiology Poptani, Harish; University of Liverpool, Cellular and Molecular Physiology Delikatny, Edward; The University of Pennsylvania, Dept of Radiology
Keywords:	Cancer therapy responses < Cancer < Applications, Multimodality probes < Exogenous Contrast Methods < Methods and Engineering, MR Spectroscopy (MRS) and Spectroscopic Imaging (MRSI) Methods < Methods and Engineering, Animal model study < Cancer < Applications, Receptors and signal pathway imaging < Cellular and molecular imaging < Applications, Cellular and molecular cancer imaging < Cellular and molecular imaging < Applications

Imaging of Cancer Lipid Metabolism in Response to Therapy

Sean Arlauckas, Ph.D.[1,2], Elizabeth A. Browning, Ph.D.[1],

Harish Poptani, Ph.D.[3], E. James Delikatny, Ph.D.*[1]

[1] Department of Radiology, Perelman School of Medicine, University of Pennsylvania, Philadelphia, PA, [2]Center for Systems Biology, Mass General Hospital, Boston MA, [3]Department of Cellular and Molecular Physiology, Institute of Regenerative Medicine, University of Liverpool, Liverpool, UK

*Address Correspondence to:

E. James Delikatny, Ph.D.

Research Professor

Department of Radiology

317 Anatomy-Chemistry Building, 3620 Hamilton Walk

Philadelphia, PA 19104, USA

Ph: 215-898-3105

Email: delikatn@pennmedicine.upenn.edu

Key words: Tumor imaging, therapy response, lipids, MR imaging, MR spectroscopy, Optical imaging

Abstract

Lipids represent a diverse array of molecules essential to the cell's structure, defense, energy, and communication. Lipid metabolism can often become dysregulated during tumor development. During cancer therapy, targeted inhibition of cell proliferation can likewise cause widespread and drastic changes in lipid composition. Molecular imaging techniques have been developed to monitor altered lipid profiles as a biomarker for cancer diagnosis and treatment response. For decades, magnetic resonance spectroscopy has been the dominant noninvasive technique for studying lipid metabolite levels. Recent insights into the oncogenic transformations driving changes in lipid metabolism have revealed new mechanisms and signaling molecules that can be exploited using optical imaging, mass spectrometry imaging, and positron emission tomography. These novel imaging modalities have provided researchers a diverse toolbox to examine changes in lipids in response to a wide array of anticancer strategies including chemotherapy, radiation therapy, signal transduction inhibitors, gene therapy, immunotherapy or a combination of these strategies. The understanding of lipid metabolism in response to cancer therapy continues to evolve as each therapeutic method emerges, and this review seeks to summarize the current field and areas of unmet needs.

Abbreviations

18F-fluorodeoxyglucose (FDG)

2,5-dihydroxybenzoic acid (DHB)

3-hydroxy-3-methyl-glutaryl-CoA (HMG-CoA)

acetyl-coenzyme A (acetyl-CoA)

acute myeloid leukemia (AML)

AMP-activated protein kinase (AMPK)

ATP-citrate lyase (ACLY)

beta-oxidation (β-Ox)

black Hole Quencher (BHQ-3)

choline kinase (ChoK)

choline transporters (ChoTs)

cisplatin (CDDP)

7-hydroxy-9H-(1,3-dichloro-9,9-dimethylacridin-2-one (DDAO)

diacylglycerol (DAG)

(4′,6-diamidino-2-phenylindole) (DAPI_

elongation-of-very-long-chain-fatty acids (ELOVL)

endoplasmic reticulum (ER)

epidermal growth factor receptor (EGFR)

fatty acid binding protein-4 (FABP-4)

G-protein coupled receptor (GPCR)

glycerophosphocholine (GPC)

hormone-sensitive lipase (HSL)

hypoxia inducible factor (HIF)

Indocyanine green (ICG)

isocitrate dehydrogenase-1 (IDH1)

lipoprotein lipase (LPL)

low density lipoprotein (LDL)

lysophosphatidylcholine (LPC)

magnetic resonance spectroscopy (MRS)

mass spectrometry imaging (MSI)

matrix-assisted laser desorption ionization (MALDI)

mono-unsaturated fatty acids (MUFAs)

nanostructure-initiator mass spectrometry (NIMS)

OKN007 (2,4-disulfophenyl-PBN)

optical coherence tomography (OCT)

PBN (α-phenyl-tert-butylnitrone)

peroxisome proliferator-activated receptor alpha (PPARα)

phosphatidylcholine (PtdCho)

phosphatidylethanolamine (PtdEtn)

phosphatidylinositol (4,5) phosphate-2 (PIP2)

phosphatidylinositol (PtdIns)

phosphatidylserine (PtdSer)

phosphocholine (PC)

phosphoethanolamine (PE)

Phosphoinositides (PI)

phospholipase (PL)

phosphomonoester (PME)

plasma membrane citrate transporter (PMCT)

polyunsaturated fatty acid (PUFA)

positron emission tomography (PET)

protein kinase C (PKC)

PtdCho-specific PLC (PC-PLC)

pyropheophorbide-a (Pyro)

reactive oxygen species (ROS)

secondary ion mass spectrometry (SIMS)

sphingosine-1-phosphate (S1P)

stearoyl-CoA desaturase-1 (SCD1)

sterol response element-binding proteins (SREBPs)

total choline (tCho)

tricarboxylic acid (TCA)

unfolded protein response (UPR)

α-cyano-4-hydroxycinnamic acid (CHCA)

Introduction

Cancer cells exist in a hyperactive state of growth and use a complex network of lipid metabolic pathways to support this growing biomass. Lipids are a broad class of compounds that include fatty acids, triglycerides, steroids, phospholipids, and sphingolipids, among others. These molecules play critical roles in cellular compartmentalization, structural barriers, communication signals, energy storage, and homeostasis. Despite high vascularization, many cancer cells exist in regions of nutrient deprivation and tumors have adopted alternative strategies to maintain sources of lipid. In some cases the altered lipid metabolic state offers a therapeutic vulnerability, while in others, adaptations to intracellular lipid composition can be used by refractory tumors to resist therapies. Because these cancer-driven aberrations in lipid metabolism often contrast the surrounding tissue, there are several molecular imaging strategies that have been developed to monitor tumor margin, stage, and treatment response.

I. Lipid Metabolism

A. Exogenous Lipid Uptake

De novo lipid synthesis pathways are crucial during embryogenesis and fetal development, but, after maturation, cells in most tissues are capable of acquiring sufficient circulating lipids to meet their biosynthetic and energetic needs (1-3). Cancer cells can access circulating lipids by overexpressing lipid-scavenging proteins. High exogenous lipids are associated with local invasive index, and obesity is also correlated with higher cancer incidence rates (4). Higher expression of low density lipoprotein (LDL) receptor has been found in transformed colorectal cells relative to normal cells (5). The LDL receptor in prostate cancer provides a major source of cellular cholesterol and essential fatty acids (6). Breast cancer and select sarcoma cells have been observed to secrete lipoprotein lipase (LPL) to release fatty acids

from triglycerides in circulating lipoproteins (7). Although macropinocytosis has been identified in cancer cells, little evidence exists to suggest that this is a relevant source of exogenous lipid *in vivo* (8). Instead, lipid binding proteins are thought to assist in the capture of lipids from the interstitial space and promote invasion (Figure 1), as overexpression of fatty acid binding protein-4 (FABP-4) has been observed on the surface of ovarian, prostate, bladder, and renal cancer cells (9,10). Fatty acid translocase, also known as CD36, is a long-chain fatty acid scavenger that contributes to high mammographic density in subjects at high-risk for breast cancer (11). Ovarian cancer cells can siphon free fatty acids from the lipid stores of the omentum by activating perilipin-A and hormone-sensitive lipase (HSL) in neighboring adipocytes (12). Studies have shown that removal of lipids from culture medium can trigger *de novo* lipid synthesis, emphasizing the dependency on lipids for cell proliferation and the adaptations cancer cells make to sustain their growing biomass (13).

B. *De Novo* Synthesis

Many cancers revert back to *de novo* lipid synthesis, and the lipogenic pathway is composed of many enzymes that are critical for tumor growth (14). Lipid synthesis starts at the energetic hub of the cell, the mitochondria, where acetyl-coenzyme A (acetyl-CoA) and oxaloacetate are condensed into citrate (Figure 1). Citrate from the TCA cycle can be shunted from the mitochondria and broken down by ATP-citrate lyase (ACLY) into acetyl-CoA. Cytosolic citrate can alternatively be sourced from the microenvironment by plasma membrane citrate transporter (PMCT)(Figure 1) (15). Besides feeding into the rate-limiting step of fatty acid synthesis, acetyl-CoA is also critical for histone acetylation and serves as a link between metabolic status and gene expression (16,17).

Acetyl-CoA serves as the 2-carbon building block used for fatty acid synthesis. The enzyme FASN combines malonyl-CoA with repeated acetyl-CoA condensations to form palmitate. Palmitate is the saturated 16-carbon fatty acid from which most complex fatty acids in the body are derived (18). FASN overexpression is associated with poor prognosis in breast cancer (19) and FASN inhibitors derived from natural products (e.g. resveratrol) and synthetic molecules (e.g. orlistat) are being studied for their anti-neoplastic effects (20). Acetyl-CoA is also a synthetic precursor to 3-hydroxy-3-methyl-glutaryl-CoA (HMG-CoA) in the cholesterol biosynthesis pathway (Figure 1). Mevalonate is then produced by HMG-CoA reductase, the target of the lipid lowering drugs, the statins. The amplification of HMG-CoA reductase in many prostate tumors creates a growth dependency on cholesterol, and suggests a possible role for statins in treating these cancers (5,21). Mevalonate is also a precursor to farnesyl-diphosphate, which can further be processed to cholesterol, or used as a substrate for protein prenylation. Isoprenoids from the mevalonate cascade are critical for membrane anchoring and activation of the growth-related G-protein subunits Ras (farnesylated), Rho (geranylgeranylation), and many others (22) (Figure 1).

Fatty acids can be chemically modified in many ways to meet the diverse range of specialized functions required for cellular function (Figure 1). Stearoyl-CoA desaturase-1 (SCD1) produces mono-unsaturated fatty acids (MUFAs) from the saturated fatty acid chains sourced exogenously or from *de novo* synthesis. Saturated fatty acid accumulation in the endoplasmic reticulum (ER) triggers autophagy-induced apoptosis by activating the unfolded protein response (UPR) (23). By modulating MUFA to saturated fatty acid ratios intracellularly, SCD1 has a regulatory effect on cell survival and proliferation (24-26). The elongation-of-very-long-chain-fatty acids (ELOVL) enzymes in the ER are responsible for polyunsaturated fatty

acid (PUFA) synthesis (27), as well as the conversion of saturated and monounsaturated fatty acids into the very long chain fatty acids (C > 18) that serve as building blocks of sphingolipids when combined with ceramide head groups (28). Free fatty acids are stored as triglycerides in lipid droplets or packed into the cell membrane as sphingolipids, cholesterol esters, or phospholipids. Lipid droplets in breast cancer cells have been found to increase with increasing malignancy and to be enriched in polyunsaturated fatty acids, especially arachidonic acid (29)

Diacylglycerol (DAG) is an important lipid second messenger that also serves as a synthetic precursor for both membrane phospholipids and lipid droplet triacylglycerides (30-33). Major membrane phospholipids include phosphatidylcholine (PtdCho), phosphatidylethanolamine (PtdEtn), phosphatidylinositol (PtdIns), phosphatidylserine (PtdSer), among others, and vary in function, location, and relative abundance. The Kennedy pathway of phospholipid synthesis describes the addition of polar head-groups to the DAG backbone, and enzymes in this pathway are responsible for the accumulation of phosphocholine (PC) and phosphoethanolamine (PE) observed in many cancers (34). Choline uptake by choline transporters (ChoTs) and phosphorylation by choline kinase (ChoK) have, in particular, been consistently linked with increased invasiveness, drug resistance, and overall malignancy (35).

C. Lipid Mobilization and Usage

Phospholipid and triacylglyceride levels are maintained by the concerted actions of catabolic enzymes that mobilize fatty acids from lipid droplets and cell membranes (36). Fatty acid release from lipid droplet storage involves lipases that can support aggressive cancer phenotypes in a manner similar to the pro-tumorigenic effects of exogenous fatty acids (37). Fatty acid release from membrane phospholipids is carried out by the phospholipase (PL) enzymes. PLA_1 and PLA_2 cleave phospholipids at the *sn*-1 and *sn*-2 positions, respectively. The

PLA_2 family of enzymes are the primary producers of arachidonic acid and three major subgroups exist: calcium-dependent or cytosolic $cPLA_2$, calcium-independent $iPLA_2$, and secretory $sPLA_2$ (38). While $cPLA_2$ has a tumor-supportive role in many cancers, $sPLA_2$ is thought to have tumor suppressive-functions (39). In contrast, iPLAs are housekeeping enzymes, primarily responsible for mobilizing lipids to maintain membrane integrity and general cellular energy metabolism during homeostasis. PLC cleaves phospholipids at the bond between glycerol and phosphate and contains pleckstrin homology domains for anchoring and cooperation with G-protein coupled receptor (GPCR) signaling networks (40). When activated by growth factor receptors, PLD hydrolyzes the phospholipid head group (e.g. choline, ethanolamine, inositol, serine) to release PA and links growth factor signaling to cell proliferation (32).

Saturated free fatty acids can be broken down into acetyl-CoA to feed into the TCA cycle, and some cancers have been found to prefer fatty acid oxidation to pyruvate oxidation, even in sufficient glucose and oxygen environments (41). β-oxidation is an important energy pathway in prostate cancers, where glycolytic rates are low, and rapid citrate utilization requires a constant supply of acetyl-CoA (42). Peroxisome proliferator-activated receptor alpha (PPARα) is a transcription factor whose activation triggers breakdown of very long chain fatty acids in the peroxisomes, and fatty acid oxidation in the mitochondria. A complex network of interactions with PUFAs, namely arachidonic and linoleic acids, regulates PPARα activity (43). Aside from their direct signaling functions (44), arachidonic acid is an important substrates for cyclooxygenase, lipoxygenase, and cytochrome enzymes that catalyze the production of the eicosanoid family of bioactive lipids that have roles in innate immunity, inflammation, cardiovascular disease, and cancer (45,46).

II. Tumor Progression and Regression

A. Oncogenic Reprogramming

A common feature of cancer cells is the metabolic transition from oxidative phosphorylation to glycolysis, during which the rate of glucose consumption far exceeds the energy requirements of the cell (14). What initially appears to be wasteful energy utilization is in fact a method to feed glucose-derived pyruvate into biosynthesis, including fatty acids (Figure 2). Glutamine has been identified in some cancers as an alternative energy source that can enter the TCA cycle (47) and provide a carbon source for citrate production (Figure 2), however the dependency on glutamine for anaplerosis varies considerably even among cancers of the same tissue (48,49). This may be due, in part, to heterogeneity in the local tissue microenvironment causing gradients in nutrients, oxygen and signaling factors that influence the energetic state of cells.

Under hypoxic conditions, solid tumors can become dependent on unsaturated fatty acid uptake from serum to prevent ER stress that can arise when rapid proliferation is unmet by nutrient availability (50). These exogenous fatty acids can arise from lipolysis in stromal cells in a manner comparable to cachexia (23). The recent resurgence of interest in cancer metabolism has improved our understanding of the adaptations tumor cells can make when fuel availability is variable. These adaptations are only possible because the common driving mutations in cancers often have direct involvement in metabolic pathways.

Many of the clinically prevalent oncogenes are capable of altering lipid uptake, production, or consumption to gain a competitive growth advantage (Figure 2). The transcription factor hypoxia inducible factor (HIF) is a downstream effector of Myc and is tightly regulated by the tumor suppressor gene p53. HIF induces FASN induction and lipid droplet formation for

energy storage to support the tumor microenvironment (18,51,52). FASN requires the reducing agent NADPH, which is produced from the pentose phosphate pathway that often becomes upregulated during cancer reprogramming (18). There is further evidence in renal cell carcinoma models that HIF2α-dependent lipid storage suppresses the ER stress response promoting tumor cell survival (53). Glutamine uptake in glioma and acute myeloid leukemia (AML) is often accompanied or driven by isocitrate dehydrogenase-1 (IDH1) mutations that reroute glutamine toward citrate to provide fatty acid and cholesterol precursors independent of the TCA cycle (Figure 2) (54,55). In hypoxic environments where glucose metabolism is diverted to anaerobic lactate production, mutations in mitochondrial IDH2 provide a continued source of citrate for lipid synthesis, by allowing reductive carboxylation of glutamine-derived α-KG (56). The oncometabolite 2-hydroxyglutarate is produced by many cancer-specific IDH1 and IDH2 mutations, and has widespread epigenetic effectors by altering DNA methylation (57-59).

AMP-activated protein kinase (AMPK) serves as an energetic sensor and master switch by inhibiting fatty acid synthesis in low energy states and stimulating consumption of fatty acids for energy in the mitochondria by β-oxidation (Figure 2). Sterol response element-binding proteins (SREBPs) (60) can activate transcription of genes involved in cholesterol and fatty acid synthesis and uptake, and are directly downstream of AMPK and the PI3K/Akt/MTOR signaling axis that includes many oncogenes (61). Epidermal growth factor receptor (EGFR) mutations are common tumor-driving factors that recruit phospholipases (62,63) and ChoKα (64) to the cell surface, leading to membrane remodeling and induction of mitogenic signals to drive cellular proliferation. Mitogenic growth signals can also come in the form of sterol-derived hormones (estrogens, progestogens, and androgens). Release of these sex hormones, their receptor expression, and the downstream signaling mediators are all common tumor-driving factors in

prostate, breast, endometrial and ovarian cancers (65). Farnesylation of Ras and geranylgeranylation of Rho GTPases are essential for downstream signaling through the phosphoinositol family of signaling lipids (66,67). Phosphoinositides (PI) comprise 10-20% of total cell phospholipids and among that fraction, phosphatidylinositol (4,5) phosphate-2 (PIP_2) and phosphatidylinositol-4-phosphate constitute approximately 0.2-1% (68-70). This class of membrane lipids plays an integral role in proliferation, apoptosis, metabolism and migration, and is pivotal to transmembrane signal transduction because it regulates the distribution of receptor tyrosine kinases, G-protein-coupled receptors, and adhesion molecules among others (71).

Metabolic disease is a risk factor for many cancer types, promoting insulin resistance, hyperactive growth signals, and evasion of apoptosis that help set the conditions for malignant transformation (72). Histological tumor grade in the breast is clinically correlated with phosphomonoester (PME) accumulation (73), such as PC and PE, detectable by MR spectroscopy (74,75). PC promotes survival and mitogenic signaling through downstream cascades such as MAPK and Akt (73,76,77). PC can be formed through the actions of the enzyme choline kinase, or by phosphatidylcholine specific phospholipase C. Phospholipid catabolism can also be a source of other mitogenic second messengers such as DAG, PA, and lysophosphatidylcholine (LPC). DAG is released following the cleavage of phospholipids by PLC (78), activates protein kinase C (PKC) resulting in the release of intracellular calcium stores and subsequent Ca^{2+}-dependent signaling. DAG and PC are also the synthetic precursors to the most abundant mammalian membrane phospholipid, PtdCho, whose levels are predictive of breast tumor grade, estrogen receptor status, and patient survival (79). It is intuitive to suspect that cancers in high adipose tissue use altered lipid metabolism to take advantage of the surrounding environment, however evidence of altered lipid metabolism in cancers that arise in

low-adipose tissues suggests that deranged lipid metabolism is a universal hallmark of cancer pathogenesis.

Variations in lipid composition are likely due to the heterogeneous nature of the tumor microenvironment, which is an ever-changing compartment of structural fibers, nutrients, cellular waste, and signaling molecules. Interstitial pH, extracellular matrix, bioactive lipids, and cytokines can alter the population and function of stromal cells and surrounding tissues. Extracellular lactate, the metabolic byproduct of aerobic glycolysis, is capable of transitioning tumor-associated macrophages from tumor-suppressive to tumor-supportive phenotypes (80,81). Biopsies of colon cancer specimens have been reported to contain high lipid deposition in regions of necrosis and infiltrating macrophages (82). These macrophages most likely resemble the immune-suppressive "alternatively-activated" phenotype, as classic (interferon gamma-induced) activation does not enhance lipid phagocytosis in human myeloid populations (83). Alternatively-activated macrophages prefer fatty acid oxidation (84) and are thought to have critical roles in clearing/remodeling necrotic tissue, recruiting new blood vessels, and regulating innate and adaptive immunity (85).

B. Lipid changes during Apoptosis/Necrosis

The role lipids play in nearly all cell survival pathways emphasizes their importance in tumor growth and invasion pathways, but lipid compartmentalization, metabolism, and signaling are also intricately involved in cell death pathways. During apoptosis, the release of lysophosphatidylcholine (LPC) and sphingosine-1-phosphate (S1P) by PLAs (86) and ceramidases (87) respectively, acts as a "find-me" signal to surrounding macrophages (88). Once recruited to the dying cell, exposed PtdSer on the apoptotic cell's surface serves as the "eat me"

signal recognized by phagocytes (89). Unlike the organized compartmentalization of apoptotic cells into non-immunogenic apoptotic bodies, necrosis is characterized by the breakdown of the plasma membrane and release of the cellular contents that often triggers an immune reaction (90). Recently, lipid peroxidase networks have been identified as key mediators of cancer cell therapy resistance by reversing a non-apoptotic form of cell death known as ferroptosis can be induced by lipid peroxide accumulation (91). Tumor cell response to therapy begins with activation of cell stress responses, which can ultimately decide the fate of the cell and surrounding tumor.

Early changes in lipid metabolism have been reported in response to a wide range of cellular stresses (92), but lipid mobilization does not necessarily commit a cell to apoptosis (93). Many cells undergoing apoptosis produce lipid droplets, although there are exceptions (94), and fatty acids are first mobilized from membrane phospholipids by PLA_2 activity (92,95). Reactive oxygen species (ROS) produced in the mitochondria of apoptotic cells are thought to inhibit the catalytically-active thiol groups on β-oxidation enzymes (96), thus free fatty acids are redirected into lipid droplets in the form of triglycerides and sterol esters (97,98). Lipid droplet formation in cancer may act as a drug reservoir to reduce intracellular concentrations of drug (99), or to absorb reactive oxygen species to protect further DNA damage (100). Lipogenesis of saturated fatty acids also makes the cell membrane less penetrable to drugs that enter by passive diffusion (101). Uptake of triglycerides by macrophages or neutrophils can dampen subsequent immune activation (102,103), providing another potential mechanism of immune escape. Ceramide accumulation regulates and can even trigger mitochondrial outer membrane permeability to fully commit a cell to apoptosis by allowing cytochrome C release to the cytosol (104). Other signs of cell stress that precede or arise during apoptosis are the rise in PUFA and glycerophosphocholine

(GPC) levels (105-107). These indicate a reprogramming of lipid metabolism and suggest that catabolic networks mobilize lipids from membrane phospholipids during this time. Many of these observations were first made using magnetic resonance spectroscopy (MRS) to non-invasively measure lipid resonances of cancer cells undergoing stress responses and apoptosis (92).

III. Imaging Metabolic Lipid Changes

The development of modern imaging techniques allows the detection of several key signaling pathways involved in lipid metabolism and its regulation/dysregulation in cancer. The ability to detect these pathways non-invasively aids in the discovery of potential targets for imaging or interventional therapies. In addition to developing probes to image lipids and alterations in lipid metabolism in mechanisms of oncogenesis, we can also image lipid-dependent or –mediated signaling in response to therapy (108).

A. Imaging lipids in tumors: MR Spectroscopy

MRS has been extensively employed for the study of biological material (from cell extracts, to homogenized tissue, and intact organisms) because it offers a non-invasive method to study the native distribution and dynamic nature of many relevant biomarkers of disease and therapeutic response. The search for disease-related metabolites requires the suppression of the overwhelming fat and water signals observed in proton MR spectra, however much can be learned from the diverse species that contribute to these lipid peaks.

B. Choline and choline metabolites

MRS has been essential in the study of lipid metabolism and for the non-invasive observation of lipid metabolism *in vitro* and *in vivo*. This is due to the ability to observe a number of lipid metabolites in ^{1}H and ^{31}P MR spectra on the basis of chemical shift discrimination. Due to the relative insensitivity of MR, observation is limited to soluble or MR-visible metabolites in the high micromolar to millimolar levels. Lipid metabolites observable in ^{31}P MR spectra, include the PME, PC and PE and the PDE, GPC and GPE. In ^{1}H spectra, observable lipid metabolites include the total choline (tCho) resonance, a composite resonance encompassing free choline, PC and GPC. Thus there is overlap in the information available between ^{31}P and ^{1}H spectra, since the choline PC and GPC resonances seen in the ^{31}P spectra are also observed in the tCho region of ^{1}H spectra. The PME and PDE resonances report on pathways relevant to phospholipid metabolism. PC and PE are generally the anabolic products of choline kinase and ethanolamine kinases, although they can also be produced by the actions of phospholipase C. The PDE resonances result from catabolism of phosphatidylcholine and phosphatidylethanolamine via the consecutive action of two phospholipases, A2 and lysophospholipase or A1.There are numerous excellent reviews on this topic (35,92,109,110), and the reader is referred to these for detailed information. However, it is worth noting that consistent elevations in PMEs and tCho have been observed in a wide range of tumors including brain, prostate, lung, skin, ovarian and breast (111,112). As a means to monitor therapeutic response, tumor choline levels have been measured using MRS in animal (113-115) and human tumors (116-120) with mixed results, at least partly due to the technical difficulties associated with acquiring choline spectra on a background of high fat in normal breast tissue. The picture is further complicated because ChoK is not the only enzyme that contributes to PC accumulation, it

can be produced directly by the actions of PLC on PtdCho, or by the hydrolysis of GPC as a source of additional choline for subsequent phosphorylation. Recent MRS applications have been used to detect changes in choline metabolism due to IDH mutations in glioma (59,121) explore the role of the glycerophosphodiesterase genes GDPD5 and GDPD6 on breast cancer cell migration/invasion (122) and profile metabolic changes in response to HIF1 and HIF2 suppression (123).

C: Imaging lipids in tumors: MR-visible lipids

Proton MRS was originally used to detect MR-visible or mobile lipid signals in cultured cells and tumor biopsies. A series of resonances were observed arising from the fatty acyl chains in neutral lipids, triglyceride and cholesterol esters, including the terminal methyl groups, the methylenes in long chain fatty acids, and olefinic MUFA/PUFA resonances (124-127). MR detects only molecules that exist in a local environment with high rotational molecular motion and thus the observed signals arise predominantly from mobile or MR-visible lipids, composed of triglycerides and cholesterol esters sequestered in lipid droplets. In animal and human tumors, the observation of these lipid resonances require the use of short echo time spectroscopic pulse sequences due to the relatively short T_2 relaxation times of mobile lipids. *In vivo* MRS studies initially used single voxel localization methods such as STEAM and PRESS for assessing the MRS pattern of lipids in tumors, due to the simplicity and accuracy of these methods. However, multi-voxel spectroscopic methods including chemical shift imaging are increasingly being used both in mouse glioma and xenograft models (128,129) as well as in human tumors (130) since these methods provide a better assessment of tumor heterogeneity. The presence of intense lipid signals from surrounding subcutaneous fat and muscle have been problematic in evaluating lipid signals by MRS methods, thus outer volume fat suppression sequences become critical. For this

reason, the majority of studies on intra-tumoral lipids have been focused on the brain where subcutaneous fat is at a minimum. However, useful insights into human tumor composition have still been made in other tumors, despite the problems associated with high fat content in peripheral tissue.

The presence of lipids in human tumors was initially reported by Kuesel *et al.* (124) where a correlation between MR-visible lipids, tumor malignancy and necrosis was observed in brain tumors. These initial findings were subsequently confirmed in *in vivo* imaging studies as well as in histologically different brain tumor types (131). An early demonstration of the sensitivity of lipid signals for accurate diagnosis of supra-tentorial brain tumors was demonstrated by Preul *et al.* (132) suggesting lipid signals as a potential biomarker for grading of astrocytomas. Correlation of lipids with malignancy was also reported in pediatric brain tumors (133) and a further study in pediatric brain tumors suggested the presence of lipids as a marker of poor survival (134). Taken together, the presence of MR-visible lipid signals seems to be a marker for malignancy and poor prognosis. In our recent review on the role of lipids in tumors (92) we argued that increased MR-visible lipids in tumors are indicative of a stress response and that their localization reflects areas of cellular hypoxia and or necrosis.

MRS methods have been used to assess changes in the metabolic profile of tumors as markers of early therapeutic response. Most xenograft and clinical studies have focused on evaluating reductions in the total choline or lactate signal as a marker of treatment response Changes in lipid signals not only suggest a positive response, but increases in PUFA, a putative marker of apoptosis (106), may also aid in understanding the mechanism of cell death induced by specific treatments.

Gene therapy induced changes in lipids

One of the first studies to implement MRS to evaluate changes in metabolism during gene therapy reported a progressive increase in the lipid resonance at 1.3 ppm in 9L rat tumors that were injected intratumorally with adenoviral HSV-*to* followed by ganciclovir treatment (135). These initial studies were followed by several studies of the HSV-*tk* positive BT4C glioma model treated with ganciclovir (106,129,136), which established accumulation of PUFA resonances as a marker of treatment induced apoptosis. The PUFA resonances arise from phospholipase A2 activity leading to hydrolysis of phospholipids in the cell membrane (137). These studies indicate that early increases in mobile lipid resonances after therapeutic intervention may be suggestive of apoptosis and positive treatment response. The temporal evolution of these resonances may be variable, with a decrease in lipid resonances during formation of scar tissue after cell death and lysis. However, the mode and nature of therapeutic interventions could affect changes in lipid resonances. A recent study involving oncolytic viral treatment of immunocompetent Syrian hamster carcinomas as well as a patient with neuroblastoma reported lower unsaturated fatty acids, as measured from the olefinic resonance at 5.3 ppm (Figure 3) in responding tumors than in non-responding tumors (138), which appears to be an exception to the norm. Unlike previous studies, which resulted in an apoptotic tumor cell death after treatment, treatment with oncolytic viruses resulted in multifocal necrosis and a substantial cellular inflammatory response. Taken together, these studies indicate that changes in PUFA resonances could possibly be used to differentiate apoptosis from necrosis, although further data is needed to substantiate this finding.

A decreased PUFA resonance, in comparison to normal breast tissue, was reported in a patient with breast cancer using selective multiple quantum coherence spectroscopy (139). In

contrast to most tumors, a decrease in total tumor lipids was observed in pancreatic cancer compared to pancreatitis as evaluated by MR studies of patient biopsy samples (140) as well as *in vivo* comparing focal pancreatitis to pancreatic adenocarcinoma (141). Although the exact reason for this apparent anomaly is unclear, the pancreatic tumor microenvironment includes stromal tissue that comprises up to 80% of the tumor mass (142). Thus, it is possible that the dominant factor contributing to the MR visible lipid signal in pancreatic cancer arises from the dynamic assortment of extracellular matrix components, infiltrating immune cells, macrophages, pancreatic stellate cells, vascular cells, fibroblasts and myofibroblasts.

Chemotherapy induced changes in lipids

There have been several MRS studies describing alterations in lipid levels in response to treatment with cytotoxic agents. Increased triglyceride resonances were observed in the malignant MDA-MB-435 breast cancer cell line treated with the anti-inflammatory agent indomethacin (143), a drug that has been shown to reduce tumor invasion and inhibit metastasis. Similar increases have also been observed in cells treated with antimitochondrial agents and other cytotoxic drugs (96,144-148). Treatment of DU145 prostate cancer cells with the differentiating agents phenylacetate or phenylbutyrate also led to a time dependent increase in lipid signals, accompanied by increased in GPC, indicating cell stress that precedes the induction of apoptosis (107,147). Increased apoptosis in BT4C glioma cells after exposure to cisplatin resulted in increases in both saturated fatty acids and PUFA resonances (149). Treatment with subcytotoxic doses of cisplatin induced similar increases in saturated and total unsaturated fatty acid (5.3 ppm) resonances in HER2+ ovarian cancer cells (150) (Figure 4). Exposure of the VEGFR tyrosine kinase inhibitor SU1498 on human U87 glioma cells induced a significant increase in lipids with a concomitant decrease in GPC (151). Although cell studies point towards

an increase in MR-visible lipid signals in tumors as a marker of response to chemotherapy, translation of these findings to *in vivo* settings have been challenging due to the confounding presence of lipid signals from hypoxic/necrotic regions in the tumor or contamination from lipid signals outside the tumor.

Many factors influence *in vivo* MRS and make it difficult to predict whether it will provide useful biomarkers for new therapeutic interventions. For example, the PI3K/mTOR inhibitor voxtali in the presence or absence of temozolomide directly alters the phosphorylation of the phospholipid PtdIns in glioblastoma tumors, but causes no detectable changes in ^{1}H MR spectra, even though hyperpolarized ^{13}C MRS showed reduced conversion of pyruvate to lactate (152). Nevertheless, many studies have successfully evaluated changes in lipid signals in response to chemotherapy in tumor xenografts. The efficacy of etoposide, a topoisomerase inhibitor, was tested on a murine lymphoma model and a significant increase in the 1.3 ppm methylene mobile lipid resonance was noted following etoposide-induced apoptosis (153). Treatment of F98 rat gliomas with the choline kinase inhibitor MN58b resulted in a significant increase in both saturated (1.3 ppm) and polyunsaturated (2.8 ppm) fatty acids (Figure 5) that correlated with increased treatment-induced apoptosis (114). Similar increases in saturated and polyunsaturated lipid resonances were observed in GL261 glioma tumors in mice treated with temozolomide (128) (Figure 6). In contrast, treatment of C6, RG2, and GL261 glioma models with the nitrones, PBN (α-phenyl-tert-butylnitrone) and OKN007 (2,4-disulfophenyl-PBN) resulted in a decrease in lipid resonances after treatment, which was attributed to a decrease in necrosis and normalization of the metabolic profile rather than the increase in apoptosis generally reported in tumor treatment studies (154). Increases in neutral lipid resonances were also correlated with tumor growth arrest and treatment response in a mouse model of HER2+

ovarian cancer treated with cisplatin (150). No changes in total choline were noted in this study, as the authors found changes in neutral lipids to be a more sensitive marker of treatment response.

Radiation therapy induced changes in lipids

Radiation therapy is one of the most commonly used therapeutic strategies for solid tumors in the clinic. Although several studies point towards increased lipid resonances in radiation-induced necrosis, relatively few studies have evaluated changes in lipid resonances as a marker of early response to radiation therapy. Cervical cancer biopsy samples obtained from patients treated with radiation therapy were studied by HR-MAS, which revealed a direct correlation between the degree of apoptosis and lipid resonances (155) confirming the observations made in cell and xenograft studies. A xenograft model of non-Hodgkin's diffuse large B cell lymphoma treated with radiation therapy demonstrated a significant increase in both mono and unsaturated lipid resonances within 3 days of treatment (156). The increase in lipid resonances corresponded with histology findings of increased apoptosis and oil red O staining, supporting the idea that unsaturated (PUFA) lipid accumulation is a marker of therapy induced apoptosis.

D. Positron Emission Tomography

Positron emission tomography (PET) measures the gamma rays produced when an electron collides with a positron emitted from a beta-decaying nucleus. PET scans require the administration of a radioactive substrate, but the high sensitivity of PET means that only tracer levels of radiolabeled material are needed. For tumor imaging, ^{18}F-fluorodeoxyglucose (FDG) is by far the most commonly employed PET tracer (Figure 7). FDG exploits the enhanced aerobic glycolysis observed in many tumors, a phenomenon known as the Warburg effect.

Overexpression of plasma membrane glucose transporters and hexokinase activity rapidly internalize FDG and phosphorylate it in the first step of glycolysis. This reaction traps FDG-6-P in the cell, but the substrate is unable to be metabolized further. FDG-PET is widely used clinically for the staging of primary tumors, but because of the ability of PET to perform a full-body scan, it is also important for the detection of metastases. FDG-PET can also be used to monitor tumor regression post-therapy, and has been used in several instances to monitor FASN inhibitor therapies due to the link between glycolysis and fatty acid synthesis (157,158). One caveat is that it is difficult to assess enhanced FDG tumor uptake in tissues with high glucose utilization (e.g. brain and heart) or in organs of excretion (e.g. kidney and bladder). There is also the potential for background labeling in metabolically active cells, such as lymphocytes in sites of inflammation. Furthermore, some tumors, such as the prostate, are not FDG avid and have relatively low uptake.

A promising alternative to FDG for tumor lipid imaging is ^{18}F or ^{11}C labeled choline (Figure 7). This strategy relies on the upregulation of choline transporters and ChoK in tumor cells. The concerted action of these components achieves tumor tissue contrast by rapidly internalizing and phosphorylating the choline mimetic radioligands. Choline PET is becoming more widely used for tumor detection, especially in the prostate (159) but also in other tumors such as gliomas (160). Choline PET has also been used to track tumor recurrence, metastasis, and response to chemo and radiotherapy (161-164). One challenge facing choline PET is the discrepancy between labeled choline tracer uptake and steady state metabolites observed using MRS (165). This could be due to intrinsic differences between choline transport and phosphorylation that manifest as differences in tracer uptake relative to steady-state levels, but it

could also be due to alternative pathways such as metabolism of the choline tracers in other organs such as liver (166).

The low FDG avidity of prostate tumors is linked to their metabolic preference for β-oxidation of fatty acids, rather than glutaminolysis or glucose metabolism, as a primary energy source (42). A variety of ^{18}F-labeled fatty acid analogs have been synthesized (Figure 7), and the metabolism of these probes effectively trap the radiolabel specifically in cells with high usage of β-oxidation (167,168). In metabolizable probes, labeling at the hydrophobic end of the molecule allows these probes to be consumed through β-oxidation. In non-metabolizable probes, chemical modifications are nearer to the carboxyl group, which still allows cell uptake and potential incorporation into phospholipids or triglycerides, but further oxidative metabolism is prevented (169). Labeled fatty acid probes, such as BMIPP (Figure 7), have been primarily employed to monitor metabolism in tissues with high levels of β-oxidation, mostly cardiac and to a lesser extent skeletal muscle (170-176). Use of these probes to study cancer has been limited, even though the use of β-oxidation as a potential cancer energy source has been known for decades (177,178).

Although the half-life of ^{11}C is quite short (20 min), it is still possible to observe ^{11}C palmitate uptake and distinguish storage in triglycerides vs metabolism by β-oxidation (179,180). Regions of high fatty acid synthesis have been imaged using ^{11}C-acetate incorporation into palmitate (181), although the intermediate acetyl-CoA has other potential metabolic fates such as the Krebs cycle or histone modification. For this reason, ^{11}C-acetate has been used to monitor prostate tumors during therapy and recurrent lesions, but is incapable of distinguishing malignant tumors from benign hyperplastic nodules (182-185). Several radiolabeled ether lipids containing PC moieties (186) have been made (Figure 7) based upon early observations of elevated

phospholipid-ethers in neoplastic tissue (187,188). Due to the preferential accumulation and retention of these alkylphosphonium analogs, ^{124}I-CLR1404 was developed and recently tested in brain tumor PET imaging where a tumor/normal brain signal ratio of 30 was reported (189). Replacement of the PET isotope with the radio-ablative ^{131}I-CLR1404 agent improved survival in tumor-bearing rodents and provided a novel theranostic platform wherein ^{124}I can assist in the planning of ^{131}I therapy.

E. Mass Spectrometry Imaging

Mass spectrometry imaging (MSI) is a powerful modality for the detailed spatial detection of protein, metabolite and drug distribution in tissues. MSI consists of a family of techniques that includes matrix-assisted laser desorption ionization (MALDI) MSI, secondary ion mass spectrometry (SIMS), matrix electrospray-MSI (ES-MSI), and nanostructure-initiator mass spectrometry (NIMS). For the detection of lipids, the most commonly used technique is MALDI MSI (190), which has a large range of applications and provides a good overall combination of spatial resolution, intact molecule sensitivity and probing depth (190). MALDI provides a critical platform for the spatial detection of lipids and lipid metabolites, as there is a lack of suitable reagents and antibodies for the analysis of tissue lipids *in situ* (191).

MSI techniques are invasive procedures, requiring the preparation and embedding of a thin tissue slice followed by rasterized destruction by laser or primary ion beams. For MALDI, tissue is embedded in a matrix such as gelatin and α-cyano-4-hydroxycinnamic acid (CHCA) or 2,5-dihydroxybenzoic acid (DHB) (192). Washing the tissues with aqueous solutions of ammonium formate or phospholipases prior to embedding can be used to enhance certain lipid species and improve signal to noise (191). MSI can detect hundreds of molecules in a single sample with a routine spatial resolution of 50−100 μm, and a small molecule resolution as high

as 5−10 μm (193). Because matrix deposition is a slow process and the application of a wet matrix to tissue can cause metabolite shift, matrix-free techniques using nanoparticle initiators have been developed and these often provide simpler spectra to interpret (194,195). These NIMS procedures provide comparable lipid profiles, but with improved spatial resolution (196).

MSI has been used extensively to study lipid in primary human tumor tissue as well as tumor cell lines and xenografts. In human tissues, a consistent observation of elevated phospholipids has been observed in cancer compared to normal tissues. This includes breast tumors and invasive ductal carcinomas compared to carcinoma *in situ* (197-199), gastric cancers (200), renal cell carcinomas (201), human lung squamous cell carcinoma (202) and colorectal carcinoma (203,204). The most frequent observation is of increased PtdCho in tumors, but increases in PtdEtn, PtdIns, and PA have also been observed (199,205,206). Some studies have demonstrated increases in ether-linked lipids (199). Lyso-phospholipids have been reported to increase in colorectal tumors, but decrease in gastric and prostate cancers (200,203,207) (Figure 8). Fatty acid levels have also been observed to increase in a number of tumors (199), but it is uncertain whether these are free fatty acids or acyl components of more complex lipids.

Studies in tumor xenografts have confirmed the general observations of increased phospholipids and ether-linked lipids in tumor tissues. Measurement of choline metabolites in breast cancer xenografts using MR spectroscopic imaging combined with MALDI-MSI revealed differences in spatial distribution with PC and choline levels concentrated in normoxic tumor regions (208). When correlated with the expression of a hypoxia-response element, PtdCho elevation was concentrated in hypoxic regions whereas LPC was elevated in necrotic regions (192,209). Further studies have indicated distinct microenvironmental lipid distribution with higher levels of ether-linked PtdEtn in viable tumor and ether-linked PtdCho in necrotic regions

(193). Elongated fatty acyl chain length in phospholipids of human lung squamous cell carcinomas was reproduced in mouse xenografts and correlated with the expression of the acyl chain elongase ELOVL6 (210). These data demonstrate the role of MSI in identifying distinct tumor microenvironments by their molecular signatures.

While MSI has revealed a number of potential lipid-related cancer markers, there are very few studies that have employed MSI lipids to monitor cancer treatment. One recent study has identified transient decreases in serum PtdCho and lyso-PtdCho associated with response to radiation in head and neck tumor patients (211). A second study has indicated that LPC (16:0) is a significant predictor of PSA recurrence in human prostate cancer patients (207). The NIMS technique is capable of simultaneous monitoring of drug accumulation and endogenous water-soluble metabolite distribution (212,213). Adopting this technique to study drugs that target lipid metabolism in tumors should be a priority in this field. These data indicate that further investigation into the utility of lipid biomarkers to assess treatment response is warranted.

F. Optical Imaging

Optical imaging is a cost-effective and relatively easy-to-use imaging modality that makes it a valuable tool for non-invasive longitudinal imaging. The range of detectable wavelengths is broad enough to allow multiplex imaging, and these principles have been applied to a number of medical diagnostic platforms, including flow cytometry, fluorescence microscopy, and diffuse optical imaging. *In vivo,* optical imaging is limited by attenuated light penetration through tissue due to scattering and absorption in the visible wavelengths. This is partially alleviated by using chromophores that absorb or emit in the near infrared region (675 – 900 nm) where absorption by hemoglobin, deoxyhemoglobin and water is at a minimum. In

addition, several endogenous proteins, such as laminin and elastin, autofluoresce and elevate the background signal during *in vivo* measurements. As a result, the observable depths of optical imaging are usually limited to 1 cm or less. Thus *in vivo* optical imaging has predominantly focused on single-channel fluorescence or bioluminescence on a macro level (< 15x magnification) in mice or other small animals. Bioluminescence is not practical in clinical settings, because it requires transfection with an invertebrate luminescent protein, but it is a highly sensitive reporter that, in the field of lipid metabolism, has been adapted to map regions of heightened fatty acid uptake (214). Advances in CCD sensitivity has recently sparked renewed interest in Cerenkov radiation as an additional source of emitted light that can be detected *in vivo* (215,216). This signal may one day offer functional information concordant with the tomographical information provided by PET (217).

New optical imaging technologies in oncology have largely followed advancements in vascular imaging. Before diffuse optical tomography became a subject of interest in mammographic screening, the observation was made that absorption of circulating hemoglobin changes in an oxygen-dependent manner (218). This was a pioneering study in translational optical imaging, but 20 years later routine clinical optical imaging remains limited outside of optical coherence tomography (OCT) in ophthalmic applications (219-221). OCT uses a rastered application of NIR light and interferometry to produce a 3-D scanning image of the retina. The use of NIR wavelengths still limits the application to surface phenomena, less than 1 cm deep in the tissue. OCT has also been employed in oncology, most notably to detect the development of esophageal tumors (222,223), With regards to lipids, OCT is most commonly used for atherosclerotic plaque detection in cadavers and patients, which is based upon its sensitivity to

lipid deposits in local vascular sites (224,225). This leads to the possibility for future applications of OCT as a method to distinguish lipid levels in treated tumor tissue.

In small animal optical imaging, enhanced contrast is often provided by the administration of exogenous NIR fluorescent compounds. There are a growing number of these molecular probes that allow for noninvasive optical imaging of lipid metabolism pathways. The probes are generally of three types: passive molecules that are used as blood pool agents and rely on leaky vasculature to accumulate at the site of pathology, targeted permanently fluorescent molecules that can be taken up selectively as substrates or inhibitors of lipid metabolic pathways, and smart quenched fluorescent molecules that can be selectively activated by enzymes. Fluorescence imaging using these probes allows for specific and localized detection of metabolic activity.

Indocyanine green (ICG) is a clinically approved blood-pooling agent that has been used for tumor detection. Collection of ICG in solid tumors has been attributed to the enhanced permeability and retention caused by disordered vasculature and insufficient lymphatic systems in tumors (226), however tumor-associated macrophages in lipid-rich regions may have an underappreciated role in this phenomenon. In atherosclerotic plaques, ICG has been observed to accumulate preferentially in the lipid-rich macrophages in both rabbits and patients (227). MRI, PET, and optical imaging of tumor-associated macrophages have been described extensively (228-230) and these methods should be used to explore co-localization of lipid profiles with immune infiltration in the tumor setting.

Lipid uptake and synthesis

Lipid uptake and synthesis are essential to the maintenance of mammalian cell membranes. For this reason, a constant source of precursors are required to maintain the

proliferative nature of the cancer cell. Tumor cells synthesize and accumulate membrane lipids, such as PtdCho, at a rate that greatly outpaces the surrounding normal tissue, and this offers an avenue that can be exploited for selective delivery of imaging and therapeutic agents. The introduction of fluorescently labeled lipid analogs into the tumor microenvironment can also be used to visualize lipid scavenger activity. Direct fluorescent labeling of PtdCho has been reported using visible fluorophores, so high background in normal tissues is a general feature of these approaches (231). A common approach is to employ fatty acid probes to which non-polar dyes such as BODIPY have been attached (232). Depending on the metabolic state of the cell, these lipid analogs can be incorporated into phospholipids or neutral lipids in lipid droplets. The alkylphosphocholine analogs described for PET imaging have also been adapted with BODIPY or heptamethine dyes for imaging of tumor margins and draining lymph nodes (233).

Choline kinase

Choline kinase catalyzes the conversion of choline to PC, and is elevated in several types of cancers. Its upregulation has been correlated with the transition of normal breast epithelium toward a malignant phenotype, and selective inhibitors have been developed for Phase I clinical trials in solid tumors (ClinicalTrials.gov, NCT01215864). Based on these studies, we developed a series of fluorescent inhibitors that selectively bind ChoK and emit fluorescence in the near infrared optical window (234). The design exploited the structural similarities between ChoK inhibitors and cyanine dyes frequently employed for optical imaging, and did not rely on dye conjugation to existing inhibitor structures (235). The probe, JAS239, showed elevated uptake in tumors that overexpressed ChoK, and more importantly, had reduced uptake in tumors after chemotherapy (236).

Phosphatidylinositol signaling pathway

Many oncogenic signaling pathways are mediated by PtdIns, which makes these lipids attractive targets for cancer imaging probes. In order to interrogate the role of these phospholipids on cell signaling, Yoon *et al.* engineered a fluorescent PIP_2 sensor to study its role in membrane remodeling, regulation of membrane proteins, and regulation of the cytoskeleton (236-238). This probe was engineered with the visible fluorophore (2-dimethyl-amino-6-acyl-naphthaline) optimized for its lipophilic properties, limiting its utility for detection of lipid dynamics *in vivo*. Because IP_3 and DAG mediate the release of intracellular calcium and are activated by lipid metabolic pathways, optical probes based upon flu-4 or BAPTA can provide an indirect means of assessing these bioactive lipids (239-241). DAG can be evaluated directly using radiolabeling (242) or using optical techniques such as FRET to detect activated DAG intercalation in the plasma membrane (243).

Phospholipases

Phospholipases are catabolic enzymes that can be targeted with lipid based quenched optical probes that are activated by enzymatic hydrolysis (39). Upregulation of $cPLA_2$ has been observed in breast and prostate cancers (112), and elevated levels of PC and phosphoethanolamine have been attributed to PLC activation in breast cancer, ovarian cancer and melanoma (109). Activatable probes with phospholipid-based structures, a linker that regulates enzyme accessibility, a quenchable fluorophore or light-emitting compound, and a cleavable quenching domain have been designed as fluorescent agents for quantifying phospholipase activity. The advantage of this approach is the enhanced signal to noise available from the continuous enzymatic release of fluorescent substrates. Enzyme activated BODIPY probes have been employed to examine phospholipase activity in many systems including the

digestive physiology of the zebra fish (244-247). While useful for cells, small transparent animals and intravital microscopy, the optical properties of BODIPY limit its detection in tissue. There are several quenched fluorophores commercially available with emission in the visible range. In the NIR range, we developed analogous probes targeting PLA_2 and PLC for *in vivo* applications (248). These self-quenching probes were composed of pyropheophorbide-*a* (Pyro) tethered to PtdEtn and a Black Hole Quencher (BHQ-3). While Pyro has an excitation maximum ~~excitable Soret band~~ at 418 nm that emits at 660 nm, its absorption peak at 670 with emission at 725 nm makes it suitable for *in vivo* imaging. The specificity of these probes to various phospholipase isoforms could be modulated by altering the spacer length between Pyro and the glycerol backbone. The resulting construct, Pyro-PtdEtn-BHQ, was highly specific to PtdCho-specific PLC (PC-PLC) both *in vitro* and *in vivo* and we used this to detected upregulation and activation of this enzyme in DU145 prostate cancer xenografts (Figure 9) (112).

Arachidonic acid, a PUFA found in the *sn*-2 position of phospholipids, is mobilized by the activity of cytosolic or cPLA2 acting on membrane-associated phospholipids. The redox activity of COX-2 catalyzes the conversion of arachidonic acid to prostaglandins that act as a lipid second messenger. Arachidonic acid is first converted to prostaglandin G2, and then the peroxidase activity of COX-2 converts it to the unstable H2 isoform that is converted to one of several homologous tissue- and function-specific isoforms of prostaglandins. It is prostaglandin E2 that is notably upregulated in several types of cancer contributing to aberrant signaling (249). In order to utilize this signal transduction pathway to image pathogenic events, there are several points of interrogation possible: using activatable probes to evaluate COX-2 activity, directly measure PGE2 levels with targeted probes, or evaluate activation of further downstream events.

Detection of cPLA2 using a cleavable construct requires a probe that contains arachidonic acid, to account for the specificity of the enzyme for this fatty acid, as well as a small enough head group to fit into the active site. Previous studies had shown that arachidonic acid esterified to visible fluorophores such as 7-hydroxycoumarin were highly specific for cPLA2 and displayed similar hydrolysis kinetics to native substrates (250). We adapted this caged fluorescence protocol using fluorophores that emit in the red wavelength range (660-680 nm) to create cPLA2 sensitive probes suitable for *in vivo* imaging. Probe selectivity could be modulated by choice of fatty acids and fluorophores, with DDAO arachidonate performing the best *in vitro,* in cells and tumors. Here, arachidonic acid provided the optimum fatty acid substrate for cPLA2 and DDAO (7-hydroxy-9H-(1,3-dichloro-9,9-dimethylacridin-2-one) was the most resistant to non-specific aqueous hydrolysis. Probe activation was shown to be proportional to cPLA2 expression levels in cells and tumors, and high relative to a non-specific control probe, DDAO palmitate.

Apoptosis

In addition to using imaging techniques to noninvasively detect components of lipid metabolism, other biomarkers can be detected that offer information pertaining to non-homeostatic states of cells and tissues *in situ*. Apoptosis is often indicative of patient response to cancer therapy, accordingly, targeting markers of apoptosis can be useful to evaluate the efficacy of various interventions (251). Among these events are plasma membrane reorganization marked by PtdSer translocation to the outer leaflet of the membrane. PtdSer translocation can be detected using labeled ligands that bind anionic phospholipids, including proteins such as Annexin 5 or synaptotagmin (252) or organic molecules such as zinc dipicolylamine (253). A number of

labeling strategies have used this approach to create apoptosis sensors for optical (254), MR (255-257) and nuclear imaging when radiolabeled with ^{99}Tc or ^{123}I (258). Annexin has shown some promise as a molecular probe for this purpose though this strategy can be limited by suboptimal pharmacokinetics (259), and non-specific labeling of necrotic cells (260).

Conclusion

Lipid metabolism is an essential component of cellular homeostasis that can become drastically altered during the process of malignant transformation. Most common driver mutations and oncogenes are related to growth cues and cellular stress responses, and many therapeutic strategies target these pathways such that the measurement of lipid metabolic changes can serve as a proxy for drug response pharmacodynamics. While MRS and PET approaches offer the ability to serially-measure lipid composition and flux, they are limited by spatial resolution. MSI and Optical Imaging, on the other hand, permit the appreciation of intratumoral heterogeneity but often require surgical exposure of the tissue site. Still, these approaches are finding increasing value in image-guided surgical resection and are experiencing fast-paced improvements in technology including the ability to image endogenous contrast, more specific probes that provide kinetic information, and sub-cellular resolution. For a balance between resolution and ability to image endogenous lipid signals without the need for new FDA-approved contrast agents, MRS remains the gold standard for measuring lipid metabolic states in tumor and other tissues. New advances including two-dimensional MRS, hyperpolarized MR spectroscopic imaging, and higher field strength MRS continue to reshape our understanding of lipid metabolic changes during tumor growth and treatment response. This comes at a critical time as therapy continues to evolve with new signal transduction inhibitors, metabolic targeting agents, and immunotherapies change the landscape of cancer care.

REFERENCES

1. Weiss L, Hoffmann GE, Schreiber R, Andres H, Fuchs E, Korber E, Kolb HJ. Fatty-acid biosynthesis in man, a pathway of minor importance. Purification, optimal assay conditions, and organ distribution of fatty-acid synthase. Biol Chem Hoppe Seyler **1986**;367(9):905-12.
2. Wagle S, Bui A, Ballard PL, Shuman H, Gonzales J, Gonzales LW. Hormonal regulation and cellular localization of fatty acid synthase in human fetal lung. Am J Physiol **1999**;277(2 Pt 1):L381-90.
3. Kusakabe T, Maeda M, Hoshi N, Sugino T, Watanabe K, Fukuda T, Suzuki T. Fatty acid synthase is expressed mainly in adult hormone-sensitive cells or cells with high lipid metabolism and in proliferating fetal cells. J Histochem Cytochem **2000**;48(5):613-22.
4. Eheman C, Henley SJ, Ballard-Barbash R, Jacobs EJ, Schymura MJ, Noone AM, Pan L, Anderson RN, Fulton JE, Kohler BA, Jemal A, Ward E, Plescia M, Ries LA, Edwards BK. Annual Report to the Nation on the status of cancer, 1975-2008, featuring cancers associated with excess weight and lack of sufficient physical activity. Cancer **2012**;118(9):2338-66.
5. Hentosh P, Yuh SH, Elson CE, Peffley DM. Sterol-independent regulation of 3-hydroxy-3-methylglutaryl coenzyme A reductase in tumor cells. Mol Carcinog **2001**;32(3):154-66.
6. Chen Y, Hughes-Fulford M. Human prostate cancer cells lack feedback regulation of low-density lipoprotein receptor and its regulator, SREBP2. Int J Cancer **2001**;91(1):41-5.
7. Kuemmerle NB, Rysman E, Lombardo PS, Flanagan AJ, Lipe BC, Wells WA, Pettus JR, Froehlich HM, Memoli VA, Morganelli PM, Swinnen JV, Timmerman LA, Chaychi L, Fricano CJ, Eisenberg BL, Coleman WB, Kinlaw WB. Lipoprotein lipase links dietary fat to solid tumor cell proliferation. Mol Cancer Ther **2011**;10(3):427-36.
8. Commisso C, Davidson SM, Soydaner-Azeloglu RG, Parker SJ, Kamphorst JJ, Hackett S, Grabocka E, Nofal M, Drebin JA, Thompson CB, Rabinowitz JD, Metallo CM, Vander Heiden MG, Bar-Sagi D. Macropinocytosis of protein is an amino acid supply route in Ras-transformed cells. Nature **2013**;497(7451):633-7.
9. Das R, Hammamieh R, Neill R, Melhem M, Jett M. Expression pattern of fatty acid-binding proteins in human normal and cancer prostate cells and tissues. Clin Cancer Res **2001**;7(6):1706-15.
10. Tolle A, Suhail S, Jung M, Jung K, Stephan C. Fatty acid binding proteins (FABPs) in prostate, bladder and kidney cancer cell lines and the use of IL-FABP as survival predictor in patients with renal cell carcinoma. BMC Cancer **2011**;11:302.
11. DeFilippis RA, Chang H, Dumont N, Rabban JT, Chen YY, Fontenay GV, Berman HK, Gauthier ML, Zhao J, Hu D, Marx JJ, Tjoe JA, Ziv E, Febbraio M, Kerlikowske K, Parvin B, Tlsty TD. CD36 repression activates a multicellular stromal program shared by high mammographic density and tumor tissues. Cancer Discov **2012**;2(9):826-39.
12. Nieman KM, Kenny HA, Penicka CV, Ladanyi A, Buell-Gutbrod R, Zillhardt MR, Romero IL, Carey MS, Mills GB, Hotamisligil GS, Yamada SD, Peter ME, Gwin K,

Lengyel E. Adipocytes promote ovarian cancer metastasis and provide energy for rapid tumor growth. Nat Med **2011**;17(11):1498-503.

13. Daniels VW, Smans K, Royaux I, Chypre M, Swinnen JV, Zaidi N. Cancer cells differentially activate and thrive on de novo lipid synthesis pathways in a low-lipid environment. PLoS One **2014**;9(9):e106913.
14. Cairns RA, Harris IS, Mak TW. Regulation of cancer cell metabolism. Nat Rev Cancer **2011**;11(2):85-95.
15. Sun J, Aluvila S, Kotaria R, Mayor JA, Walters DE, Kaplan RS. Mitochondrial and Plasma Membrane Citrate Transporters: Discovery of Selective Inhibitors and Application to Structure/Function Analysis. Mol Cell Pharmacol **2010**;2(3):101-10.
16. Zaidi N, Swinnen JV, Smans K. ATP-citrate lyase: a key player in cancer metabolism. Cancer Res **2012**;72(15):3709-14.
17. Bauer DE, Hatzivassiliou G, Zhao F, Andreadis C, Thompson CB. ATP citrate lyase is an important component of cell growth and transformation. Oncogene **2005**;24(41):6314-22.
18. Menendez JA, Lupu R. Fatty acid synthase and the lipogenic phenotype in cancer pathogenesis. Nat Rev Cancer **2007**;7(10):763-77.
19. Kuhajda FP, Jenner K, Wood FD, Hennigar RA, Jacobs LB, Dick JD, Pasternack GR. Fatty acid synthesis: a potential selective target for antineoplastic therapy. Proc Natl Acad Sci U S A **1994**;91(14):6379-83.
20. Mullen GE, Yet L. Progress in the development of fatty acid synthase inhibitors as anticancer targets. Bioorg Med Chem Lett **2015**;25(20):4363-9.
21. Zhuang L, Kim J, Adam RM, Solomon KR, Freeman MR. Cholesterol targeting alters lipid raft composition and cell survival in prostate cancer cells and xenografts. J Clin Invest **2005**;115(4):959-68.
22. Roberts PJ, Mitin N, Keller PJ, Chenette EJ, Madigan JP, Currin RO, Cox AD, Wilson O, Kirschmeier P, Der CJ. Rho Family GTPase modification and dependence on CAAX motif-signaled posttranslational modification. J Biol Chem **2008**;283(37):25150-63.
23. Ackerman D, Simon MC. Hypoxia, lipids, and cancer: surviving the harsh tumor microenvironment. Trends Cell Biol **2014**;24(8):472-8.
24. Huang GM, Jiang QH, Cai C, Qu M, Shen W. SCD1 negatively regulates autophagy-induced cell death in human hepatocellular carcinoma through inactivation of the AMPK signaling pathway. Cancer Lett **2015**;358(2):180-90.
25. Scaglia N, Igal RA. Stearoyl-CoA desaturase is involved in the control of proliferation, anchorage-independent growth, and survival in human transformed cells. J Biol Chem **2005**;280(27):25339-49.
26. Chen L, Ren J, Yang L, Li Y, Fu J, Tian Y, Qiu F, Liu Z, Qiu Y. Stearoyl-CoA desaturase-1 mediated cell apoptosis in colorectal cancer by promoting ceramide synthesis. Sci Rep **2016**;6:19665.
27. Jakobsson A, Westerberg R, Jacobsson A. Fatty acid elongases in mammals: their regulation and roles in metabolism. Prog Lipid Res **2006**;45(3):237-49.
28. Denic V, Weissman JS. A molecular caliper mechanism for determining very long-chain fatty acid length. Cell **2007**;130(4):663-77.

29. Abramczyk H, Surmacki J, Kopec M, Olejnik AK, Lubecka-Pietruszewska K, Fabianowska-Majewska K. The role of lipid droplets and adipocytes in cancer. Raman imaging of cell cultures: MCF10A, MCF7, and MDA-MB-231 compared to adipocytes in cancerous human breast tissue. Analyst **2015**;140(7):2224-35.
30. Griner EM, Kazanietz MG. Protein kinase C and other diacylglycerol effectors in cancer. Nat Rev Cancer **2007**;7(4):281-94.
31. Lin ME, Herr DR, Chun J. Lysophosphatidic acid (LPA) receptors: signaling properties and disease relevance. Prostaglandins Other Lipid Mediat **2010**;91(3-4):130-8.
32. Foster DA, Salloum D, Menon D, Frias MA. Phospholipase D and the maintenance of phosphatidic acid levels for regulation of mammalian target of rapamycin (mTOR). J Biol Chem **2014**;289(33):22583-8.
33. Bagnato C, Igal RA. Overexpression of diacylglycerol acyltransferase-1 reduces phospholipid synthesis, proliferation, and invasiveness in simian virus 40-transformed human lung fibroblasts. J Biol Chem **2003**;278(52):52203-11.
34. Daly PF, Lyon RC, Faustino PJ, Cohen JS. Phospholipid metabolism in cancer cells monitored by 31P NMR spectroscopy. J Biol Chem **1987**;262(31):14875-8.
35. Glunde K, Bhujwalla ZM, Ronen SM. Choline metabolism in malignant transformation. Nat Rev Cancer **2011**;11(12):835-48.
36. Currie E, Schulze A, Zechner R, Walther TC, Farese RV, Jr. Cellular fatty acid metabolism and cancer. Cell Metab **2013**;18(2):153-61.
37. Nomura DK, Long JZ, Niessen S, Hoover HS, Ng SW, Cravatt BF. Monoacylglycerol lipase regulates a fatty acid network that promotes cancer pathogenesis. Cell **2010**;140(1):49-61.
38. Murakami M, Taketomi Y, Miki Y, Sato H, Hirabayashi T, Yamamoto K. Recent progress in phospholipase A(2) research: from cells to animals to humans. Prog Lipid Res **2011**;50(2):152-92.
39. Park JB, Lee CS, Jang JH, Ghim J, Kim YJ, You S, Hwang D, Suh PG, Ryu SH. Phospholipase signalling networks in cancer. Nat Rev Cancer **2012**;12(11):782-92.
40. Kadamur G, Ross EM. Mammalian phospholipase C. Annu Rev Physiol **2013**;75:127-54.
41. Samudio I, Harmancey R, Fiegl M, Kantarjian H, Konopleva M, Korchin B, Kaluarachchi K, Bornmann W, Duvvuri S, Taegtmeyer H, Andreeff M. Pharmacologic inhibition of fatty acid oxidation sensitizes human leukemia cells to apoptosis induction. J Clin Invest **2010**;120(1):142-56.
42. Liu Y. Fatty acid oxidation is a dominant bioenergetic pathway in prostate cancer. Prostate Cancer Prostatic Dis **2006**;9(3):230-4.
43. Zuo X, Wu Y, Morris JS, Stimmel JB, Leesnitzer LM, Fischer SM, Lippman SM, Shureiqi I. Oxidative metabolism of linoleic acid modulates PPAR-beta/delta suppression of PPAR-gamma activity. Oncogene **2006**;25(8):1225-41.
44. Brash AR. Arachidonic acid as a bioactive molecule. J Clin Invest **2001**;107(11):1339-45.
45. Dennis EA, Norris PC. Eicosanoid storm in infection and inflammation. Nat Rev Immunol **2015**;15(8):511-23.

46. Harizi H, Corcuff JB, Gualde N. Arachidonic-acid-derived eicosanoids: roles in biology and immunopathology. Trends Mol Med **2008**;14(10):461-9.
47. Wise DR, Thompson CB. Glutamine addiction: a new therapeutic target in cancer. Trends Biochem Sci **2010**;35(8):427-33.
48. Cheng T, Sudderth J, Yang C, Mullen AR, Jin ES, Mates JM, DeBerardinis RJ. Pyruvate carboxylase is required for glutamine-independent growth of tumor cells. Proc Natl Acad Sci U S A **2011**;108(21):8674-9.
49. Hensley CT, Wasti AT, DeBerardinis RJ. Glutamine and cancer: cell biology, physiology, and clinical opportunities. J Clin Invest **2013**;123(9):3678-84.
50. Young RM, Ackerman D, Quinn ZL, Mancuso A, Gruber M, Liu L, Giannoukos DN, Bobrovnikova-Marjon E, Diehl JA, Keith B, Simon MC. Dysregulated mTORC1 renders cells critically dependent on desaturated lipids for survival under tumor-like stress. Genes Dev **2013**;27(10):1115-31.
51. Doe MR, Ascano JM, Kaur M, Cole MD. Myc posttranscriptionally induces HIF1 protein and target gene expression in normal and cancer cells. Cancer Res **2012**;72(4):949-57.
52. Ravi R, Mookerjee B, Bhujwalla ZM, Sutter CH, Artemov D, Zeng Q, Dillehay LE, Madan A, Semenza GL, Bedi A. Regulation of tumor angiogenesis by p53-induced degradation of hypoxia-inducible factor 1alpha. Genes Dev **2000**;14(1):34-44.
53. Qiu B, Ackerman D, Sanchez DJ, Li B, Ochocki JD, Grazioli A, Bobrovnikova-Marjon E, Diehl JA, Keith B, Simon MC. HIF2alpha-Dependent Lipid Storage Promotes Endoplasmic Reticulum Homeostasis in Clear-Cell Renal Cell Carcinoma. Cancer Discov **2015**;5(6):652-67.
54. Dang L, White DW, Gross S, Bennett BD, Bittinger MA, Driggers EM, Fantin VR, Jang HG, Jin S, Keenan MC, Marks KM, Prins RM, Ward PS, Yen KE, Liau LM, Rabinowitz JD, Cantley LC, Thompson CB, Vander Heiden MG, Su SM. Cancer-associated IDH1 mutations produce 2-hydroxyglutarate. Nature **2009**;462(7274):739-44.
55. Metallo CM, Gameiro PA, Bell EL, Mattaini KR, Yang J, Hiller K, Jewell CM, Johnson ZR, Irvine DJ, Guarente L, Kelleher JK, Vander Heiden MG, Iliopoulos O, Stephanopoulos G. Reductive glutamine metabolism by IDH1 mediates lipogenesis under hypoxia. Nature **2011**;481(7381):380-4.
56. Wise DR, Ward PS, Shay JE, Cross JR, Gruber JJ, Sachdeva UM, Platt JM, DeMatteo RG, Simon MC, Thompson CB. Hypoxia promotes isocitrate dehydrogenase-dependent carboxylation of alpha-ketoglutarate to citrate to support cell growth and viability. Proc Natl Acad Sci U S A **2011**;108(49):19611-6.
57. Lu C, Ward PS, Kapoor GS, Rohle D, Turcan S, Abdel-Wahab O, Edwards CR, Khanin R, Figueroa ME, Melnick A, Wellen KE, O'Rourke DM, Berger SL, Chan TA, Levine RL, Mellinghoff IK, Thompson CB. IDH mutation impairs histone demethylation and results in a block to cell differentiation. Nature **2012**;483(7390):474-8.
58. Losman JA, Kaelin WG, Jr. What a difference a hydroxyl makes: mutant IDH, (R)-2-hydroxyglutarate, and cancer. Genes Dev **2013**;27(8):836-52.
59. Leather T, Jenkinson MD, Das K, Poptani H. Magnetic Resonance Spectroscopy for Detection of 2-Hydroxyglutarate as a Biomarker for IDH Mutation in Gliomas. Metabolites **2017**;7(2).

60. Guo D, Bell EH, Mischel P, Chakravarti A. Targeting SREBP-1-driven lipid metabolism to treat cancer. Curr Pharm Des **2014**;20(15):2619-26.
61. Lewis CA, Brault C, Peck B, Bensaad K, Griffiths B, Mitter R, Chakravarty P, East P, Dankworth B, Alibhai D, Harris AL, Schulze A. SREBP maintains lipid biosynthesis and viability of cancer cells under lipid- and oxygen-deprived conditions and defines a gene signature associated with poor survival in glioblastoma multiforme. Oncogene **2015**;34(40):5128-40.
62. Kim SW, Hayashi M, Lo JF, Yang Y, Yoo JS, Lee JD. ADP-ribosylation factor 4 small GTPase mediates epidermal growth factor receptor-dependent phospholipase D2 activation. J Biol Chem **2003**;278(4):2661-8.
63. Tvorogov D, Carpenter G. EGF-dependent association of phospholipase C-gamma1 with c-Cbl. Exp Cell Res **2002**;277(1):86-94.
64. Miyake T, Parsons SJ. Functional interactions between Choline kinase alpha, epidermal growth factor receptor and c-Src in breast cancer cell proliferation. Oncogene **2012**;31(11):1431-41.
65. Key TJ, Allen NE, Verkasalo PK, Banks E. Energy balance and cancer: the role of sex hormones. Proc Nutr Soc **2001**;60(1):81-9.
66. Cantley LC. The phosphoinositide 3-kinase pathway. Science **2002**;296(5573):1655-7.
67. Takai Y, Sasaki T, Matozaki T. Small GTP-binding proteins. Physiol Rev **2001**;81(1):153-208.
68. Balla T. Phosphoinositides: tiny lipids with giant impact on cell regulation. Physiol Rev **2013**;93(3):1019-137.
69. Nasuhoglu C, Feng S, Mao J, Yamamoto M, Yin HL, Earnest S, Barylko B, Albanesi JP, Hilgemann DW. Nonradioactive analysis of phosphatidylinositides and other anionic phospholipids by anion-exchange high-performance liquid chromatography with suppressed conductivity detection. Anal Biochem **2002**;301(2):243-54.
70. Wenk MR, Lucast L, Di Paolo G, Romanelli AJ, Suchy SF, Nussbaum RL, Cline GW, Shulman GI, McMurray W, De Camilli P. Phosphoinositide profiling in complex lipid mixtures using electrospray ionization mass spectrometry. Nat Biotechnol **2003**;21(7):813-7.
71. Santos CR, Schulze A. Lipid metabolism in cancer. FEBS J **2012**;279(15):2610-23.
72. Hashmi S, Wang Y, Suman DS, Parhar RS, Collison K, Conca W, Al-Mohanna F, Gaugler R. Human cancer: is it linked to dysfunctional lipid metabolism? Biochim Biophys Acta **2014**;1850(2):352-64.
73. Ramirez de Molina A, Gutierrez R, Ramos MA, Silva JM, Silva J, Bonilla F, Sanchez JJ, Lacal JC. Increased choline kinase activity in human breast carcinomas: clinical evidence for a potential novel antitumor strategy. Oncogene **2002**;21(27):4317-22.
74. Daly PF, Cohen JS. Magnetic resonance spectroscopy of tumors and potential in vivo clinical applications: a review. Cancer Res **1989**;49(4):770-9.
75. Negendank W. Studies of human tumors by MRS: a review. NMR Biomed **1992**;5(5):303-24.

76. Yalcin A, Clem B, Makoni S, Clem A, Nelson K, Thornburg J, Siow D, Lane AN, Brock SE, Goswami U, Eaton JW, Telang S, Chesney J. Selective inhibition of choline kinase simultaneously attenuates MAPK and PI3K/AKT signaling. Oncogene **2010**;29(1):139-49.

77. Iorio E, Mezzanzanica D, Alberti P, Spadaro F, Ramoni C, D'Ascenzo S, Millimaggi D, Pavan A, Dolo V, Canevari S, Podo F. Alterations of choline phospholipid metabolism in ovarian tumor progression. Cancer Res **2005**;65(20):9369-76.

78. Cocco L, Follo MY, Manzoli L, Suh PG. Phosphoinositide-specific phospholipase C in health and disease. J Lipid Res **2015**;56(10):1853-60.

79. Hilvo M, Denkert C, Lehtinen L, Muller B, Brockmoller S, Seppanen-Laakso T, Budczies J, Bucher E, Yetukuri L, Castillo S, Berg E, Nygren H, Sysi-Aho M, Griffin JL, Fiehn O, Loibl S, Richter-Ehrenstein C, Radke C, Hyotylainen T, Kallioniemi O, Iljin K, Oresic M. Novel theranostic opportunities offered by characterization of altered membrane lipid metabolism in breast cancer progression. Cancer Res **2011**;71(9):3236-45.

80. Husain Z, Huang Y, Seth P, Sukhatme VP. Tumor-derived lactate modifies antitumor immune response: effect on myeloid-derived suppressor cells and NK cells. J Immunol **2013**;191(3):1486-95.

81. Colegio OR, Chu NQ, Szabo AL, Chu T, Rhebergen AM, Jairam V, Cyrus N, Brokowski CE, Eisenbarth SC, Phillips GM, Cline GW, Phillips AJ, Medzhitov R. Functional polarization of tumour-associated macrophages by tumour-derived lactic acid. Nature **2014**;513(7519):559-63.

82. Ende D, Rutter A, Russell P, Mountford CE. Chemical shift imaging of human colorectal tissue (ex vivo). NMR Biomed **1996**;9(4):179-83.

83. King NJ, Delikatny EJ, Holmes KT. 1H magnetic resonance spectroscopy of primary human and murine cells of the myeloid lineage. Immunomethods **1994**;4(2):188-98.

84. Pearce EL, Pearce EJ. Metabolic pathways in immune cell activation and quiescence. Immunity **2013**;38(4):633-43.

85. Noy R, Pollard JW. Tumor-associated macrophages: from mechanisms to therapy. Immunity **2014**;41(1):49-61.

86. Lauber K, Bohn E, Krober SM, Xiao YJ, Blumenthal SG, Lindemann RK, Marini P, Wiedig C, Zobywalski A, Baksh S, Xu Y, Autenrieth IB, Schulze-Osthoff K, Belka C, Stuhler G, Wesselborg S. Apoptotic cells induce migration of phagocytes via caspase-3-mediated release of a lipid attraction signal. Cell **2003**;113(6):717-30.

87. Gude DR, Alvarez SE, Paugh SW, Mitra P, Yu J, Griffiths R, Barbour SE, Milstien S, Spiegel S. Apoptosis induces expression of sphingosine kinase 1 to release sphingosine-1-phosphate as a "come-and-get-me" signal. FASEB J **2008**;22(8):2629-38.

88. Savill J, Dransfield I, Gregory C, Haslett C. A blast from the past: clearance of apoptotic cells regulates immune responses. Nat Rev Immunol **2002**;2(12):965-75.

89. Ravichandran KS. Find-me and eat-me signals in apoptotic cell clearance: progress and conundrums. J Exp Med **2010**;207(9):1807-17.

90. Edinger AL, Thompson CB. Death by design: apoptosis, necrosis and autophagy. Curr Opin Cell Biol **2004**;16(6):663-9.

91. Viswanathan VS, Ryan MJ, Dhruv HD, Gill S, Eichhoff OM, Seashore-Ludlow B, Kaffenberger SD, Eaton JK, Shimada K, Aguirre AJ, Viswanathan SR, Chattopadhyay S, Tamayo P, Yang WS, Rees MG, Chen S, Boskovic ZV, Javaid S, Huang C, Wu X, Tseng YY, Roider EM, Gao D, Cleary JM, Wolpin BM, Mesirov JP, Haber DA, Engelman JA, Boehm JS, Kotz JD, Hon CS, Chen Y, Hahn WC, Levesque MP, Doench JG, Berens ME, Shamji AF, Clemons PA, Stockwell BR, Schreiber SL. Dependency of a therapy-resistant state of cancer cells on a lipid peroxidase pathway. Nature **2017**;547(7664):453-7.

92. Delikatny EJ, Chawla S, Leung DJ, Poptani H. MR-visible lipids and the tumor microenvironment. NMR Biomed **2011**;24(6):592-611.

93. Milkevitch M, Jeitner TM, Beardsley NJ, Delikatny EJ. Lovastatin enhances phenylbutyrate-induced MR-visible glycerophosphocholine but not apoptosis in DU145 prostate cells. Biochim Biophys Acta **2007**;1771(9):1166-76.

94. Iorio E, Di Vito M, Spadaro F, Ramoni C, Lococo E, Carnevale R, Lenti L, Strom R, Podo F. Triacsin C inhibits the formation of 1H NMR-visible mobile lipids and lipid bodies in HuT 78 apoptotic cells. Biochim Biophys Acta **2003**;1634(1-2):1-14.

95. Miki Y, Mukae S, Murakami M, Ishikawa Y, Ishii T, Ohki H, Matsumoto M, Komiyama K. Butyrate inhibits oral cancer cell proliferation and regulates expression of secretory phospholipase A2-X and COX-2. Anticancer Res **2007**;27(3B):1493-502.

96. Boren J, Brindle KM. Apoptosis-induced mitochondrial dysfunction causes cytoplasmic lipid droplet formation. Cell Death Differ **2012**;19(9):1561-70.

97. Farese RV, Jr., Walther TC. Lipid droplets finally get a little R-E-S-P-E-C-T. Cell **2009**;139(5):855-60.

98. Guo Y, Walther TC, Rao M, Stuurman N, Goshima G, Terayama K, Wong JS, Vale RD, Walter P, Farese RV. Functional genomic screen reveals genes involved in lipid-droplet formation and utilization. Nature **2008**;453(7195):657-61.

99. Morjani H, Aouali N, Belhoussine R, Veldman RJ, Levade T, Manfait M. Elevation of glucosylceramide in multidrug-resistant cancer cells and accumulation in cytoplasmic droplets. Int J Cancer **2001**;94(2):157-65.

100. Bensaad K, Favaro E, Lewis CA, Peck B, Lord S, Collins JM, Pinnick KE, Wigfield S, Buffa FM, Li JL, Zhang Q, Wakelam MJ, Karpe F, Schulze A, Harris AL. Fatty acid uptake and lipid storage induced by HIF-1alpha contribute to cell growth and survival after hypoxia-reoxygenation. Cell Rep **2014**;9(1):349-65.

101. Rysman E, Brusselmans K, Scheys K, Timmermans L, Derua R, Munck S, Van Veldhoven PP, Waltregny D, Daniels VW, Machiels J, Vanderhoydonc F, Smans K, Waelkens E, Verhoeven G, Swinnen JV. De novo lipogenesis protects cancer cells from free radicals and chemotherapeutics by promoting membrane lipid saturation. Cancer Res **2010**;70(20):8117-26.

102. Mukundan L, Odegaard JI, Morel CR, Heredia JE, Mwangi JW, Ricardo-Gonzalez RR, Goh YP, Eagle AR, Dunn SE, Awakuni JU, Nguyen KD, Steinman L, Michie SA, Chawla A. PPAR-delta senses and orchestrates clearance of apoptotic cells to promote tolerance. Nat Med **2009**;15(11):1266-72.

103. Wright LC, Groot Obbink KL, Delikatny EJ, Santangelo RT, Sorrell TC. The origin of ^{1}H NMR-visible triacylglycerol in human neutrophils: high fatty acid environments result in preferential sequestration of palmitic acid into plasma membrane triacylglycerol. European Journal of Biochemistry **2000**;267:68-78.

104. Huang C, Freter C. Lipid metabolism, apoptosis and cancer therapy. Int J Mol Sci **2015**;16(1):924-49.

105. Podo F, Canevari S, Canese R, Pisanu ME, Ricci A, Iorio E. MR evaluation of response to targeted treatment in cancer cells. NMR Biomed **2011**;24(6):648-72.

106. Hakumaki JM, Poptani H, Sandmair AM, Yla-Herttuala S, Kauppinen RA. 1H MRS detects polyunsaturated fatty acid accumulation during gene therapy of glioma: implications for the in vivo detection of apoptosis. Nat Med **1999**;5(11):1323-7.

107. Milkevitch M, Shim H, Pilatus U, Pickup S, Wehrle JP, Samid D, Poptani H, Glickson JD, Delikatny EJ. Increases in NMR-visible lipid and glycerophosphocholine during phenylbutyrate-induced apoptosis in human prostate cancer cells. Biochim Biophys Acta **2005**;1734(1):1-12.

108. Greenhough A, Smartt HJ, Moore AE, Roberts HR, Williams AC, Paraskeva C, Kaidi A. The COX-2/PGE2 pathway: key roles in the hallmarks of cancer and adaptation to the tumour microenvironment. Carcinogenesis **2009**;30(3):377-86.

109. Podo F. Tumour phospholipid metabolism. NMR Biomed **1999**;12(7):413-39.

110. Ackerstaff E, Glunde K, Bhujwalla ZM. Choline phospholipid metabolism: a target in cancer cells? J Cell Biochem **2003**;90(3):525-33.

111. Glunde K, Jie C, Bhujwalla ZM. Molecular causes of the aberrant choline phospholipid metabolism in breast cancer. Cancer Research **2004**;64(12):4270-6.

112. Mawn TM, Popov AV, Beardsley NJ, Stefflova K, Milkevitch M, Zheng G, Delikatny EJ. In Vivo Detection of Phospholipase C by Enzyme-Activated Near-Infrared Probes. Bioconjugate Chem **2011**;22(12):2434-43.

113. Al-Saffar NM, Troy H, Ramirez de Molina A, Jackson LE, Madhu B, Griffiths JR, Leach MO, Workman P, Lacal JC, Judson IR, Chung YL. Noninvasive magnetic resonance spectroscopic pharmacodynamic markers of the choline kinase inhibitor MN58b in human carcinoma models. Cancer Res **2006**;66(1):427-34.

114. Kumar M, Arlauckas SP, Saksena S, Verma G, Ittyerah R, Pickup S, Popov AV, Delikatny EJ, Poptani H. Magnetic resonance spectroscopy for detection of choline kinase inhibition in the treatment of brain tumors. Mol Cancer Ther **2015**;14(4):899-908.

115. van Asten JJ, Vettukattil R, Buckle T, Rottenberg S, van Leeuwen F, Bathen TF, Heerschap A. Increased levels of choline metabolites are an early marker of docetaxel treatment response in BRCA1-mutated mouse mammary tumors: an assessment by ex vivo proton magnetic resonance spectroscopy. J Transl Med **2015**;13:114.

116. Sharma U, Baek HM, Su MY, Jagannathan NR. In vivo 1H MRS in the assessment of the therapeutic response of breast cancer patients. NMR Biomed **2011**;24(6):700-11.

117. Danishad KK, Sharma U, Sah RG, Seenu V, Parshad R, Jagannathan NR. Assessment of therapeutic response of locally advanced breast cancer (LABC) patients undergoing

neoadjuvant chemotherapy (NACT) monitored using sequential magnetic resonance spectroscopic imaging (MRSI). NMR Biomed **2010**;23(3):233-41.

118. Bathen TF, Heldahl MG, Sitter B, Vettukattil R, Bofin A, Lundgren S, Gribbestad IS. In vivo MRS of locally advanced breast cancer: characteristics related to negative or positive choline detection and early monitoring of treatment response. MAGMA **2011**;24(6):347-57.
119. Drisis S, Flamen P, Ignatiadis M, Metens T, Chao SL, Chintinne M, Lemort M. Total choline quantification measured by 1H MR spectroscopy as early predictor of response after neoadjuvant treatment for locally advanced breast cancer: The impact of immunohistochemical status. J Magn Reson Imaging **2018**.
120. Bolan PJ, Kim E, Herman BA, Newstead GM, Rosen MA, Schnall MD, Pisano ED, Weatherall PT, Morris EA, Lehman CD, Garwood M, Nelson MT, Yee D, Polin SM, Esserman LJ, Gatsonis CA, Metzger GJ, Newitt DC, Partridge SC, Hylton NM, Investigators ATtI-. MR spectroscopy of breast cancer for assessing early treatment response: Results from the ACRIN 6657 MRS trial. J Magn Reson Imaging **2017**;46(1):290-302.
121. Viswanath P, Radoul M, Izquierdo-Garcia JL, Ong WQ, Luchman HA, Cairncross JG, Huang B, Pieper RO, Phillips JJ, Ronen SM. 2-Hydroxyglutarate-Mediated Autophagy of the Endoplasmic Reticulum Leads to an Unusual Downregulation of Phospholipid Biosynthesis in Mutant IDH1 Gliomas. Cancer Res **2018**.
122. Cao MD, Cheng M, Rizwan A, Jiang L, Krishnamachary B, Bhujwalla ZM, Bathen TF, Glunde K. Targeting choline phospholipid metabolism: GDPD5 and GDPD6 silencing decrease breast cancer cell proliferation, migration, and invasion. NMR Biomed **2016**;29(8):1098-107.
123. Bharti SK, Mironchik Y, Wildes F, Penet MF, Goggins E, Krishnamachary B, Bhujwalla ZM. Metabolic consequences of HIF silencing in a triple negative human breast cancer xenograft. Oncotarget **2018**;9(20):15326-39.
124. Kuesel AC, Sutherland GR, Halliday W, Smith IC. 1H MRS of high grade astrocytomas: mobile lipid accumulation in necrotic tissue. NMR Biomed **1994**;7(3):149-55.
125. Delikatny EJ, Russell P, Hunter JC, Hancock R, Atkinson KH, van Haaften-Day C, Mountford CE. Proton MR and human cervical neoplasia: ex vivo spectroscopy allows distinction of invasive carcinoma of the cervix from carcinoma in situ and other preinvasive lesions. Radiology **1993**;188(3):791-6.
126. Mountford CE, Grossman G, Reid G, Fox RM. Characterization of transformed cells and tumours by proton nuclear magnetic resonance spectroscopy. Cancer Research **1982**;42:2270-6.
127. Cross KJ, Holmes KT, Mountford CE, Wright PE. Assignment of acyl chain resonances from membranes of mammalian cells by two-dimensional NMR methods. Biochemistry **1984**;23:5895-7.
128. Delgado-Goni T, Julia-Sape M, Candiota AP, Pumarola M, Arus C. Molecular imaging coupled to pattern recognition distinguishes response to temozolomide in preclinical glioblastoma. NMR Biomed **2014**;27(11):1333-45.

129. Liimatainen T, Hakumaki JM, Kauppinen RA, Ala-Korpela M. Monitoring of gliomas in vivo by diffusion MRI and (1)H MRS during gene therapy-induced apoptosis: interrelationships between water diffusion and mobile lipids. NMR Biomed **2009**;22(3):272-9.

130. Chawla S, Krejza J, Vossough A, Zhang Y, Kapoor GS, Wang S, O'Rourke DM, Melhem ER, Poptani H. Differentiation between oligodendroglioma genotypes using dynamic susceptibility contrast perfusion-weighted imaging and proton MR spectroscopy. AJNR Am J Neuroradiol **2013**;34(8):1542-9.

131. Doblas S, He T, Saunders D, Hoyle J, Smith N, Pye Q, Lerner M, Jensen RL, Towner RA. In vivo characterization of several rodent glioma models by 1H MRS. NMR Biomed **2012**;25(4):685-94.

132. Preul MC, Caramanos Z, Collins DL, Villemure JG, Leblanc R, Olivier A, Pokrupa R, Arnold DL. Accurate, noninvasive diagnosis of human brain tumors by using proton magnetic resonance spectroscopy. Nat Med **1996**;2(3):323-5.

133. Astrakas LG, Zurakowski D, Tzika AA, Zarifi MK, Anthony DC, De Girolami U, Tarbell NJ, Black PM. Noninvasive magnetic resonance spectroscopic imaging biomarkers to predict the clinical grade of pediatric brain tumors. Clin Cancer Res **2004**;10(24):8220-8.

134. Wilson M, Cummins CL, Macpherson L, Sun Y, Natarajan K, Grundy RG, Arvanitis TN, Kauppinen RA, Peet AC. Magnetic resonance spectroscopy metabolite profiles predict survival in paediatric brain tumours. Eur J Cancer **2013**;49(2):457-64.

135. Ross BD, Chenevert TL, Kim B, Ben-Yoseph O. Magnetic Resonance Imaging and Spectroscopy: Application to Experimental Neuro-Oncology. Q Magn Reson Biol Med **1994**;1(2):89-106.

136. Liimatainen T, Hakumaki J, Tkac I, Grohn O. Ultra-short echo time spectroscopic imaging in rats: implications for monitoring lipids in glioma gene therapy. NMR Biomed **2006**;19(5):554-9.

137. Liimatainen TJ, Erkkila AT, Valonen P, Vidgren H, Lakso M, Wong G, Grohn OH, Yla-Herttuala S, Hakumaki JM. 1H MR spectroscopic imaging of phospholipase-mediated membrane lipid release in apoptotic rat glioma in vivo. Magn Reson Med **2008**;59(6):1232-8.

138. Hemminki O, Immonen R, Narvainen J, Kipar A, Paasonen J, Jokivarsi KT, Yli-Ollila H, Soininen P, Partanen K, Joensuu T, Parvianen S, Pesonen SK, Koski A, Vaha-Koskela M, Cerullo V, Pesonen S, Grohn OH, Hemminki A. In vivo magnetic resonance imaging and spectroscopy identifies oncolytic adenovirus responders. Int J Cancer **2014**;134(12):2878-90.

139. He Q, Shkarin P, Hooley RJ, Lannin DR, Weinreb JC, Bossuyt VI. In vivo MR spectroscopic imaging of polyunsaturated fatty acids (PUFA) in healthy and cancerous breast tissues by selective multiple-quantum coherence transfer (Sel-MQC): a preliminary study. Magn Reson Med **2007**;58(6):1079-85.

140. Wang AS, Lodi A, Rivera LB, Izquierdo-Garcia JL, Firpo MA, Mulvihill SJ, Tempero MA, Bergers G, Ronen SM. HR-MAS MRS of the pancreas reveals reduced lipid and elevated lactate and taurine associated with early pancreatic cancer. NMR Biomed **2014**;27(11):1361-70.

141. Cho SG, Lee DH, Lee KY, Ji H, Lee KH, Ros PR, Suh CH. Differentiation of chronic focal pancreatitis from pancreatic carcinoma by in vivo proton magnetic resonance spectroscopy. J Comput Assist Tomogr **2005**;29(2):163-9.

142. Erkan M, Hausmann S, Michalski CW, Fingerle AA, Dobritz M, Kleeff J, Friess H. The role of stroma in pancreatic cancer: diagnostic and therapeutic implications. Nat Rev Gastroenterol Hepatol **2012**;9(8):454-67.

143. Ackerstaff E, Gimi B, Artemov D, Bhujwalla ZM. Anti-inflammatory agent indomethacin reduces invasion and alters metabolism in a human breast cancer cell line. Neoplasia **2007**;9(3):222-35.

144. Delikatny EJ, Cooper WA, Brammah S, Sathasivam N, Rideout DC. Nuclear magnetic resonance-visible lipid induced by cationic lipophilic chemotherapeutic agents are accompanied by increased lipid droplet formation and damaged mitochondria. Cancer Research **2002**;62:1394-400.

145. Blankenberg FG, Katsikis PD, Storrs RW, Beaulieu C, Spielman D, Chen JY, Naumovski L, Tait JF. Quantitative analysis of apoptotic cell death using proton nuclear magnetic resonance spectroscopy. Blood **1997**;89(10):3778-86.

146. Iorio E, Di Vito M, Spadaro F, Ramoni C, Lococo E, Carnevale R, Lenti L, Strom R, Podo F. Triacsin C inhibits the formation of 1H NMR-visible mobile lipids and lipid bodies in HuT 78 apoptotic cells. Biochimica et Biophysica Acta **2003**;1634(1-2):1-14.

147. Milkevitch M, Beardsley NJ, Delikatny EJ. Phenylbutyrate induces apoptosis and lipid accumulations via a peroxisome proliferator-activated receptor gamma-dependent pathway. NMR in Biomedicine **2010**;23(5):473-9.

148. Roman SK, Jeitner TM, Hancock R, Cooper WA, Rideout DC, Delikatny EJ. Induction of magnetic resonance-visible lipid in a transformed human breast cell line by tetraphenylphosphonium chloride. International Journal of Cancer **1997**;73:570-9.

149. Mirbahai L, Wilson M, Shaw CS, McConville C, Malcomson RD, Kauppinen RA, Peet AC. Lipid biomarkers of glioma cell growth arrest and cell death detected by 1 H magic angle spinning MRS. NMR Biomed **2012**;25(11):1253-62.

150. Pisanu ME, Ricci A, Paris L, Surrentino E, Liliac L, Bagnoli M, Canevari S, Mezzanzanica D, Podo F, Iorio E, Canese R. Monitoring response to cytostatic cisplatin in a HER2(+) ovary cancer model by MRI and in vitro and in vivo MR spectroscopy. Br J Cancer **2014**;110(3):625-35.

151. Mesti T, Savarin P, Triba MN, Le Moyec L, Ocvirk J, Banissi C, Carpentier AF. Metabolic impact of anti-angiogenic agents on U87 glioma cells. PLoS One **2014**;9(6):e99198.

152. Radoul M, Chaumeil MM, Eriksson P, Wang AS, Phillips JJ, Ronen SM. MR Studies of Glioblastoma Models Treated with Dual PI3K/mTOR Inhibitor and Temozolomide:Metabolic Changes Are Associated with Enhanced Survival. Mol Cancer Ther **2016**;15(5):1113-22.

153. Schmitz JE, Kettunen MI, Hu DE, Brindle KM. 1H MRS-visible lipids accumulate during apoptosis of lymphoma cells in vitro and in vivo. Magn Reson Med **2005**;54(1):43-50.

154. He T, Doblas S, Saunders D, Casteel R, Lerner M, Ritchey JW, Snider T, Floyd RA, Towner RA. Effects of PBN and OKN007 in rodent glioma models assessed by 1H MR spectroscopy. Free Radic Biol Med **2011**;51(2):490-502.

155. Lyng H, Sitter B, Bathen TF, Jensen LR, Sundfor K, Kristensen GB, Gribbestad IS. Metabolic mapping by use of high-resolution magic angle spinning 1H MR spectroscopy for assessment of apoptosis in cervical carcinomas. BMC Cancer **2007**;7:11.

156. Lee SC, Poptani H, Pickup S, Jenkins WT, Kim S, Koch CJ, Delikatny EJ, Glickson JD. Early detection of radiation therapy response in non-Hodgkin's lymphoma xenografts by in vivo 1H magnetic resonance spectroscopy and imaging. NMR Biomed **2010**;23(6):624-32.

157. Lee JS, Orita H, Gabrielson K, Alvey S, Hagemann RL, Kuhajda FP, Gabrielson E, Pomper MG. FDG-PET for pharmacodynamic assessment of the fatty acid synthase inhibitor C75 in an experimental model of lung cancer. Pharm Res **2007**;24(6):1202-7.

158. Sankaranarayanapillai M, Zhang N, Baggerly KA, Gelovani JG. Metabolic shifts induced by fatty acid synthase inhibitor orlistat in non-small cell lung carcinoma cells provide novel pharmacodynamic biomarkers for positron emission tomography and magnetic resonance spectroscopy. Mol Imaging Biol **2013**;15(2):136-47.

159. Beauregard JM, Williams SG, Degrado TR, Roselt P, Hicks RJ. Pilot comparison of F-fluorocholine and F-fluorodeoxyglucose PET/CT with conventional imaging in prostate cancer. J Med Imaging Radiat Oncol **2010**;54(4):325-32.

160. Sollini M, Sghedoni R, Erba PA, Cavuto S, Froio A, De Berti G, Pisanello A, Fraternali A, Iori M, Iaccarino C, Asti M, Filice A, Versari A. Diagnostic performances of [18f]fluorocholine positron emission tomography in brain tumors. Q J Nucl Med Mol Imaging **2015**;62(2):209-19.

161. Reske SN, Moritz S, Kull T. [11C]Choline-PET/CT for outcome prediction of salvage radiotherapy of local relapsing prostate carcinoma. Q J Nucl Med Mol Imaging **2012**;56(5):430-9.

162. Beheshti M, Vali R, Waldenberger P, Fitz F, Nader M, Loidl W, Broinger G, Stoiber F, Foglman I, Langsteger W. Detection of bone metastases in patients with prostate cancer by 18F fluorocholine and 18F fluoride PET-CT: a comparative study. Eur J Nucl Med Mol Imaging **2008**;35(10):1766-74.

163. Kitajima K, Murphy RC, Nathan MA, Froemming AT, Hagen CE, Takahashi N, Kawashima A. Detection of recurrent prostate cancer after radical prostatectomy: comparison of 11C-choline PET/CT with pelvic multiparametric MR imaging with endorectal coil. J Nucl Med **2014**;55(2):223-32.

164. Giovacchini G, Picchio M, Garcia-Parra R, Briganti A, Abdollah F, Gianolli L, Schindler C, Montorsi F, Messa C, Fazio F. 11C-choline PET/CT predicts prostate cancer-specific survival in patients with biochemical failure during androgen-deprivation therapy. J Nucl Med **2014**;55(2):233-41.

165. Rommel D, Bol A, Abarca-Quinones J, Peeters F, Robert A, Labar D, Galant C, Gregoire V, Duprez T. Rodent rhabdomyosarcoma: comparison between total choline concentration at H-MRS and [18F]-fluoromethylcholine uptake at PET using accurate methods for collecting data. Mol Imaging Biol **2010**;12(4):415-23.

166. Challapalli A, Aboagye EO. Positron Emission Tomography Imaging of Tumor Cell Metabolism and Application to Therapy Response Monitoring. Front Oncol **2016**;6:44.
167. Eckelman WC, Babich JW. Synthesis and validation of fatty acid analogs radiolabeled by nonisotopic substitution. J Nucl Cardiol **2007**;14(3 Suppl):S100-9.
168. Pandey MK, Belanger AP, Wang S, DeGrado TR. Structure dependence of long-chain [18F]fluorothia fatty acids as myocardial fatty acid oxidation probes. J Med Chem **2012**;55(23):10674-84.
169. Kataoka K, Nohara R, Hosokawa R, Hirai T, Okuda K, Li-Guang C, Fujibayashi Y, Fujita M, Konishi J, Sasayama S. Myocardial lipid metabolism in compensated and advanced stages of heart failure: evaluation by canine pacing model with BMIPP. J Nucl Med **2001**;42(1):124-9.
170. Tamaki N, Morita K, Kuge Y, Tsukamoto E. The role of fatty acids in cardiac imaging. J Nucl Med **2000**;41(9):1525-34.
171. DeGrado TR, Wang S, Holden JE, Nickles RJ, Taylor M, Stone CK. Synthesis and preliminary evaluation of (18)F-labeled 4-thia palmitate as a PET tracer of myocardial fatty acid oxidation. Nucl Med Biol **2000**;27(3):221-31.
172. DeGrado TR, Kitapci MT, Wang S, Ying J, Lopaschuk GD. Validation of 18F-fluoro-4-thia-palmitate as a PET probe for myocardial fatty acid oxidation: effects of hypoxia and composition of exogenous fatty acids. J Nucl Med **2006**;47(1):173-81.
173. Taylor M, Wallhaus TR, Degrado TR, Russell DC, Stanko P, Nickles RJ, Stone CK. An evaluation of myocardial fatty acid and glucose uptake using PET with [18F]fluoro-6-thia-heptadecanoic acid and [18F]FDG in Patients with Congestive Heart Failure. J Nucl Med **2001**;42(1):55-62.
174. DeGrado TR, Bhattacharyya F, Pandey MK, Belanger AP, Wang S. Synthesis and preliminary evaluation of 18-(18)F-fluoro-4-thia-oleate as a PET probe of fatty acid oxidation. J Nucl Med **2010**;51(8):1310-7.
175. Tu Z, Li S, Sharp TL, Herrero P, Dence CS, Gropler RJ, Mach RH. Synthesis and evaluation of 15-(4-(2-[(1)(8)F]Fluoroethoxy)phenyl)pentadecanoic acid: a potential PET tracer for studying myocardial fatty acid metabolism. Bioconjug Chem **2010**;21(12):2313-9.
176. Maki MT, Haaparanta M, Nuutila P, Oikonen V, Luotolahti M, Eskola O, Knuuti JM. Free fatty acid uptake in the myocardium and skeletal muscle using fluorine-18-fluoro-6-thia-heptadecanoic acid. J Nucl Med **1998**;39(8):1320-7.
177. Zaidi N, Lupien L, Kuemmerle NB, Kinlaw WB, Swinnen JV, Smans K. Lipogenesis and lipolysis: the pathways exploited by the cancer cells to acquire fatty acids. Prog Lipid Res **2013**;52(4):585-9.
178. Camarda R, Zhou AY, Kohnz RA, Balakrishnan S, Mahieu C, Anderton B, Eyob H, Kajimura S, Tward A, Krings G, Nomura DK, Goga A. Inhibition of fatty acid oxidation as a therapy for MYC-overexpressing triple-negative breast cancer. Nat Med **2016**;22(4):427-32.
179. Han Q, Cao Y, Gathaiya NW, Kemp BJ, Jensen MD. Free fatty acid flux measured using [1-(11)C]palmitate positron emission tomography and [U-(13)C]palmitate in humans. Am J Physiol Endocrinol Metab **2017**:ajpendo002842017.

180. Christensen NL, Jakobsen S, Schacht AC, Munk OL, Alstrup AKO, Tolbod LP, Harms HJ, Nielsen S, Gormsen LC. Whole-Body Biodistribution, Dosimetry, and Metabolite Correction of [(11)C]Palmitate: A PET Tracer for Imaging of Fatty Acid Metabolism. Mol Imaging **2017**;16:1536012117734485.

181. Vavere AL, Kridel SJ, Wheeler FB, Lewis JS. 1-11C-acetate as a PET radiopharmaceutical for imaging fatty acid synthase expression in prostate cancer. J Nucl Med **2008**;49(2):327-34.

182. Oyama N, Akino H, Kanamaru H, Suzuki Y, Muramoto S, Yonekura Y, Sadato N, Yamamoto K, Okada K. 11C-acetate PET imaging of prostate cancer. J Nucl Med **2002**;43(2):181-6.

183. Mena E, Turkbey B, Mani H, Adler S, Valera VA, Bernardo M, Shah V, Pohida T, McKinney Y, Kwarteng G, Daar D, Lindenberg ML, Eclarinal P, Wade R, Linehan WM, Merino MJ, Pinto PA, Choyke PL, Kurdziel KA. 11C-Acetate PET/CT in localized prostate cancer: a study with MRI and histopathologic correlation. J Nucl Med **2012**;53(4):538-45.

184. Wachter S, Tomek S, Kurtaran A, Wachter-Gerstner N, Djavan B, Becherer A, Mitterhauser M, Dobrozemsky G, Li S, Potter R, Dudczak R, Kletter K. 11C-acetate positron emission tomography imaging and image fusion with computed tomography and magnetic resonance imaging in patients with recurrent prostate cancer. J Clin Oncol **2006**;24(16):2513-9.

185. Haseebuddin M, Dehdashti F, Siegel BA, Liu J, Roth EB, Nepple KG, Siegel CL, Fischer KC, Kibel AS, Andriole GL, Miller TR. 11C-acetate PET/CT before radical prostatectomy: nodal staging and treatment failure prediction. J Nucl Med **2013**;54(5):699-706.

186. Snyder F, Wood R. Alkyl and alk-1-enyl ethers of glycerol in lipids from normal and neoplastic human tissues. Cancer Res **1969**;29(1):251-7.

187. Meyer KL, Schwendner SW, Counsell RE. Potential tumor or organ-imaging agents. 30. Radioiodinated phospholipid ethers. J Med Chem **1989**;32(9):2142-7.

188. Rampy MA, Pinchuk AN, Weichert JP, Skinner RW, Fisher SJ, Wahl RL, Gross MD, Counsell RE. Synthesis and biological evaluation of radioiodinated phospholipid ether stereoisomers. J Med Chem **1995**;38(16):3156-62.

189. Weichert JP, Clark PA, Kandela IK, Vaccaro AM, Clarke W, Longino MA, Pinchuk AN, Farhoud M, Swanson KI, Floberg JM, Grudzinski J, Titz B, Traynor AM, Chen HE, Hall LT, Pazoles CJ, Pickhardt PJ, Kuo JS. Alkylphosphocholine analogs for broad-spectrum cancer imaging and therapy. Sci Transl Med **2014**;6(240):240ra75.

190. Gode D, Volmer DA. Lipid imaging by mass spectrometry - a review. Analyst **2013**;138(5):1289-315.

191. Yalcin EB, de la Monte SM. Review of matrix-assisted laser desorption ionization-imaging mass spectrometry for lipid biochemical histopathology. J Histochem Cytochem **2015**;63(10):762-71.

192. Chughtai K, Jiang L, Greenwood TR, Glunde K, Heeren RM. Mass spectrometry images acylcarnitines, phosphatidylcholines, and sphingomyelin in MDA-MB-231 breast tumor models. J Lipid Res **2013**;54(2):333-44.

193. Fernandez R, Garate J, Lage S, Teres S, Higuera M, Bestard-Escalas J, Lopez DH, Guardiola-Serrano F, Escriba PV, Barcelo-Coblijn G, Fernandez JA. Identification of Biomarkers of Necrosis in Xenografts Using Imaging Mass Spectrometry. J Am Soc Mass Spectrom **2016**;27(2):244-54.

194. Northen TR, Yanes O, Northen MT, Marrinucci D, Uritboonthai W, Apon J, Golledge SL, Nordstrom A, Siuzdak G. Clathrate nanostructures for mass spectrometry. Nature **2007**;449(7165):1033-6.

195. Vidova V, Novak P, Strohalm M, Pol J, Havlicek V, Volny M. Laser desorption-ionization of lipid transfers: tissue mass spectrometry imaging without MALDI matrix. Anal Chem **2010**;82(12):4994-7.

196. Sturm RM, Greer T, Chen R, Hensen B, Li L. Comparison of NIMS and MALDI platforms for neuropeptide and lipid mass spectrometric imaging in C. borealis brain tissue. Anal Methods **2013**;5(6):1623-8.

197. Mao X, He J, Li T, Lu Z, Sun J, Meng Y, Abliz Z, Chen J. Application of imaging mass spectrometry for the molecular diagnosis of human breast tumors. Sci Rep **2016**;6:21043.

198. Ide Y, Waki M, Hayasaka T, Nishio T, Morita Y, Tanaka H, Sasaki T, Koizumi K, Matsunuma R, Hosokawa Y, Ogura H, Shiiya N, Setou M. Human breast cancer tissues contain abundant phosphatidylcholine(36ratio1) with high stearoyl-CoA desaturase-1 expression. PLoS One **2013**;8(4):e61204.

199. Guenther S, Muirhead LJ, Speller AV, Golf O, Strittmatter N, Ramakrishnan R, Goldin RD, Jones E, Veselkov K, Nicholson J, Darzi A, Takats Z. Spatially resolved metabolic phenotyping of breast cancer by desorption electrospray ionization mass spectrometry. Cancer Res **2015**;75(9):1828-37.

200. Uehara T, Kikuchi H, Miyazaki S, Iino I, Setoguchi T, Hiramatsu Y, Ohta M, Kamiya K, Morita Y, Tanaka H, Baba S, Hayasaka T, Setou M, Konno H. Overexpression of Lysophosphatidylcholine Acyltransferase 1 and Concomitant Lipid Alterations in Gastric Cancer. Ann Surg Oncol **2016**;23 Suppl 2:206-13.

201. Jones EE, Powers TW, Neely BA, Cazares LH, Troyer DA, Parker AS, Drake RR. MALDI imaging mass spectrometry profiling of proteins and lipids in clear cell renal cell carcinoma. Proteomics **2014**;14(7-8):924-35.

202. Wei Y, Chen L, Zhou W, Chingin K, Ouyang Y, Zhu T, Wen H, Ding J, Xu J, Chen H. Tissue spray ionization mass spectrometry for rapid recognition of human lung squamous cell carcinoma. Sci Rep **2015**;5:10077.

203. Mirnezami R, Spagou K, Vorkas PA, Lewis MR, Kinross J, Want E, Shion H, Goldin RD, Darzi A, Takats Z, Holmes E, Cloarec O, Nicholson JK. Chemical mapping of the colorectal cancer microenvironment via MALDI imaging mass spectrometry (MALDI-MSI) reveals novel cancer-associated field effects. Mol Oncol **2014**;8(1):39-49.

204. Kurabe N, Hayasaka T, Ogawa M, Masaki N, Ide Y, Waki M, Nakamura T, Kurachi K, Kahyo T, Shinmura K, Midorikawa Y, Sugiyama Y, Setou M, Sugimura H. Accumulated phosphatidylcholine (16:0/16:1) in human colorectal cancer; possible involvement of LPCAT4. Cancer Sci **2013**;104(10):1295-302.

205. Kawashima M, Iwamoto N, Kawaguchi-Sakita N, Sugimoto M, Ueno T, Mikami Y, Terasawa K, Sato TA, Tanaka K, Shimizu K, Toi M. High-resolution imaging mass

spectrometry reveals detailed spatial distribution of phosphatidylinositols in human breast cancer. Cancer Sci **2013**;104(10):1372-9.

206. Goto T, Terada N, Inoue T, Nakayama K, Okada Y, Yoshikawa T, Miyazaki Y, Uegaki M, Sumiyoshi S, Kobayashi T, Kamba T, Yoshimura K, Ogawa O. The expression profile of phosphatidylinositol in high spatial resolution imaging mass spectrometry as a potential biomarker for prostate cancer. PLoS One **2014**;9(2):e90242.
207. Goto T, Terada N, Inoue T, Kobayashi T, Nakayama K, Okada Y, Yoshikawa T, Miyazaki Y, Uegaki M, Utsunomiya N, Makino Y, Sumiyoshi S, Yamasaki T, Kamba T, Ogawa O. Decreased expression of lysophosphatidylcholine (16:0/OH) in high resolution imaging mass spectrometry independently predicts biochemical recurrence after surgical treatment for prostate cancer. Prostate **2015**;75(16):1821-30.
208. Amstalden van Hove ER, Blackwell TR, Klinkert I, Eijkel GB, Heeren RM, Glunde K. Multimodal mass spectrometric imaging of small molecules reveals distinct spatio-molecular signatures in differentially metastatic breast tumor models. Cancer Res **2010**;70(22):9012-21.
209. Jiang L, Chughtai K, Purvine SO, Bhujwalla ZM, Raman V, Pasa-Tolic L, Heeren RM, Glunde K. MALDI-Mass Spectrometric Imaging Revealing Hypoxia-Driven Lipids and Proteins in a Breast Tumor Model. Anal Chem **2015**;87(12):5947-56.
210. Marien E, Meister M, Muley T, Gomez Del Pulgar T, Derua R, Spraggins JM, Van de Plas R, Vanderhoydonc F, Machiels J, Binda MM, Dehairs J, Willette Brown J, Hu Y, Dienemann H, Thomas M, Schnabel PA, Caprioli RM, Lacal JC, Waelkens E, Swinnen JV. Phospholipid profiling identifies acyl chain elongation as a ubiquitous trait and potential target for the treatment of lung squamous cell carcinoma. Oncotarget **2016**;7(11):12582-97.
211. Jelonek K, Pietrowska M, Ros M, Zagdanski A, Suchwalko A, Polanska J, Marczyk M, Rutkowski T, Skladowski K, Clench MR, Widlak P. Radiation-induced changes in serum lipidome of head and neck cancer patients. Int J Mol Sci **2014**;15(4):6609-24.
212. Woo HK, Northen TR, Yanes O, Siuzdak G. Nanostructure-initiator mass spectrometry: a protocol for preparing and applying NIMS surfaces for high-sensitivity mass analysis. Nat Protoc **2008**;3(8):1341-9.
213. O'Brien PJ, Lee M, Spilker ME, Zhang CC, Yan Z, Nichols TC, Li W, Johnson CH, Patti GJ, Siuzdak G. Monitoring metabolic responses to chemotherapy in single cells and tumors using nanostructure-initiator mass spectrometry (NIMS) imaging. Cancer Metab **2013**;1(1):4.
214. Park HM, Russo KA, Karateev G, Park M, Dubikovskaya E, Kriegsfeld LJ, Stahl A. A System for In Vivo Imaging of Hepatic Free Fatty Acid Uptake. Gastroenterology **2016**;152(1):78-81.
215. Thorek D, Robertson R, Bacchus WA, Hahn J, Rothberg J, Beattie BJ, Grimm J. Cerenkov imaging - a new modality for molecular imaging. Am J Nucl Med Mol Imaging **2012**;2(2):163-73.
216. Thorek DL, Ogirala A, Beattie BJ, Grimm J. Quantitative imaging of disease signatures through radioactive decay signal conversion. Nat Med **2013**;19(10):1345-50.

217. Czupryna J, Kachur AV, Blankemeyer E, Popov AV, Arroyo AD, Karp JS, Delikatny EJ. Cerenkov-specific contrast agents for detection of pH in vivo. J Nucl Med **2015**;56(3):483-8.

218. Yodh, A., Chance B. Spectroscopy and Imaging with Diffusing Light Physics Today **1995**;48(3):34.

219. Jia Y, Bailey ST, Hwang TS, McClintic SM, Gao SS, Pennesi ME, Flaxel CJ, Lauer AK, Wilson DJ, Hornegger J, Fujimoto JG, Huang D. Quantitative optical coherence tomography angiography of vascular abnormalities in the living human eye. Proc Natl Acad Sci U S A **2015**;112(18):E2395-402.

220. Shemonski ND, South FA, Liu YZ, Adie SG, Carney PS, Boppart SA. Computational high-resolution optical imaging of the living human retina. Nat Photonics **2015**;9:440-3.

221. Spaide RF, Klancnik JM, Jr., Cooney MJ. Retinal vascular layers imaged by fluorescein angiography and optical coherence tomography angiography. JAMA Ophthalmol **2015**;133(1):45-50.

222. Ughi GJ, Gora MJ, Swager AF, Soomro A, Grant C, Tiernan A, Rosenberg M, Sauk JS, Nishioka NS, Tearney GJ. Automated segmentation and characterization of esophageal wall in vivo by tethered capsule optical coherence tomography endomicroscopy. Biomed Opt Express **2016**;7(2):409-19.

223. Bouma BE, Tearney GJ, Compton CC, Nishioka NS. High-resolution imaging of the human esophagus and stomach in vivo using optical coherence tomography. Gastrointest Endosc **2000**;51(4 Pt 1):467-74.

224. Jang IK, Bouma BE, Kang DH, Park SJ, Park SW, Seung KB, Choi KB, Shishkov M, Schlendorf K, Pomerantsev E, Houser SL, Aretz HT, Tearney GJ. Visualization of coronary atherosclerotic plaques in patients using optical coherence tomography: comparison with intravascular ultrasound. J Am Coll Cardiol **2002**;39(4):604-9.

225. Prabhu D, Mehanna E, Gargesha M, Wen D, Brandt E, van Ditzhuijzen NS, Chamie D, Yamamoto H, Fujino Y, Farmazilian A, Patel J, Costa M, Bezerra HG, Wilson DL. 3D registration of intravascular optical coherence tomography and cryo-image volumes for microscopic-resolution validation. Proc SPIE Int Soc Opt Eng **2016**;9788.

226. Jiang JX, Keating JJ, Jesus EM, Judy RP, Madajewski B, Venegas O, Okusanya OT, Singhal S. Optimization of the enhanced permeability and retention effect for near-infrared imaging of solid tumors with indocyanine green. Am J Nucl Med Mol Imaging **2015**;5(4):390-400.

227. Vinegoni C, Botnaru I, Aikawa E, Calfon MA, Iwamoto Y, Folco EJ, Ntziachristos V, Weissleder R, Libby P, Jaffer FA. Indocyanine green enables near-infrared fluorescence imaging of lipid-rich, inflamed atherosclerotic plaques. Sci Transl Med **2011**;3(84):84ra45.

228. Weissleder R, Nahrendorf M, Pittet MJ. Imaging macrophages with nanoparticles. Nat Mater **2014**;13(2):125-38.

229. Leimgruber A, Berger C, Cortez-Retamozo V, Etzrodt M, Newton AP, Waterman P, Figueiredo JL, Kohler RH, Elpek N, Mempel TR, Swirski FK, Nahrendorf M, Weissleder R, Pittet MJ. Behavior of endogenous tumor-associated macrophages assessed in vivo using a functionalized nanoparticle. Neoplasia **2009**;11(5):459-68, 2 p following 68.

230. Shao H, Yoon TJ, Liong M, Weissleder R, Lee H. Magnetic nanoparticles for biomedical NMR-based diagnostics. Beilstein J Nanotechnol **2010**;1:142-54.

231. Villa AM, Caporizzo E, Papagni A, Miozzo L, Del Buttero P, Grilli MD, Amboldi N, Fazio F, Doglia SM, Giglioni B. Choline and phosphatidylcholine fluorescent derivatives localization in carcinoma cells studied by laser scanning confocal fluorescence microscopy. Eur J Cancer **2005**;41(10):1453-9.

232. Thumser AE, Storch J. Characterization of a BODIPY-labeled fluorescent fatty acid analogue. Binding to fatty acid-binding proteins, intracellular localization, and metabolism. Mol Cell Biochem **2007**;299(1-2):67-73.

233. Korb ML, Warram JM, Grudzinski J, Weichert J, Jeffery J, Rosenthal EL. Breast cancer imaging using the near-infrared fluorescent agent, CLR1502. Mol Imaging **2014**;13.

234. Arlauckas SP, Popov AV, Delikatny EJ. Direct Inhibition of Choline Kinase by a Near-Infrared Fluorescent Carbocyanine. Molecular Cancer Therapeutics **2014**;13(9):2149-58.

235. Vinegoni C, Dubach JM, Thurber GM, Miller MA, Mazitschek R, Weissleder R. Advances in measuring single-cell pharmacology in vivo. Drug Discov Today **2015**;20(9):1087-92.

236. Arlauckas SP, Kumar M, Popov AV, Poptani H, Delikatny EJ. Near infrared fluorescent imaging of choline kinase alpha expression and inhibition in breast tumors. Oncotarget **2017**;8(10):16518-30.

237. Yoon Y, Lee PJ, Kurilova S, Cho W. In situ quantitative imaging of cellular lipids using molecular sensors. Nat Chem **2011**;3(11):868-74.

238. Di Paolo G, De Camilli P. Phosphoinositides in cell regulation and membrane dynamics. Nature **2006**;443(7112):651-7.

239. Verderame MF. pp60v-src transformation of rat cells but not chicken cells strongly correlates with low-affinity phosphopeptide binding by the SH2 domain. Mol Biol Cell **1997**;8(5):843-54.

240. Caers J, Peymen K, Suetens N, Temmerman L, Janssen T, Schoofs L, Beets I. Characterization of G protein-coupled receptors by a fluorescence-based calcium mobilization assay. J Vis Exp **2014**(89):e51516.

241. Bazzi MD, Nelsestuen GL. Association of protein kinase C with phospholipid vesicles. Biochemistry **1987**;26(1):115-22.

242. Peddie CJ, Blight K, Wilson E, Melia C, Marrison J, Carzaniga R, Domart MC, O'Toole P, Larijani B, Collinson LM. Correlative and integrated light and electron microscopy of in-resin GFP fluorescence, used to localise diacylglycerol in mammalian cells. Ultramicroscopy **2014**;143:3-14.

243. Sato M, Ueda Y, Umezawa Y. Imaging diacylglycerol dynamics at organelle membranes. Nat Methods **2006**;3(10):797-9.

244. Farber SA, Pack M, Ho SY, Johnson ID, Wagner DS, Dosch R, Mullins MC, Hendrickson HS, Hendrickson EK, Halpern ME. Genetic analysis of digestive physiology using fluorescent phospholipid reporters. Science **2001**;292(5520):1385-8.

245. Hama K, Provost E, Baranowski TC, Rubinstein AL, Anderson JL, Leach SD, Farber SA. In vivo imaging of zebrafish digestive organ function using multiple quenched fluorescent reporters. Am J Physiol Gastrointest Liver Physiol **2009**;296(2):G445-53.

246. Hendrickson HS, Hendrickson EK, Johnson ID, Farber SA. Intramolecularly quenched BODIPY-labeled phospholipid analogs in phospholipase A(2) and platelet-activating factor acetylhydrolase assays and in vivo fluorescence imaging. Anal Biochem **1999**;276(1):27-35.

247. Fraher D, Sanigorski A, Mellett NA, Meikle PJ, Sinclair AJ, Gibert Y. Zebrafish Embryonic Lipidomic Analysis Reveals that the Yolk Cell Is Metabolically Active in Processing Lipid. Cell Rep **2016**;14(6):1317-29.

248. Popov AV, Mawn TM, Kim S, Zheng G, Delikatny EJ. Design and synthesis of phospholipase C and A2-activatable near-infrared fluorescent smart probes. Bioconjug Chem **2010**;21(10):1724-7.

249. Nakanishi M, Rosenberg DW. Multifaceted roles of PGE2 in inflammation and cancer. Semin Immunopathol **2013**;35(2):123-37.

250. Huang Z, Laliberte F, Tremblay NM, Weech PK, Street IP. A continuous fluorescence-based assay for the human high-molecular-weight cytosolic phospholipase A2. Anal Biochem **1994**;222(1):110-5.

251. Zeng W, Wang X, Xu P, Liu G, Eden HS, Chen X. Molecular imaging of apoptosis: from micro to macro. Theranostics **2015**;5(6):559-82.

252. Zhao M, Beauregard DA, Loizou L, Davletov B, Brindle KM. Non-invasive detection of apoptosis using magnetic resonance imaging and a targeted contrast agent. Nat Med **2001**;7(11):1241-4.

253. Rice DR, Clear KJ, Smith BD. Imaging and therapeutic applications of zinc(ii)-dipicolylamine molecular probes for anionic biomembranes. Chem Commun (Camb) **2016**;52(57):8787-801.

254. Koulov AV, Stucker KA, Lakshmi C, Robinson JP, Smith BD. Detection of apoptotic cells using a synthetic fluorescent sensor for membrane surfaces that contain phosphatidylserine. Cell Death Differ **2003**;10(12):1357-9.

255. Neves AA, Krishnan AS, Kettunen MI, Hu DE, Backer MM, Davletov B, Brindle KM. A paramagnetic nanoprobe to detect tumor cell death using magnetic resonance imaging. Nano Lett **2007**;7(5):1419-23.

256. Jung HI, Kettunen MI, Davletov B, Brindle KM. Detection of apoptosis using the C2A domain of synaptotagmin I. Bioconjug Chem **2004**;15(5):983-7.

257. Surman AJ, Bonnet CS, Lowe MP, Kenny GD, Bell JD, Toth E, Vilar R. A Pyrophosphate-Responsive Gadolinium(III) MRI Contrast Agent. Chem - Eur J **2011**;17(1):223-30, S/1-S/16.

258. Fang W, Wang F, Ji S, Zhu X, Meier HT, Hellman RS, Brindle KM, Davletov B, Zhao M. SPECT imaging of myocardial infarction using 99mTc-labeled C2A domain of synaptotagmin I in a porcine ischemia-reperfusion model. Nucl Med Biol **2007**;34(8):917-23.

259. Niu G, Chen X. Apoptosis imaging: beyond annexin V. J Nucl Med **2010**;51(11):1659-62.

260. Alam IS, Neves AA, Witney TH, Boren J, Brindle KM. Comparison of the C2A domain of synaptotagmin-I and annexin-V as probes for detecting cell death. Bioconjug Chem **2010**;21(5):884-91.

Figure Legends

Figure 1: Lipid metabolism pathways in the cell. Glucose transported into the cell is metabolized to pyruvate via the glycolytic pathway, and can be fed into the tricarboxylic acid (TCA) cycle for ATP production in the mitochondria. Citrate from the TCA cycle or from exogenous sources is converted to Acetyl-CoA in the cytoplasm and can be used for cholesterol or fatty acid (e.g. palmitate) biosynthesis. Cholesterol produced in this fashion can be used to synthesize membranes or be incorporated into sterols. Fatty acids can be desaturated or extended and then incorporated into triglycerides or incorporated into phospholipids via the Kennedy Pathway. Cholesterol and triglycerides fatty acids can also be taken up through specific transport mechanisms. The resulting lipid droplets, shown in the inset, contain fatty acids stored in phospholipid and fatty acid form that can be mobilized by phospholipases and lipases, respectively. Beta-oxidation (β-Ox) of free fatty acids from lipid droplets can be triggered to meet energy needs. In place of the third acyl group ($Acyl_3$) attached to the glycerol moiety of triacylglycerides (orange oval), phospholipids have a phosphorylated polar head group (yellow sphere) that confers water solubility and creates organized bi-layer and micelle structures. Phospholipases can also elicit 2^{nd} messenger signaling cascades by releasing bioactive fatty acids (e.g. sphingolipids, eicosanoids) and/or polar head groups in response to growth or stress cues. External cell signaling cues can also be transmitted by lipids in the case of isoprenylation and subsequent transport of small GTPases to dock with G protein-coupled receptors (GPCRs) on the cell surface.

Figure 2: Major lipid metabolic pathways altered in cancer cells. Metabolic reprogramming during malignant transformation mimics autonomous growth signaling in unicellular organisms. Common oncogenes in the PI3K/Akt/MTOR pathway, are often mutated

or upregulated due to their presence downstream of external growth factors and their ability to re-route cellular carbon sources toward fatty acid utilization as an energy source. Cancer cells can also supply the TCA cycle from glucose via aberrant glycolysis and from glutamine via IDH mutations, although the contributions of these pathways differ greatly depending on the energy needs of the cell. The transcription factor Myc promotes many malignant processes in cancer cells because it is a master regulator capable of triggering survival pathways in response to hypoxia and nutrient deprivation. Hypoxic conditions are a factor in many solid tumors and influence the local tumor microenvironment by dampening the immune response and activating hypoxia-inducible factor-1α (HIF1α), which among other things, initiates the regulatory function of sterol regulatory element binding protein 1 (SREBP-1) on fatty acid synthesis. Free fatty acids such as palmitate are used as energy sources or converted to bioactive eicosanoids to dampen the immune response and stabilize the ER stress that can result from saturated fatty acid accumulation.

Figure 3: Changes in lipid metabolism in response to oncolytic viral treatment of Syrian hamster carcinomas. The oncolytic viral treatment induces coagulative necrosis, which is seen as hypo-intense areas within the tumor on T_2-weighted MR image. *In vivo* MRS from the voxel (overlaid on the image) is shown on the right demonstrating resonances from unsaturated fatty acids, taurine and choline. ~~Unlike the increased PUFA resonances observed during apoptosis (Figure 3), no~~ No changes in PUFA resonances were observed in coagulative necrosis resulting from oncolytic viral treatment. Reprinted with permission from (138).

Figure 4. A) Confocal micrographs of SKOV3.ip cells treated for 48 h with cisplatin (CDDP) show increased lipid droplets as measured by Nile red staining, compared to untreated controls (CTRL). Fixed cells were counterstained with phalloidin 488 for actin (green) and DAPI for nuclei (blue). Scale bar represents 23.8 µm. (B) ^{1}H NMR spectra of intact SKOV3.ip cells treated with 5 mM CDDP for 48 h (red) show increases in mobile lipids compared with untreated control cells (black). Labeled lipid resonances include: methine protons at 5.3 ppm (-CH=CH-); fatty chain methylene group at 1.3 ppm (-$(CH2)_n$)- ; methyl group at 0.9 ppm (-CH_3) ; and total choline (tCho) at 3.2 ppm (-N.$(CH_3)_3$). Reprinted with permission from (150).

Figure 5: Increased lipids in response to choline kinase inhibition as an alternate therapy for the treatment of gliomas. *In vivo* MRS from an untreated F98 rat glioma (bottom spectrum) and after 5 days of treatment with a choline kinase inhibitor, MN58b (top spectrum). Increased mono-unsaturated lipid peaks (1.3 ppm) are evident with treatment. In addition, a significant increase in the poly-unsaturated fatty acids (PUFA, 2.8 ppm), indicating apoptotic cell death. As expected, a decrease in the total choline (tCho) peak was also observed in response to choline kinase inhibition. The MR image demonstrates placement of the voxel for MRS studies. Reprinted with permission from (114).

Figure 6: Single voxel ^{1}H MR spectra from a GL261 tumor implanted into a mouse brain. Treatment with three cycles of temozolomide led to significant (*) increases in mobile lipid:Cre and tCho:Cre resonances at 28 days post inoculation (left) compared to spectra acquired before treatment (tight). Labeled resonances: Cho (choline: 3.2 ppm, Cre (creatine): 3.3

ppm, MLs (mobile lipid methylenes): 1.3 ppm, PUFAs: 2.8 ppm. Reprinted with permission from (128).

Figure 7: Chemical structure of the common PET tracers used for detection of lipid metabolism. The radioactive isotope is denoted in red.

Figure 8: MALDI-MSI images and corresponding H&E sections from human colorectal tumors (A-C) and adjacent tumor free regions (D-F). A selective projection of *m/z* 478.3 onto MALDI-MSI images reveals elevations in 1-palmitoyl-lysophosphatidylcholine in cancer-containing areas compared to the non-tumor bearing tissue sections. Elevations in *m/z* 504.3, representing 1-oleoyl-lysophosphatidylcholine, were also observed in this study. Reprinted with permission from (203).

Figure 9: *In vivo* NIR fluorescence imaging of phospholipase activity using the PC-PLC activatable probe Pyro-PL-BHQ in DU145 prostate tumor xenografts. Each mouse received 80 nmol *i.v.* of (A) Pyro-PtdEtn, a permanently fluorescent analog used as a control, (B) Pyro-PtdEtn-BHQ or (C) Pyro-PtdEtn-BHQ plus pre- and post- injections of the PC-PLC inhibitor D609. The fluorescence intensity from Pyro-PL-BHQ activation peaked at 6-7 h, and was inhibited by D609 treatment. Fluorescence persisted for up to 31 h in tumor tissue (T) excised from mice when compared to muscle (M) control. Reprinted with permission from (112).

Imaging of Cancer Lipid Metabolism in Response to Therapy

Sean Arlauckas, Ph.D.[1,2], Elizabeth A. Browning, Ph.D.[1],

Harish Poptani, Ph.D.[3], E. James Delikatny, Ph.D.*[1]

[1] Department of Radiology, Perelman School of Medicine, University of Pennsylvania, Philadelphia, PA, [2]Center for Systems Biology, Mass General Hospital, Boston MA, [3]Department of Cellular and Molecular Physiology, Institute of Regenerative Medicine, University of Liverpool, Liverpool, UK

*Address Correspondence to:

E. James Delikatny, Ph.D.

Research Professor

Department of Radiology

317 Anatomy-Chemistry Building, 3620 Hamilton Walk

Philadelphia, PA 19104, USA

Ph: 215-898-3105

Email: delikatn@pennmedicine.upenn.edu

Key words: Tumor imaging, therapy response, lipids, MR imaging, MR spectroscopy, Optical imaging

Abstract

Lipids represent a diverse array of molecules essential to the cell's structure, defense, energy, and communication. Lipid metabolism can often become dysregulated during tumor development. During cancer therapy, targeted inhibition of cell proliferation can likewise cause widespread and drastic changes in lipid composition. Molecular imaging techniques have been developed to monitor altered lipid profiles as a biomarker for cancer diagnosis and treatment response. For decades, magnetic resonance spectroscopy has been the dominant noninvasive technique for studying lipid metabolite levels. Recent insights into the oncogenic transformations driving changes in lipid metabolism have revealed new mechanisms and signaling molecules that can be exploited using optical imaging, mass spectrometry imaging, and positron emission tomography. These novel imaging modalities have provided researchers a diverse toolbox to examine changes in lipids in response to a wide array of anticancer strategies including chemotherapy, radiation therapy, signal transduction inhibitors, gene therapy, immunotherapy or a combination of these strategies. The understanding of lipid metabolism in response to cancer therapy continues to evolve as each therapeutic method emerges, and this review seeks to summarize the current field and areas of unmet needs.

Abbreviations

18F-fluorodeoxyglucose (FDG)

2,5-dihydroxybenzoic acid (DHB)

3-hydroxy-3-methyl-glutaryl-CoA (HMG-CoA)

acetyl-coenzyme A (acetyl-CoA)

acute myeloid leukemia (AML)

AMP-activated protein kinase (AMPK)

ATP-citrate lyase (ACLY)

beta-oxidation (β-Ox)

black Hole Quencher (BHQ-3)

choline kinase (ChoK)

choline transporters (ChoTs)

cisplatin (CDDP)

7-hydroxy-9H-(1,3-dichloro-9,9-dimethylacridin-2-one (DDAO)

diacylglycerol (DAG)

(4′,6-diamidino-2-phenylindole) (DAPI_

elongation-of-very-long-chain-fatty acids (ELOVL)

endoplasmic reticulum (ER)

epidermal growth factor receptor (EGFR)

fatty acid binding protein-4 (FABP-4)

G-protein coupled receptor (GPCR)

glycerophosphocholine (GPC)

hormone-sensitive lipase (HSL)

hypoxia inducible factor (HIF)

Indocyanine green (ICG)

isocitrate dehydrogenase-1 (IDH1)

lipoprotein lipase (LPL)

low density lipoprotein (LDL)

lysophosphatidylcholine (LPC)

magnetic resonance spectroscopy (MRS)

mass spectrometry imaging (MSI)

matrix-assisted laser desorption ionization (MALDI)

mono-unsaturated fatty acids (MUFAs)

nanostructure-initiator mass spectrometry (NIMS)

OKN007 (2,4-disulfophenyl-PBN)

optical coherence tomography (OCT)

PBN (α-phenyl-tert-butylnitrone)

peroxisome proliferator-activated receptor alpha (PPARα)

phosphatidylcholine (PtdCho)

phosphatidylethanolamine (PtdEtn)

phosphatidylinositol (4,5) phosphate-2 (PIP2)

phosphatidylinositol (PtdIns)

phosphatidylserine (PtdSer)

phosphocholine (PC)

phosphoethanolamine (PE)

Phosphoinositides (PI)

phospholipase (PL)

phosphomonoester (PME)

plasma membrane citrate transporter (PMCT)

polyunsaturated fatty acid (PUFA)

positron emission tomography (PET)

protein kinase C (PKC)

PtdCho-specific PLC (PC-PLC)

pyropheophorbide-a (Pyro)

reactive oxygen species (ROS)

secondary ion mass spectrometry (SIMS)

sphingosine-1-phosphate (S1P)

stearoyl-CoA desaturase-1 (SCD1)

sterol response element-binding proteins (SREBPs)

total choline (tCho)

tricarboxylic acid (TCA)

unfolded protein response (UPR)

α-cyano-4-hydroxycinnamic acid (CHCA)

Introduction

Cancer cells exist in a hyperactive state of growth and use a complex network of lipid metabolic pathways to support this growing biomass. Lipids are a broad class of compounds that include fatty acids, triglycerides, steroids, phospholipids, and sphingolipids, among others. These molecules play critical roles in cellular compartmentalization, structural barriers, communication signals, energy storage, and homeostasis. Despite high vascularization, many cancer cells exist in regions of nutrient deprivation and tumors have adopted alternative strategies to maintain sources of lipid. In some cases the altered lipid metabolic state offers a therapeutic vulnerability, while in others, adaptations to intracellular lipid composition can be used by refractory tumors to resist therapies. Because these cancer-driven aberrations in lipid metabolism often contrast the surrounding tissue, there are several molecular imaging strategies that have been developed to monitor tumor margin, stage, and treatment response.

I. Lipid Metabolism

A. Exogenous Lipid Uptake

De novo lipid synthesis pathways are crucial during embryogenesis and fetal development, but, after maturation, cells in most tissues are capable of acquiring sufficient circulating lipids to meet their biosynthetic and energetic needs (1-3). Cancer cells can access circulating lipids by overexpressing lipid-scavenging proteins. High exogenous lipids are associated with local invasive index, and obesity is also correlated with higher cancer incidence rates (4). Higher expression of low density lipoprotein (LDL) receptor has been found in transformed colorectal cells relative to normal cells (5). The LDL receptor in prostate cancer provides a major source of cellular cholesterol and essential fatty acids (6). Breast cancer and select sarcoma cells have been observed to secrete lipoprotein lipase (LPL) to release fatty acids

from triglycerides in circulating lipoproteins (7). Although macropinocytosis has been identified in cancer cells, little evidence exists to suggest that this is a relevant source of exogenous lipid *in vivo* (8). Instead, lipid binding proteins are thought to assist in the capture of lipids from the interstitial space and promote invasion (Figure 1), as overexpression of fatty acid binding protein-4 (FABP-4) has been observed on the surface of ovarian, prostate, bladder, and renal cancer cells (9,10). Fatty acid translocase, also known as CD36, is a long-chain fatty acid scavenger that contributes to high mammographic density in subjects at high-risk for breast cancer (11). Ovarian cancer cells can siphon free fatty acids from the lipid stores of the omentum by activating perilipin-A and hormone-sensitive lipase (HSL) in neighboring adipocytes (12). Studies have shown that removal of lipids from culture medium can trigger *de novo* lipid synthesis, emphasizing the dependency on lipids for cell proliferation and the adaptations cancer cells make to sustain their growing biomass (13).

B. *De Novo* Synthesis

Many cancers revert back to *de novo* lipid synthesis, and the lipogenic pathway is composed of many enzymes that are critical for tumor growth (14). Lipid synthesis starts at the energetic hub of the cell, the mitochondria, where acetyl-coenzyme A (acetyl-CoA) and oxaloacetate are condensed into citrate (Figure 1). Citrate from the TCA cycle can be shunted from the mitochondria and broken down by ATP-citrate lyase (ACLY) into acetyl-CoA. Cytosolic citrate can alternatively be sourced from the microenvironment by plasma membrane citrate transporter (PMCT)(Figure 1) (15). Besides feeding into the rate-limiting step of fatty acid synthesis, acetyl-CoA is also critical for histone acetylation and serves as a link between metabolic status and gene expression (16,17).

Acetyl-CoA serves as the 2-carbon building block used for fatty acid synthesis. The enzyme FASN combines malonyl-CoA with repeated acetyl-CoA condensations to form palmitate. Palmitate is the saturated 16-carbon fatty acid from which most complex fatty acids in the body are derived (18). FASN overexpression is associated with poor prognosis in breast cancer (19) and FASN inhibitors derived from natural products (e.g. resveratrol) and synthetic molecules (e.g. orlistat) are being studied for their anti-neoplastic effects (20). Acetyl-CoA is also a synthetic precursor to 3-hydroxy-3-methyl-glutaryl-CoA (HMG-CoA) in the cholesterol biosynthesis pathway (Figure 1). Mevalonate is then produced by HMG-CoA reductase, the target of the lipid lowering drugs, the statins. The amplification of HMG-CoA reductase in many prostate tumors creates a growth dependency on cholesterol, and suggests a possible role for statins in treating these cancers (5,21). Mevalonate is also a precursor to farnesyl-diphosphate, which can further be processed to cholesterol, or used as a substrate for protein prenylation. Isoprenoids from the mevalonate cascade are critical for membrane anchoring and activation of the growth-related G-protein subunits Ras (farnesylated), Rho (geranylgeranylation), and many others (22) (Figure 1).

Fatty acids can be chemically modified in many ways to meet the diverse range of specialized functions required for cellular function (Figure 1). Stearoyl-CoA desaturase-1 (SCD1) produces mono-unsaturated fatty acids (MUFAs) from the saturated fatty acid chains sourced exogenously or from *de novo* synthesis. Saturated fatty acid accumulation in the endoplasmic reticulum (ER) triggers autophagy-induced apoptosis by activating the unfolded protein response (UPR) (23). By modulating MUFA to saturated fatty acid ratios intracellularly, SCD1 has a regulatory effect on cell survival and proliferation (24-26). The elongation-of-very-long-chain-fatty acids (ELOVL) enzymes in the ER are responsible for polyunsaturated fatty

acid (PUFA) synthesis (27), as well as the conversion of saturated and monounsaturated fatty acids into the very long chain fatty acids (C > 18) that serve as building blocks of sphingolipids when combined with ceramide head groups (28). Free fatty acids are stored as triglycerides in lipid droplets or packed into the cell membrane as sphingolipids, cholesterol esters, or phospholipids. Lipid droplets in breast cancer cells have been found to increase with increasing malignancy and to be enriched in polyunsaturated fatty acids, especially arachidonic acid (29)

Diacylglycerol (DAG) is an important lipid second messenger that also serves as a synthetic precursor for both membrane phospholipids and lipid droplet triacylglycerides (30-33). Major membrane phospholipids include phosphatidylcholine (PtdCho), phosphatidylethanolamine (PtdEtn), phosphatidylinositol (PtdIns), phosphatidylserine (PtdSer), among others, and vary in function, location, and relative abundance. The Kennedy pathway of phospholipid synthesis describes the addition of polar head-groups to the DAG backbone, and enzymes in this pathway are responsible for the accumulation of phosphocholine (PC) and phosphoethanolamine (PE) observed in many cancers (34). Choline uptake by choline transporters (ChoTs) and phosphorylation by choline kinase (ChoK) have, in particular, been consistently linked with increased invasiveness, drug resistance, and overall malignancy (35).

C. Lipid Mobilization and Usage

Phospholipid and triacylglyceride levels are maintained by the concerted actions of catabolic enzymes that mobilize fatty acids from lipid droplets and cell membranes (36). Fatty acid release from lipid droplet storage involves lipases that can support aggressive cancer phenotypes in a manner similar to the pro-tumorigenic effects of exogenous fatty acids (37). Fatty acid release from membrane phospholipids is carried out by the phospholipase (PL) enzymes. PLA_1 and PLA_2 cleave phospholipids at the *sn*-1 and *sn*-2 positions, respectively. The

PLA_2 family of enzymes are the primary producers of arachidonic acid and three major subgroups exist: calcium-dependent or cytosolic $cPLA_2$, calcium-independent $iPLA_2$, and secretory $sPLA_2$ (38). While $cPLA_2$ has a tumor-supportive role in many cancers, $sPLA_2$ is thought to have tumor suppressive-functions (39). In contrast, iPLAs are housekeeping enzymes, primarily responsible for mobilizing lipids to maintain membrane integrity and general cellular energy metabolism during homeostasis. PLC cleaves phospholipids at the bond between glycerol and phosphate and contains pleckstrin homology domains for anchoring and cooperation with G-protein coupled receptor (GPCR) signaling networks (40). When activated by growth factor receptors, PLD hydrolyzes the phospholipid head group (e.g. choline, ethanolamine, inositol, serine) to release PA and links growth factor signaling to cell proliferation (32).

Saturated free fatty acids can be broken down into acetyl-CoA to feed into the TCA cycle, and some cancers have been found to prefer fatty acid oxidation to pyruvate oxidation, even in sufficient glucose and oxygen environments (41). β-oxidation is an important energy pathway in prostate cancers, where glycolytic rates are low, and rapid citrate utilization requires a constant supply of acetyl-CoA (42). Peroxisome proliferator-activated receptor alpha (PPARα) is a transcription factor whose activation triggers breakdown of very long chain fatty acids in the peroxisomes, and fatty acid oxidation in the mitochondria. A complex network of interactions with PUFAs, namely arachidonic and linoleic acids, regulates PPARα activity (43). Aside from their direct signaling functions (44), arachidonic acid is an important substrates for cyclooxygenase, lipoxygenase, and cytochrome enzymes that catalyze the production of the eicosanoid family of bioactive lipids that have roles in innate immunity, inflammation, cardiovascular disease, and cancer (45,46).

II. Tumor Progression and Regression

A. Oncogenic Reprogramming

A common feature of cancer cells is the metabolic transition from oxidative phosphorylation to glycolysis, during which the rate of glucose consumption far exceeds the energy requirements of the cell (14). What initially appears to be wasteful energy utilization is in fact a method to feed glucose-derived pyruvate into biosynthesis, including fatty acids (Figure 2). Glutamine has been identified in some cancers as an alternative energy source that can enter the TCA cycle (47) and provide a carbon source for citrate production (Figure 2), however the dependency on glutamine for anaplerosis varies considerably even among cancers of the same tissue (48,49). This may be due, in part, to heterogeneity in the local tissue microenvironment causing gradients in nutrients, oxygen and signaling factors that influence the energetic state of cells.

Under hypoxic conditions, solid tumors can become dependent on unsaturated fatty acid uptake from serum to prevent ER stress that can arise when rapid proliferation is unmet by nutrient availability (50). These exogenous fatty acids can arise from lipolysis in stromal cells in a manner comparable to cachexia (23). The recent resurgence of interest in cancer metabolism has improved our understanding of the adaptations tumor cells can make when fuel availability is variable. These adaptations are only possible because the common driving mutations in cancers often have direct involvement in metabolic pathways.

Many of the clinically prevalent oncogenes are capable of altering lipid uptake, production, or consumption to gain a competitive growth advantage (Figure 2). The transcription factor hypoxia inducible factor (HIF) is a downstream effector of Myc and is tightly regulated by the tumor suppressor gene p53. HIF induces FASN induction and lipid droplet formation for

energy storage to support the tumor microenvironment (18,51,52). FASN requires the reducing agent NADPH, which is produced from the pentose phosphate pathway that often becomes upregulated during cancer reprogramming (18). There is further evidence in renal cell carcinoma models that HIF2α-dependent lipid storage suppresses the ER stress response promoting tumor cell survival (53). Glutamine uptake in glioma and acute myeloid leukemia (AML) is often accompanied or driven by isocitrate dehydrogenase-1 (IDH1) mutations that reroute glutamine toward citrate to provide fatty acid and cholesterol precursors independent of the TCA cycle (Figure 2) (54,55). In hypoxic environments where glucose metabolism is diverted to anaerobic lactate production, mutations in mitochondrial IDH2 provide a continued source of citrate for lipid synthesis, by allowing reductive carboxylation of glutamine-derived α-KG (56). The oncometabolite 2-hydroxyglutarate is produced by many cancer-specific IDH1 and IDH2 mutations, and has widespread epigenetic effectors by altering DNA methylation (57-59).

AMP-activated protein kinase (AMPK) serves as an energetic sensor and master switch by inhibiting fatty acid synthesis in low energy states and stimulating consumption of fatty acids for energy in the mitochondria by β-oxidation (Figure 2). Sterol response element-binding proteins (SREBPs) (60) can activate transcription of genes involved in cholesterol and fatty acid synthesis and uptake, and are directly downstream of AMPK and the PI3K/Akt/MTOR signaling axis that includes many oncogenes (61). Epidermal growth factor receptor (EGFR) mutations are common tumor-driving factors that recruit phospholipases (62,63) and ChoKα (64) to the cell surface, leading to membrane remodeling and induction of mitogenic signals to drive cellular proliferation. Mitogenic growth signals can also come in the form of sterol-derived hormones (estrogens, progestogens, and androgens). Release of these sex hormones, their receptor expression, and the downstream signaling mediators are all common tumor-driving factors in

prostate, breast, endometrial and ovarian cancers (65). Farnesylation of Ras and geranylgeranylation of Rho GTPases are essential for downstream signaling through the phosphoinositol family of signaling lipids (66,67). Phosphoinositides (PI) comprise 10-20% of total cell phospholipids and among that fraction, phosphatidylinositol (4,5) phosphate-2 (PIP_2) and phosphatidylinositol-4-phosphate constitute approximately 0.2-1% (68-70). This class of membrane lipids plays an integral role in proliferation, apoptosis, metabolism and migration, and is pivotal to transmembrane signal transduction because it regulates the distribution of receptor tyrosine kinases, G-protein-coupled receptors, and adhesion molecules among others (71).

Metabolic disease is a risk factor for many cancer types, promoting insulin resistance, hyperactive growth signals, and evasion of apoptosis that help set the conditions for malignant transformation (72). Histological tumor grade in the breast is clinically correlated with phosphomonoester (PME) accumulation (73), such as PC and PE, detectable by MR spectroscopy (74,75). PC promotes survival and mitogenic signaling through downstream cascades such as MAPK and Akt (73,76,77). PC can be formed through the actions of the enzyme choline kinase, or by phosphatidylcholine specific phospholipase C. Phospholipid catabolism can also be a source of other mitogenic second messengers such as DAG, PA, and lysophosphatidylcholine (LPC). DAG is released following the cleavage of phospholipids by PLC (78), activates protein kinase C (PKC) resulting in the release of intracellular calcium stores and subsequent Ca^{2+}-dependent signaling. DAG and PC are also the synthetic precursors to the most abundant mammalian membrane phospholipid, PtdCho, whose levels are predictive of breast tumor grade, estrogen receptor status, and patient survival (79). It is intuitive to suspect that cancers in high adipose tissue use altered lipid metabolism to take advantage of the surrounding environment, however evidence of altered lipid metabolism in cancers that arise in

low-adipose tissues suggests that deranged lipid metabolism is a universal hallmark of cancer pathogenesis.

Variations in lipid composition are likely due to the heterogeneous nature of the tumor microenvironment, which is an ever-changing compartment of structural fibers, nutrients, cellular waste, and signaling molecules. Interstitial pH, extracellular matrix, bioactive lipids, and cytokines can alter the population and function of stromal cells and surrounding tissues. Extracellular lactate, the metabolic byproduct of aerobic glycolysis, is capable of transitioning tumor-associated macrophages from tumor-suppressive to tumor-supportive phenotypes (80,81). Biopsies of colon cancer specimens have been reported to contain high lipid deposition in regions of necrosis and infiltrating macrophages (82). These macrophages most likely resemble the immune-suppressive "alternatively-activated" phenotype, as classic (interferon gamma-induced) activation does not enhance lipid phagocytosis in human myeloid populations (83). Alternatively-activated macrophages prefer fatty acid oxidation (84) and are thought to have critical roles in clearing/remodeling necrotic tissue, recruiting new blood vessels, and regulating innate and adaptive immunity (85).

B. Lipid changes during Apoptosis/Necrosis

The role lipids play in nearly all cell survival pathways emphasizes their importance in tumor growth and invasion pathways, but lipid compartmentalization, metabolism, and signaling are also intricately involved in cell death pathways. During apoptosis, the release of lysophosphatidylcholine (LPC) and sphingosine-1-phosphate (S1P) by PLAs (86) and ceramidases (87) respectively, acts as a "find-me" signal to surrounding macrophages (88). Once recruited to the dying cell, exposed PtdSer on the apoptotic cell's surface serves as the "eat me"

signal recognized by phagocytes (89). Unlike the organized compartmentalization of apoptotic cells into non-immunogenic apoptotic bodies, necrosis is characterized by the breakdown of the plasma membrane and release of the cellular contents that often triggers an immune reaction (90). Recently, lipid peroxidase networks have been identified as key mediators of cancer cell therapy resistance by reversing a non-apoptotic form of cell death known as ferroptosis can be induced by lipid peroxide accumulation (91). Tumor cell response to therapy begins with activation of cell stress responses, which can ultimately decide the fate of the cell and surrounding tumor.

Early changes in lipid metabolism have been reported in response to a wide range of cellular stresses (92), but lipid mobilization does not necessarily commit a cell to apoptosis (93). Many cells undergoing apoptosis produce lipid droplets, although there are exceptions (94), and fatty acids are first mobilized from membrane phospholipids by PLA_2 activity (92,95). Reactive oxygen species (ROS) produced in the mitochondria of apoptotic cells are thought to inhibit the catalytically-active thiol groups on β-oxidation enzymes (96), thus free fatty acids are redirected into lipid droplets in the form of triglycerides and sterol esters (97,98). Lipid droplet formation in cancer may act as a drug reservoir to reduce intracellular concentrations of drug (99), or to absorb reactive oxygen species to protect further DNA damage (100). Lipogenesis of saturated fatty acids also makes the cell membrane less penetrable to drugs that enter by passive diffusion (101). Uptake of triglycerides by macrophages or neutrophils can dampen subsequent immune activation (102,103), providing another potential mechanism of immune escape. Ceramide accumulation regulates and can even trigger mitochondrial outer membrane permeability to fully commit a cell to apoptosis by allowing cytochrome C release to the cytosol (104). Other signs of cell stress that precede or arise during apoptosis are the rise in PUFA and glycerophosphocholine

(GPC) levels (105-107). These indicate a reprogramming of lipid metabolism and suggest that catabolic networks mobilize lipids from membrane phospholipids during this time. Many of these observations were first made using magnetic resonance spectroscopy (MRS) to non-invasively measure lipid resonances of cancer cells undergoing stress responses and apoptosis (92).

III. Imaging Metabolic Lipid Changes

The development of modern imaging techniques allows the detection of several key signaling pathways involved in lipid metabolism and its regulation/dysregulation in cancer. The ability to detect these pathways non-invasively aids in the discovery of potential targets for imaging or interventional therapies. In addition to developing probes to image lipids and alterations in lipid metabolism in mechanisms of oncogenesis, we can also image lipid-dependent or –mediated signaling in response to therapy (108).

A. Imaging lipids in tumors: MR Spectroscopy

MRS has been extensively employed for the study of biological material (from cell extracts, to homogenized tissue, and intact organisms) because it offers a non-invasive method to study the native distribution and dynamic nature of many relevant biomarkers of disease and therapeutic response. The search for disease-related metabolites requires the suppression of the overwhelming fat and water signals observed in proton MR spectra, however much can be learned from the diverse species that contribute to these lipid peaks.

B. Choline and choline metabolites

MRS has been essential in the study of lipid metabolism and for the non-invasive observation of lipid metabolism *in vitro* and *in vivo*. This is due to the ability to observe a number of lipid metabolites in ^{1}H and ^{31}P MR spectra on the basis of chemical shift discrimination. Due to the relative insensitivity of MR, observation is limited to soluble or MR-visible metabolites in the high micromolar to millimolar levels. Lipid metabolites observable in ^{31}P MR spectra, include the PME, PC and PE and the PDE, GPC and GPE. In ^{1}H spectra, observable lipid metabolites include the total choline (tCho) resonance, a composite resonance encompassing free choline, PC and GPC. Thus there is overlap in the information available between ^{31}P and ^{1}H spectra, since the choline PC and GPC resonances seen in the ^{31}P spectra are also observed in the tCho region of ^{1}H spectra. The PME and PDE resonances report on pathways relevant to phospholipid metabolism. PC and PE are generally the anabolic products of choline kinase and ethanolamine kinases, although they can also be produced by the actions of phospholipase C. The PDE resonances result from catabolism of phosphatidylcholine and phosphatidylethanolamine via the consecutive action of two phospholipases, A2 and lysophospholipase or A1.There are numerous excellent reviews on this topic (35,92,109,110), and the reader is referred to these for detailed information. However, it is worth noting that consistent elevations in PMEs and tCho have been observed in a wide range of tumors including brain, prostate, lung, skin, ovarian and breast (111,112). As a means to monitor therapeutic response, tumor choline levels have been measured using MRS in animal (113-115) and human tumors (116-120) with mixed results, at least partly due to the technical difficulties associated with acquiring choline spectra on a background of high fat in normal breast tissue. The picture is further complicated because ChoK is not the only enzyme that contributes to PC accumulation, it

can be produced directly by the actions of PLC on PtdCho, or by the hydrolysis of GPC as a source of additional choline for subsequent phosphorylation. Recent MRS applications have been used to detect changes in choline metabolism due to IDH mutations in glioma (59,121) explore the role of the glycerophosphodiesterase genes GDPD5 and GDPD6 on breast cancer cell migration/invasion (122) and profile metabolic changes in response to HIF1 and HIF2 suppression (123).

C: Imaging lipids in tumors: MR-visible lipids

Proton MRS was originally used to detect MR-visible or mobile lipid signals in cultured cells and tumor biopsies. A series of resonances were observed arising from the fatty acyl chains in neutral lipids, triglyceride and cholesterol esters, including the terminal methyl groups, the methylenes in long chain fatty acids, and olefinic MUFA/PUFA resonances (124-127). MR detects only molecules that exist in a local environment with high rotational molecular motion and thus the observed signals arise predominantly from mobile or MR-visible lipids, composed of triglycerides and cholesterol esters sequestered in lipid droplets. In animal and human tumors, the observation of these lipid resonances require the use of short echo time spectroscopic pulse sequences due to the relatively short T_2 relaxation times of mobile lipids. *In vivo* MRS studies initially used single voxel localization methods such as STEAM and PRESS for assessing the MRS pattern of lipids in tumors, due to the simplicity and accuracy of these methods. However, multi-voxel spectroscopic methods including chemical shift imaging are increasingly being used both in mouse glioma and xenograft models (128,129) as well as in human tumors (130) since these methods provide a better assessment of tumor heterogeneity. The presence of intense lipid signals from surrounding subcutaneous fat and muscle have been problematic in evaluating lipid signals by MRS methods, thus outer volume fat suppression sequences become critical. For this

reason, the majority of studies on intra-tumoral lipids have been focused on the brain where subcutaneous fat is at a minimum. However, useful insights into human tumor composition have still been made in other tumors, despite the problems associated with high fat content in peripheral tissue.

The presence of lipids in human tumors was initially reported by Kuesel *et al.* (124) where a correlation between MR-visible lipids, tumor malignancy and necrosis was observed in brain tumors. These initial findings were subsequently confirmed in *in vivo* imaging studies as well as in histologically different brain tumor types (131). An early demonstration of the sensitivity of lipid signals for accurate diagnosis of supra-tentorial brain tumors was demonstrated by Preul *et al.* (132) suggesting lipid signals as a potential biomarker for grading of astrocytomas. Correlation of lipids with malignancy was also reported in pediatric brain tumors (133) and a further study in pediatric brain tumors suggested the presence of lipids as a marker of poor survival (134). Taken together, the presence of MR-visible lipid signals seems to be a marker for malignancy and poor prognosis. In our recent review on the role of lipids in tumors (92) we argued that increased MR-visible lipids in tumors are indicative of a stress response and that their localization reflects areas of cellular hypoxia and or necrosis.

MRS methods have been used to assess changes in the metabolic profile of tumors as markers of early therapeutic response. Most xenograft and clinical studies have focused on evaluating reductions in the total choline or lactate signal as a marker of treatment response Changes in lipid signals not only suggest a positive response, but increases in PUFA, a putative marker of apoptosis (106), may also aid in understanding the mechanism of cell death induced by specific treatments.

Gene therapy induced changes in lipids

One of the first studies to implement MRS to evaluate changes in metabolism during gene therapy reported a progressive increase in the lipid resonance at 1.3 ppm in 9L rat tumors that were injected intratumorally with adenoviral HSV-*to* followed by ganciclovir treatment (135). These initial studies were followed by several studies of the HSV-*tk* positive BT4C glioma model treated with ganciclovir (106,129,136), which established accumulation of PUFA resonances as a marker of treatment induced apoptosis. The PUFA resonances arise from phospholipase A2 activity leading to hydrolysis of phospholipids in the cell membrane (137). These studies indicate that early increases in mobile lipid resonances after therapeutic intervention may be suggestive of apoptosis and positive treatment response. The temporal evolution of these resonances may be variable, with a decrease in lipid resonances during formation of scar tissue after cell death and lysis. However, the mode and nature of therapeutic interventions could affect changes in lipid resonances. A recent study involving oncolytic viral treatment of immunocompetent Syrian hamster carcinomas as well as a patient with neuroblastoma reported lower unsaturated fatty acids, as measured from the olefinic resonance at 5.3 ppm (Figure 3) in responding tumors than in non-responding tumors (138), which appears to be an exception to the norm. Unlike previous studies, which resulted in an apoptotic tumor cell death after treatment, treatment with oncolytic viruses resulted in multifocal necrosis and a substantial cellular inflammatory response. Taken together, these studies indicate that changes in PUFA resonances could possibly be used to differentiate apoptosis from necrosis, although further data is needed to substantiate this finding.

A decreased PUFA resonance, in comparison to normal breast tissue, was reported in a patient with breast cancer using selective multiple quantum coherence spectroscopy (139). In

contrast to most tumors, a decrease in total tumor lipids was observed in pancreatic cancer compared to pancreatitis as evaluated by MR studies of patient biopsy samples (140) as well as *in vivo* comparing focal pancreatitis to pancreatic adenocarcinoma (141). Although the exact reason for this apparent anomaly is unclear, the pancreatic tumor microenvironment includes stromal tissue that comprises up to 80% of the tumor mass (142). Thus, it is possible that the dominant factor contributing to the MR visible lipid signal in pancreatic cancer arises from the dynamic assortment of extracellular matrix components, infiltrating immune cells, macrophages, pancreatic stellate cells, vascular cells, fibroblasts and myofibroblasts.

Chemotherapy induced changes in lipids

There have been several MRS studies describing alterations in lipid levels in response to treatment with cytotoxic agents. Increased triglyceride resonances were observed in the malignant MDA-MB-435 breast cancer cell line treated with the anti-inflammatory agent indomethacin (143), a drug that has been shown to reduce tumor invasion and inhibit metastasis. Similar increases have also been observed in cells treated with antimitochondrial agents and other cytotoxic drugs (96,144-148). Treatment of DU145 prostate cancer cells with the differentiating agents phenylacetate or phenylbutyrate also led to a time dependent increase in lipid signals, accompanied by increased in GPC, indicating cell stress that precedes the induction of apoptosis (107,147). Increased apoptosis in BT4C glioma cells after exposure to cisplatin resulted in increases in both saturated fatty acids and PUFA resonances (149). Treatment with subcytotoxic doses of cisplatin induced similar increases in saturated and total unsaturated fatty acid (5.3 ppm) resonances in HER2+ ovarian cancer cells (150) (Figure 4). Exposure of the VEGFR tyrosine kinase inhibitor SU1498 on human U87 glioma cells induced a significant increase in lipids with a concomitant decrease in GPC (151). Although cell studies point towards

an increase in MR-visible lipid signals in tumors as a marker of response to chemotherapy, translation of these findings to *in vivo* settings have been challenging due to the confounding presence of lipid signals from hypoxic/necrotic regions in the tumor or contamination from lipid signals outside the tumor.

Many factors influence *in vivo* MRS and make it difficult to predict whether it will provide useful biomarkers for new therapeutic interventions. For example, the PI3K/mTOR inhibitor voxtali in the presence or absence of temozolomide directly alters the phosphorylation of the phospholipid PtdIns in glioblastoma tumors, but causes no detectable changes in ^{1}H MR spectra, even though hyperpolarized ^{13}C MRS showed reduced conversion of pyruvate to lactate (152). Nevertheless, many studies have successfully evaluated changes in lipid signals in response to chemotherapy in tumor xenografts. The efficacy of etoposide, a topoisomerase inhibitor, was tested on a murine lymphoma model and a significant increase in the 1.3 ppm methylene mobile lipid resonance was noted following etoposide-induced apoptosis (153). Treatment of F98 rat gliomas with the choline kinase inhibitor MN58b resulted in a significant increase in both saturated (1.3 ppm) and polyunsaturated (2.8 ppm) fatty acids (Figure 5) that correlated with increased treatment-induced apoptosis (114). Similar increases in saturated and polyunsaturated lipid resonances were observed in GL261 glioma tumors in mice treated with temozolomide (128) (Figure 6). In contrast, treatment of C6, RG2, and GL261 glioma models with the nitrones, PBN (α-phenyl-tert-butylnitrone) and OKN007 (2,4-disulfophenyl-PBN) resulted in a decrease in lipid resonances after treatment, which was attributed to a decrease in necrosis and normalization of the metabolic profile rather than the increase in apoptosis generally reported in tumor treatment studies (154). Increases in neutral lipid resonances were also correlated with tumor growth arrest and treatment response in a mouse model of HER2+

ovarian cancer treated with cisplatin (150). No changes in total choline were noted in this study, as the authors found changes in neutral lipids to be a more sensitive marker of treatment response.

Radiation therapy induced changes in lipids

Radiation therapy is one of the most commonly used therapeutic strategies for solid tumors in the clinic. Although several studies point towards increased lipid resonances in radiation-induced necrosis, relatively few studies have evaluated changes in lipid resonances as a marker of early response to radiation therapy. Cervical cancer biopsy samples obtained from patients treated with radiation therapy were studied by HR-MAS, which revealed a direct correlation between the degree of apoptosis and lipid resonances (155) confirming the observations made in cell and xenograft studies. A xenograft model of non-Hodgkin's diffuse large B cell lymphoma treated with radiation therapy demonstrated a significant increase in both mono and unsaturated lipid resonances within 3 days of treatment (156). The increase in lipid resonances corresponded with histology findings of increased apoptosis and oil red O staining, supporting the idea that unsaturated (PUFA) lipid accumulation is a marker of therapy induced apoptosis.

D. Positron Emission Tomography

Positron emission tomography (PET) measures the gamma rays produced when an electron collides with a positron emitted from a beta-decaying nucleus. PET scans require the administration of a radioactive substrate, but the high sensitivity of PET means that only tracer levels of radiolabeled material are needed. For tumor imaging, ^{18}F-fluorodeoxyglucose (FDG) is by far the most commonly employed PET tracer (Figure 7). FDG exploits the enhanced aerobic glycolysis observed in many tumors, a phenomenon known as the Warburg effect.

Overexpression of plasma membrane glucose transporters and hexokinase activity rapidly internalize FDG and phosphorylate it in the first step of glycolysis. This reaction traps FDG-6-P in the cell, but the substrate is unable to be metabolized further. FDG-PET is widely used clinically for the staging of primary tumors, but because of the ability of PET to perform a full-body scan, it is also important for the detection of metastases. FDG-PET can also be used to monitor tumor regression post-therapy, and has been used in several instances to monitor FASN inhibitor therapies due to the link between glycolysis and fatty acid synthesis (157,158). One caveat is that it is difficult to assess enhanced FDG tumor uptake in tissues with high glucose utilization (e.g. brain and heart) or in organs of excretion (e.g. kidney and bladder). There is also the potential for background labeling in metabolically active cells, such as lymphocytes in sites of inflammation. Furthermore, some tumors, such as the prostate, are not FDG avid and have relatively low uptake.

A promising alternative to FDG for tumor lipid imaging is ^{18}F or ^{11}C labeled choline (Figure 7). This strategy relies on the upregulation of choline transporters and ChoK in tumor cells. The concerted action of these components achieves tumor tissue contrast by rapidly internalizing and phosphorylating the choline mimetic radioligands. Choline PET is becoming more widely used for tumor detection, especially in the prostate (159) but also in other tumors such as gliomas (160). Choline PET has also been used to track tumor recurrence, metastasis, and response to chemo and radiotherapy (161-164). One challenge facing choline PET is the discrepancy between labeled choline tracer uptake and steady state metabolites observed using MRS (165). This could be due to intrinsic differences between choline transport and phosphorylation that manifest as differences in tracer uptake relative to steady-state levels, but it

could also be due to alternative pathways such as metabolism of the choline tracers in other organs such as liver (166).

The low FDG avidity of prostate tumors is linked to their metabolic preference for β-oxidation of fatty acids, rather than glutaminolysis or glucose metabolism, as a primary energy source (42). A variety of ^{18}F-labeled fatty acid analogs have been synthesized (Figure 7), and the metabolism of these probes effectively trap the radiolabel specifically in cells with high usage of β-oxidation (167,168). In metabolizable probes, labeling at the hydrophobic end of the molecule allows these probes to be consumed through β-oxidation. In non-metabolizable probes, chemical modifications are nearer to the carboxyl group, which still allows cell uptake and potential incorporation into phospholipids or triglycerides, but further oxidative metabolism is prevented (169). Labeled fatty acid probes, such as BMIPP (Figure 7), have been primarily employed to monitor metabolism in tissues with high levels of β-oxidation, mostly cardiac and to a lesser extent skeletal muscle (170-176). Use of these probes to study cancer has been limited, even though the use of β-oxidation as a potential cancer energy source has been known for decades (177,178).

Although the half-life of ^{11}C is quite short (20 min), it is still possible to observe ^{11}C palmitate uptake and distinguish storage in triglycerides vs metabolism by β-oxidation (179,180). Regions of high fatty acid synthesis have been imaged using ^{11}C-acetate incorporation into palmitate (181), although the intermediate acetyl-CoA has other potential metabolic fates such as the Krebs cycle or histone modification. For this reason, ^{11}C-acetate has been used to monitor prostate tumors during therapy and recurrent lesions, but is incapable of distinguishing malignant tumors from benign hyperplastic nodules (182-185). Several radiolabeled ether lipids containing PC moieties (186) have been made (Figure 7) based upon early observations of elevated

phospholipid-ethers in neoplastic tissue (187,188). Due to the preferential accumulation and retention of these alkylphosphonium analogs, ^{124}I-CLR1404 was developed and recently tested in brain tumor PET imaging where a tumor/normal brain signal ratio of 30 was reported (189). Replacement of the PET isotope with the radio-ablative ^{131}I-CLR1404 agent improved survival in tumor-bearing rodents and provided a novel theranostic platform wherein ^{124}I can assist in the planning of ^{131}I therapy.

E. Mass Spectrometry Imaging

Mass spectrometry imaging (MSI) is a powerful modality for the detailed spatial detection of protein, metabolite and drug distribution in tissues. MSI consists of a family of techniques that includes matrix-assisted laser desorption ionization (MALDI) MSI, secondary ion mass spectrometry (SIMS), matrix electrospray-MSI (ES-MSI), and nanostructure-initiator mass spectrometry (NIMS). For the detection of lipids, the most commonly used technique is MALDI MSI (190), which has a large range of applications and provides a good overall combination of spatial resolution, intact molecule sensitivity and probing depth (190). MALDI provides a critical platform for the spatial detection of lipids and lipid metabolites, as there is a lack of suitable reagents and antibodies for the analysis of tissue lipids *in situ* (191).

MSI techniques are invasive procedures, requiring the preparation and embedding of a thin tissue slice followed by rasterized destruction by laser or primary ion beams. For MALDI, tissue is embedded in a matrix such as gelatin and α-cyano-4-hydroxycinnamic acid (CHCA) or 2,5-dihydroxybenzoic acid (DHB) (192). Washing the tissues with aqueous solutions of ammonium formate or phospholipases prior to embedding can be used to enhance certain lipid species and improve signal to noise (191). MSI can detect hundreds of molecules in a single sample with a routine spatial resolution of 50−100 μm, and a small molecule resolution as high

as 5−10 μm (193). Because matrix deposition is a slow process and the application of a wet matrix to tissue can cause metabolite shift, matrix-free techniques using nanoparticle initiators have been developed and these often provide simpler spectra to interpret (194,195). These NIMS procedures provide comparable lipid profiles, but with improved spatial resolution (196).

MSI has been used extensively to study lipid in primary human tumor tissue as well as tumor cell lines and xenografts. In human tissues, a consistent observation of elevated phospholipids has been observed in cancer compared to normal tissues. This includes breast tumors and invasive ductal carcinomas compared to carcinoma *in situ* (197-199), gastric cancers (200), renal cell carcinomas (201), human lung squamous cell carcinoma (202) and colorectal carcinoma (203,204). The most frequent observation is of increased PtdCho in tumors, but increases in PtdEtn, PtdIns, and PA have also been observed (199,205,206). Some studies have demonstrated increases in ether-linked lipids (199). Lyso-phospholipids have been reported to increase in colorectal tumors, but decrease in gastric and prostate cancers (200,203,207) (Figure 8). Fatty acid levels have also been observed to increase in a number of tumors (199), but it is uncertain whether these are free fatty acids or acyl components of more complex lipids.

Studies in tumor xenografts have confirmed the general observations of increased phospholipids and ether-linked lipids in tumor tissues. Measurement of choline metabolites in breast cancer xenografts using MR spectroscopic imaging combined with MALDI-MSI revealed differences in spatial distribution with PC and choline levels concentrated in normoxic tumor regions (208). When correlated with the expression of a hypoxia-response element, PtdCho elevation was concentrated in hypoxic regions whereas LPC was elevated in necrotic regions (192,209). Further studies have indicated distinct microenvironmental lipid distribution with higher levels of ether-linked PtdEtn in viable tumor and ether-linked PtdCho in necrotic regions

(193). Elongated fatty acyl chain length in phospholipids of human lung squamous cell carcinomas was reproduced in mouse xenografts and correlated with the expression of the acyl chain elongase ELOVL6 (210). These data demonstrate the role of MSI in identifying distinct tumor microenvironments by their molecular signatures.

While MSI has revealed a number of potential lipid-related cancer markers, there are very few studies that have employed MSI lipids to monitor cancer treatment. One recent study has identified transient decreases in serum PtdCho and lyso-PtdCho associated with response to radiation in head and neck tumor patients (211). A second study has indicated that LPC (16:0) is a significant predictor of PSA recurrence in human prostate cancer patients (207). The NIMS technique is capable of simultaneous monitoring of drug accumulation and endogenous water-soluble metabolite distribution (212,213). Adopting this technique to study drugs that target lipid metabolism in tumors should be a priority in this field. These data indicate that further investigation into the utility of lipid biomarkers to assess treatment response is warranted.

F. Optical Imaging

Optical imaging is a cost-effective and relatively easy-to-use imaging modality that makes it a valuable tool for non-invasive longitudinal imaging. The range of detectable wavelengths is broad enough to allow multiplex imaging, and these principles have been applied to a number of medical diagnostic platforms, including flow cytometry, fluorescence microscopy, and diffuse optical imaging. *In vivo,* optical imaging is limited by attenuated light penetration through tissue due to scattering and absorption in the visible wavelengths. This is partially alleviated by using chromophores that absorb or emit in the near infrared region (675 – 900 nm) where absorption by hemoglobin, deoxyhemoglobin and water is at a minimum. In

addition, several endogenous proteins, such as laminin and elastin, autofluoresce and elevate the background signal during *in vivo* measurements. As a result, the observable depths of optical imaging are usually limited to 1 cm or less. Thus *in vivo* optical imaging has predominantly focused on single-channel fluorescence or bioluminescence on a macro level (< 15x magnification) in mice or other small animals. Bioluminescence is not practical in clinical settings, because it requires transfection with an invertebrate luminescent protein, but it is a highly sensitive reporter that, in the field of lipid metabolism, has been adapted to map regions of heightened fatty acid uptake (214). Advances in CCD sensitivity has recently sparked renewed interest in Cerenkov radiation as an additional source of emitted light that can be detected *in vivo* (215,216). This signal may one day offer functional information concordant with the tomographical information provided by PET (217).

New optical imaging technologies in oncology have largely followed advancements in vascular imaging. Before diffuse optical tomography became a subject of interest in mammographic screening, the observation was made that absorption of circulating hemoglobin changes in an oxygen-dependent manner (218). This was a pioneering study in translational optical imaging, but 20 years later routine clinical optical imaging remains limited outside of optical coherence tomography (OCT) in ophthalmic applications (219-221). OCT uses a rastered application of NIR light and interferometry to produce a 3-D scanning image of the retina. The use of NIR wavelengths still limits the application to surface phenomena, less than 1 cm deep in the tissue. OCT has also been employed in oncology, most notably to detect the development of esophageal tumors (222,223), With regards to lipids, OCT is most commonly used for atherosclerotic plaque detection in cadavers and patients, which is based upon its sensitivity to

lipid deposits in local vascular sites (224,225). This leads to the possibility for future applications of OCT as a method to distinguish lipid levels in treated tumor tissue.

In small animal optical imaging, enhanced contrast is often provided by the administration of exogenous NIR fluorescent compounds. There are a growing number of these molecular probes that allow for noninvasive optical imaging of lipid metabolism pathways. The probes are generally of three types: passive molecules that are used as blood pool agents and rely on leaky vasculature to accumulate at the site of pathology, targeted permanently fluorescent molecules that can be taken up selectively as substrates or inhibitors of lipid metabolic pathways, and smart quenched fluorescent molecules that can be selectively activated by enzymes. Fluorescence imaging using these probes allows for specific and localized detection of metabolic activity.

Indocyanine green (ICG) is a clinically approved blood-pooling agent that has been used for tumor detection. Collection of ICG in solid tumors has been attributed to the enhanced permeability and retention caused by disordered vasculature and insufficient lymphatic systems in tumors (226), however tumor-associated macrophages in lipid-rich regions may have an underappreciated role in this phenomenon. In atherosclerotic plaques, ICG has been observed to accumulate preferentially in the lipid-rich macrophages in both rabbits and patients (227). MRI, PET, and optical imaging of tumor-associated macrophages have been described extensively (228-230) and these methods should be used to explore co-localization of lipid profiles with immune infiltration in the tumor setting.

Lipid uptake and synthesis

Lipid uptake and synthesis are essential to the maintenance of mammalian cell membranes. For this reason, a constant source of precursors are required to maintain the

proliferative nature of the cancer cell. Tumor cells synthesize and accumulate membrane lipids, such as PtdCho, at a rate that greatly outpaces the surrounding normal tissue, and this offers an avenue that can be exploited for selective delivery of imaging and therapeutic agents. The introduction of fluorescently labeled lipid analogs into the tumor microenvironment can also be used to visualize lipid scavenger activity. Direct fluorescent labeling of PtdCho has been reported using visible fluorophores, so high background in normal tissues is a general feature of these approaches (231). A common approach is to employ fatty acid probes to which non-polar dyes such as BODIPY have been attached (232). Depending on the metabolic state of the cell, these lipid analogs can be incorporated into phospholipids or neutral lipids in lipid droplets. The alkylphosphocholine analogs described for PET imaging have also been adapted with BODIPY or heptamethine dyes for imaging of tumor margins and draining lymph nodes (233).

Choline kinase

Choline kinase catalyzes the conversion of choline to PC, and is elevated in several types of cancers. Its upregulation has been correlated with the transition of normal breast epithelium toward a malignant phenotype, and selective inhibitors have been developed for Phase I clinical trials in solid tumors (ClinicalTrials.gov, NCT01215864). Based on these studies, we developed a series of fluorescent inhibitors that selectively bind ChoK and emit fluorescence in the near infrared optical window (234). The design exploited the structural similarities between ChoK inhibitors and cyanine dyes frequently employed for optical imaging, and did not rely on dye conjugation to existing inhibitor structures (235). The probe, JAS239, showed elevated uptake in tumors that overexpressed ChoK, and more importantly, had reduced uptake in tumors after chemotherapy (236).

Phosphatidylinositol signaling pathway

Many oncogenic signaling pathways are mediated by PtdIns, which makes these lipids attractive targets for cancer imaging probes. In order to interrogate the role of these phospholipids on cell signaling, Yoon *et al.* engineered a fluorescent PIP_2 sensor to study its role in membrane remodeling, regulation of membrane proteins, and regulation of the cytoskeleton (236-238). This probe was engineered with the visible fluorophore (2-dimethyl-amino-6-acyl-naphthaline) optimized for its lipophilic properties, limiting its utility for detection of lipid dynamics *in vivo*. Because IP_3 and DAG mediate the release of intracellular calcium and are activated by lipid metabolic pathways, optical probes based upon flu-4 or BAPTA can provide an indirect means of assessing these bioactive lipids (239-241). DAG can be evaluated directly using radiolabeling (242) or using optical techniques such as FRET to detect activated DAG intercalation in the plasma membrane (243).

Phospholipases

Phospholipases are catabolic enzymes that can be targeted with lipid based quenched optical probes that are activated by enzymatic hydrolysis (39). Upregulation of $cPLA_2$ has been observed in breast and prostate cancers (112), and elevated levels of PC and phosphoethanolamine have been attributed to PLC activation in breast cancer, ovarian cancer and melanoma (109). Activatable probes with phospholipid-based structures, a linker that regulates enzyme accessibility, a quenchable fluorophore or light-emitting compound, and a cleavable quenching domain have been designed as fluorescent agents for quantifying phospholipase activity. The advantage of this approach is the enhanced signal to noise available from the continuous enzymatic release of fluorescent substrates. Enzyme activated BODIPY probes have been employed to examine phospholipase activity in many systems including the

digestive physiology of the zebra fish (244-247). While useful for cells, small transparent animals and intravital microscopy, the optical properties of BODIPY limit its detection in tissue. There are several quenched fluorophores commercially available with emission in the visible range. In the NIR range, we developed analogous probes targeting PLA_2 and PLC for *in vivo* applications (248). These self-quenching probes were composed of pyropheophorbide-*a* (Pyro) tethered to PtdEtn and a Black Hole Quencher (BHQ-3). While Pyro has an excitation maximum ~~excitable Soret band~~ at 418 nm that emits at 660 nm, its absorption peak at 670 with emission at 725 nm makes it suitable for *in vivo* imaging. The specificity of these probes to various phospholipase isoforms could be modulated by altering the spacer length between Pyro and the glycerol backbone. The resulting construct, Pyro-PtdEtn-BHQ, was highly specific to PtdCho-specific PLC (PC-PLC) both *in vitro* and *in vivo* and we used this to detected upregulation and activation of this enzyme in DU145 prostate cancer xenografts (Figure 9) (112).

Arachidonic acid, a PUFA found in the *sn*-2 position of phospholipids, is mobilized by the activity of cytosolic or cPLA2 acting on membrane-associated phospholipids. The redox activity of COX-2 catalyzes the conversion of arachidonic acid to prostaglandins that act as a lipid second messenger. Arachidonic acid is first converted to prostaglandin G2, and then the peroxidase activity of COX-2 converts it to the unstable H2 isoform that is converted to one of several homologous tissue- and function-specific isoforms of prostaglandins. It is prostaglandin E2 that is notably upregulated in several types of cancer contributing to aberrant signaling (249). In order to utilize this signal transduction pathway to image pathogenic events, there are several points of interrogation possible: using activatable probes to evaluate COX-2 activity, directly measure PGE2 levels with targeted probes, or evaluate activation of further downstream events.

Detection of cPLA2 using a cleavable construct requires a probe that contains arachidonic acid, to account for the specificity of the enzyme for this fatty acid, as well as a small enough head group to fit into the active site. Previous studies had shown that arachidonic acid esterified to visible fluorophores such as 7-hydroxycoumarin were highly specific for cPLA2 and displayed similar hydrolysis kinetics to native substrates (250). We adapted this caged fluorescence protocol using fluorophores that emit in the red wavelength range (660-680 nm) to create cPLA2 sensitive probes suitable for *in vivo* imaging. Probe selectivity could be modulated by choice of fatty acids and fluorophores, with DDAO arachidonate performing the best *in vitro,* in cells and tumors. Here, arachidonic acid provided the optimum fatty acid substrate for cPLA2 and DDAO (7-hydroxy-9H-(1,3-dichloro-9,9-dimethylacridin-2-one) was the most resistant to non-specific aqueous hydrolysis. Probe activation was shown to be proportional to cPLA2 expression levels in cells and tumors, and high relative to a non-specific control probe, DDAO palmitate.

Apoptosis

In addition to using imaging techniques to noninvasively detect components of lipid metabolism, other biomarkers can be detected that offer information pertaining to non-homeostatic states of cells and tissues *in situ*. Apoptosis is often indicative of patient response to cancer therapy, accordingly, targeting markers of apoptosis can be useful to evaluate the efficacy of various interventions (251). Among these events are plasma membrane reorganization marked by PtdSer translocation to the outer leaflet of the membrane. PtdSer translocation can be detected using labeled ligands that bind anionic phospholipids, including proteins such as Annexin 5 or synaptotagmin (252) or organic molecules such as zinc dipicolylamine (253). A number of

labeling strategies have used this approach to create apoptosis sensors for optical (254), MR (255-257) and nuclear imaging when radiolabeled with ^{99}Tc or ^{123}I (258). Annexin has shown some promise as a molecular probe for this purpose though this strategy can be limited by suboptimal pharmacokinetics (259), and non-specific labeling of necrotic cells (260).

Conclusion

Lipid metabolism is an essential component of cellular homeostasis that can become drastically altered during the process of malignant transformation. Most common driver mutations and oncogenes are related to growth cues and cellular stress responses, and many therapeutic strategies target these pathways such that the measurement of lipid metabolic changes can serve as a proxy for drug response pharmacodynamics. While MRS and PET approaches offer the ability to serially-measure lipid composition and flux, they are limited by spatial resolution. MSI and Optical Imaging, on the other hand, permit the appreciation of intratumoral heterogeneity but often require surgical exposure of the tissue site. Still, these approaches are finding increasing value in image-guided surgical resection and are experiencing fast-paced improvements in technology including the ability to image endogenous contrast, more specific probes that provide kinetic information, and sub-cellular resolution. For a balance between resolution and ability to image endogenous lipid signals without the need for new FDA-approved contrast agents, MRS remains the gold standard for measuring lipid metabolic states in tumor and other tissues. New advances including two-dimensional MRS, hyperpolarized MR spectroscopic imaging, and higher field strength MRS continue to reshape our understanding of lipid metabolic changes during tumor growth and treatment response. This comes at a critical time as therapy continues to evolve with new signal transduction inhibitors, metabolic targeting agents, and immunotherapies change the landscape of cancer care.

REFERENCES

1. Weiss L, Hoffmann GE, Schreiber R, Andres H, Fuchs E, Korber E, Kolb HJ. Fatty-acid biosynthesis in man, a pathway of minor importance. Purification, optimal assay conditions, and organ distribution of fatty-acid synthase. Biol Chem Hoppe Seyler **1986**;367(9):905-12.
2. Wagle S, Bui A, Ballard PL, Shuman H, Gonzales J, Gonzales LW. Hormonal regulation and cellular localization of fatty acid synthase in human fetal lung. Am J Physiol **1999**;277(2 Pt 1):L381-90.
3. Kusakabe T, Maeda M, Hoshi N, Sugino T, Watanabe K, Fukuda T, Suzuki T. Fatty acid synthase is expressed mainly in adult hormone-sensitive cells or cells with high lipid metabolism and in proliferating fetal cells. J Histochem Cytochem **2000**;48(5):613-22.
4. Eheman C, Henley SJ, Ballard-Barbash R, Jacobs EJ, Schymura MJ, Noone AM, Pan L, Anderson RN, Fulton JE, Kohler BA, Jemal A, Ward E, Plescia M, Ries LA, Edwards BK. Annual Report to the Nation on the status of cancer, 1975-2008, featuring cancers associated with excess weight and lack of sufficient physical activity. Cancer **2012**;118(9):2338-66.
5. Hentosh P, Yuh SH, Elson CE, Peffley DM. Sterol-independent regulation of 3-hydroxy-3-methylglutaryl coenzyme A reductase in tumor cells. Mol Carcinog **2001**;32(3):154-66.
6. Chen Y, Hughes-Fulford M. Human prostate cancer cells lack feedback regulation of low-density lipoprotein receptor and its regulator, SREBP2. Int J Cancer **2001**;91(1):41-5.
7. Kuemmerle NB, Rysman E, Lombardo PS, Flanagan AJ, Lipe BC, Wells WA, Pettus JR, Froehlich HM, Memoli VA, Morganelli PM, Swinnen JV, Timmerman LA, Chaychi L, Fricano CJ, Eisenberg BL, Coleman WB, Kinlaw WB. Lipoprotein lipase links dietary fat to solid tumor cell proliferation. Mol Cancer Ther **2011**;10(3):427-36.
8. Commisso C, Davidson SM, Soydaner-Azeloglu RG, Parker SJ, Kamphorst JJ, Hackett S, Grabocka E, Nofal M, Drebin JA, Thompson CB, Rabinowitz JD, Metallo CM, Vander Heiden MG, Bar-Sagi D. Macropinocytosis of protein is an amino acid supply route in Ras-transformed cells. Nature **2013**;497(7451):633-7.
9. Das R, Hammamieh R, Neill R, Melhem M, Jett M. Expression pattern of fatty acid-binding proteins in human normal and cancer prostate cells and tissues. Clin Cancer Res **2001**;7(6):1706-15.
10. Tolle A, Suhail S, Jung M, Jung K, Stephan C. Fatty acid binding proteins (FABPs) in prostate, bladder and kidney cancer cell lines and the use of IL-FABP as survival predictor in patients with renal cell carcinoma. BMC Cancer **2011**;11:302.
11. DeFilippis RA, Chang H, Dumont N, Rabban JT, Chen YY, Fontenay GV, Berman HK, Gauthier ML, Zhao J, Hu D, Marx JJ, Tjoe JA, Ziv E, Febbraio M, Kerlikowske K, Parvin B, Tlsty TD. CD36 repression activates a multicellular stromal program shared by high mammographic density and tumor tissues. Cancer Discov **2012**;2(9):826-39.
12. Nieman KM, Kenny HA, Penicka CV, Ladanyi A, Buell-Gutbrod R, Zillhardt MR, Romero IL, Carey MS, Mills GB, Hotamisligil GS, Yamada SD, Peter ME, Gwin K,

Lengyel E. Adipocytes promote ovarian cancer metastasis and provide energy for rapid tumor growth. Nat Med **2011**;17(11):1498-503.

13. Daniels VW, Smans K, Royaux I, Chypre M, Swinnen JV, Zaidi N. Cancer cells differentially activate and thrive on de novo lipid synthesis pathways in a low-lipid environment. PLoS One **2014**;9(9):e106913.
14. Cairns RA, Harris IS, Mak TW. Regulation of cancer cell metabolism. Nat Rev Cancer **2011**;11(2):85-95.
15. Sun J, Aluvila S, Kotaria R, Mayor JA, Walters DE, Kaplan RS. Mitochondrial and Plasma Membrane Citrate Transporters: Discovery of Selective Inhibitors and Application to Structure/Function Analysis. Mol Cell Pharmacol **2010**;2(3):101-10.
16. Zaidi N, Swinnen JV, Smans K. ATP-citrate lyase: a key player in cancer metabolism. Cancer Res **2012**;72(15):3709-14.
17. Bauer DE, Hatzivassiliou G, Zhao F, Andreadis C, Thompson CB. ATP citrate lyase is an important component of cell growth and transformation. Oncogene **2005**;24(41):6314-22.
18. Menendez JA, Lupu R. Fatty acid synthase and the lipogenic phenotype in cancer pathogenesis. Nat Rev Cancer **2007**;7(10):763-77.
19. Kuhajda FP, Jenner K, Wood FD, Hennigar RA, Jacobs LB, Dick JD, Pasternack GR. Fatty acid synthesis: a potential selective target for antineoplastic therapy. Proc Natl Acad Sci U S A **1994**;91(14):6379-83.
20. Mullen GE, Yet L. Progress in the development of fatty acid synthase inhibitors as anticancer targets. Bioorg Med Chem Lett **2015**;25(20):4363-9.
21. Zhuang L, Kim J, Adam RM, Solomon KR, Freeman MR. Cholesterol targeting alters lipid raft composition and cell survival in prostate cancer cells and xenografts. J Clin Invest **2005**;115(4):959-68.
22. Roberts PJ, Mitin N, Keller PJ, Chenette EJ, Madigan JP, Currin RO, Cox AD, Wilson O, Kirschmeier P, Der CJ. Rho Family GTPase modification and dependence on CAAX motif-signaled posttranslational modification. J Biol Chem **2008**;283(37):25150-63.
23. Ackerman D, Simon MC. Hypoxia, lipids, and cancer: surviving the harsh tumor microenvironment. Trends Cell Biol **2014**;24(8):472-8.
24. Huang GM, Jiang QH, Cai C, Qu M, Shen W. SCD1 negatively regulates autophagy-induced cell death in human hepatocellular carcinoma through inactivation of the AMPK signaling pathway. Cancer Lett **2015**;358(2):180-90.
25. Scaglia N, Igal RA. Stearoyl-CoA desaturase is involved in the control of proliferation, anchorage-independent growth, and survival in human transformed cells. J Biol Chem **2005**;280(27):25339-49.
26. Chen L, Ren J, Yang L, Li Y, Fu J, Tian Y, Qiu F, Liu Z, Qiu Y. Stearoyl-CoA desaturase-1 mediated cell apoptosis in colorectal cancer by promoting ceramide synthesis. Sci Rep **2016**;6:19665.
27. Jakobsson A, Westerberg R, Jacobsson A. Fatty acid elongases in mammals: their regulation and roles in metabolism. Prog Lipid Res **2006**;45(3):237-49.
28. Denic V, Weissman JS. A molecular caliper mechanism for determining very long-chain fatty acid length. Cell **2007**;130(4):663-77.

29. Abramczyk H, Surmacki J, Kopec M, Olejnik AK, Lubecka-Pietruszewska K, Fabianowska-Majewska K. The role of lipid droplets and adipocytes in cancer. Raman imaging of cell cultures: MCF10A, MCF7, and MDA-MB-231 compared to adipocytes in cancerous human breast tissue. Analyst **2015**;140(7):2224-35.
30. Griner EM, Kazanietz MG. Protein kinase C and other diacylglycerol effectors in cancer. Nat Rev Cancer **2007**;7(4):281-94.
31. Lin ME, Herr DR, Chun J. Lysophosphatidic acid (LPA) receptors: signaling properties and disease relevance. Prostaglandins Other Lipid Mediat **2010**;91(3-4):130-8.
32. Foster DA, Salloum D, Menon D, Frias MA. Phospholipase D and the maintenance of phosphatidic acid levels for regulation of mammalian target of rapamycin (mTOR). J Biol Chem **2014**;289(33):22583-8.
33. Bagnato C, Igal RA. Overexpression of diacylglycerol acyltransferase-1 reduces phospholipid synthesis, proliferation, and invasiveness in simian virus 40-transformed human lung fibroblasts. J Biol Chem **2003**;278(52):52203-11.
34. Daly PF, Lyon RC, Faustino PJ, Cohen JS. Phospholipid metabolism in cancer cells monitored by 31P NMR spectroscopy. J Biol Chem **1987**;262(31):14875-8.
35. Glunde K, Bhujwalla ZM, Ronen SM. Choline metabolism in malignant transformation. Nat Rev Cancer **2011**;11(12):835-48.
36. Currie E, Schulze A, Zechner R, Walther TC, Farese RV, Jr. Cellular fatty acid metabolism and cancer. Cell Metab **2013**;18(2):153-61.
37. Nomura DK, Long JZ, Niessen S, Hoover HS, Ng SW, Cravatt BF. Monoacylglycerol lipase regulates a fatty acid network that promotes cancer pathogenesis. Cell **2010**;140(1):49-61.
38. Murakami M, Taketomi Y, Miki Y, Sato H, Hirabayashi T, Yamamoto K. Recent progress in phospholipase A(2) research: from cells to animals to humans. Prog Lipid Res **2011**;50(2):152-92.
39. Park JB, Lee CS, Jang JH, Ghim J, Kim YJ, You S, Hwang D, Suh PG, Ryu SH. Phospholipase signalling networks in cancer. Nat Rev Cancer **2012**;12(11):782-92.
40. Kadamur G, Ross EM. Mammalian phospholipase C. Annu Rev Physiol **2013**;75:127-54.
41. Samudio I, Harmancey R, Fiegl M, Kantarjian H, Konopleva M, Korchin B, Kaluarachchi K, Bornmann W, Duvvuri S, Taegtmeyer H, Andreeff M. Pharmacologic inhibition of fatty acid oxidation sensitizes human leukemia cells to apoptosis induction. J Clin Invest **2010**;120(1):142-56.
42. Liu Y. Fatty acid oxidation is a dominant bioenergetic pathway in prostate cancer. Prostate Cancer Prostatic Dis **2006**;9(3):230-4.
43. Zuo X, Wu Y, Morris JS, Stimmel JB, Leesnitzer LM, Fischer SM, Lippman SM, Shureiqi I. Oxidative metabolism of linoleic acid modulates PPAR-beta/delta suppression of PPAR-gamma activity. Oncogene **2006**;25(8):1225-41.
44. Brash AR. Arachidonic acid as a bioactive molecule. J Clin Invest **2001**;107(11):1339-45.
45. Dennis EA, Norris PC. Eicosanoid storm in infection and inflammation. Nat Rev Immunol **2015**;15(8):511-23.

46. Harizi H, Corcuff JB, Gualde N. Arachidonic-acid-derived eicosanoids: roles in biology and immunopathology. Trends Mol Med **2008**;14(10):461-9.
47. Wise DR, Thompson CB. Glutamine addiction: a new therapeutic target in cancer. Trends Biochem Sci **2010**;35(8):427-33.
48. Cheng T, Sudderth J, Yang C, Mullen AR, Jin ES, Mates JM, DeBerardinis RJ. Pyruvate carboxylase is required for glutamine-independent growth of tumor cells. Proc Natl Acad Sci U S A **2011**;108(21):8674-9.
49. Hensley CT, Wasti AT, DeBerardinis RJ. Glutamine and cancer: cell biology, physiology, and clinical opportunities. J Clin Invest **2013**;123(9):3678-84.
50. Young RM, Ackerman D, Quinn ZL, Mancuso A, Gruber M, Liu L, Giannoukos DN, Bobrovnikova-Marjon E, Diehl JA, Keith B, Simon MC. Dysregulated mTORC1 renders cells critically dependent on desaturated lipids for survival under tumor-like stress. Genes Dev **2013**;27(10):1115-31.
51. Doe MR, Ascano JM, Kaur M, Cole MD. Myc posttranscriptionally induces HIF1 protein and target gene expression in normal and cancer cells. Cancer Res **2012**;72(4):949-57.
52. Ravi R, Mookerjee B, Bhujwalla ZM, Sutter CH, Artemov D, Zeng Q, Dillehay LE, Madan A, Semenza GL, Bedi A. Regulation of tumor angiogenesis by p53-induced degradation of hypoxia-inducible factor 1alpha. Genes Dev **2000**;14(1):34-44.
53. Qiu B, Ackerman D, Sanchez DJ, Li B, Ochocki JD, Grazioli A, Bobrovnikova-Marjon E, Diehl JA, Keith B, Simon MC. HIF2alpha-Dependent Lipid Storage Promotes Endoplasmic Reticulum Homeostasis in Clear-Cell Renal Cell Carcinoma. Cancer Discov **2015**;5(6):652-67.
54. Dang L, White DW, Gross S, Bennett BD, Bittinger MA, Driggers EM, Fantin VR, Jang HG, Jin S, Keenan MC, Marks KM, Prins RM, Ward PS, Yen KE, Liau LM, Rabinowitz JD, Cantley LC, Thompson CB, Vander Heiden MG, Su SM. Cancer-associated IDH1 mutations produce 2-hydroxyglutarate. Nature **2009**;462(7274):739-44.
55. Metallo CM, Gameiro PA, Bell EL, Mattaini KR, Yang J, Hiller K, Jewell CM, Johnson ZR, Irvine DJ, Guarente L, Kelleher JK, Vander Heiden MG, Iliopoulos O, Stephanopoulos G. Reductive glutamine metabolism by IDH1 mediates lipogenesis under hypoxia. Nature **2011**;481(7381):380-4.
56. Wise DR, Ward PS, Shay JE, Cross JR, Gruber JJ, Sachdeva UM, Platt JM, DeMatteo RG, Simon MC, Thompson CB. Hypoxia promotes isocitrate dehydrogenase-dependent carboxylation of alpha-ketoglutarate to citrate to support cell growth and viability. Proc Natl Acad Sci U S A **2011**;108(49):19611-6.
57. Lu C, Ward PS, Kapoor GS, Rohle D, Turcan S, Abdel-Wahab O, Edwards CR, Khanin R, Figueroa ME, Melnick A, Wellen KE, O'Rourke DM, Berger SL, Chan TA, Levine RL, Mellinghoff IK, Thompson CB. IDH mutation impairs histone demethylation and results in a block to cell differentiation. Nature **2012**;483(7390):474-8.
58. Losman JA, Kaelin WG, Jr. What a difference a hydroxyl makes: mutant IDH, (R)-2-hydroxyglutarate, and cancer. Genes Dev **2013**;27(8):836-52.
59. Leather T, Jenkinson MD, Das K, Poptani H. Magnetic Resonance Spectroscopy for Detection of 2-Hydroxyglutarate as a Biomarker for IDH Mutation in Gliomas. Metabolites **2017**;7(2).

60. Guo D, Bell EH, Mischel P, Chakravarti A. Targeting SREBP-1-driven lipid metabolism to treat cancer. Curr Pharm Des **2014**;20(15):2619-26.

61. Lewis CA, Brault C, Peck B, Bensaad K, Griffiths B, Mitter R, Chakravarty P, East P, Dankworth B, Alibhai D, Harris AL, Schulze A. SREBP maintains lipid biosynthesis and viability of cancer cells under lipid- and oxygen-deprived conditions and defines a gene signature associated with poor survival in glioblastoma multiforme. Oncogene **2015**;34(40):5128-40.

62. Kim SW, Hayashi M, Lo JF, Yang Y, Yoo JS, Lee JD. ADP-ribosylation factor 4 small GTPase mediates epidermal growth factor receptor-dependent phospholipase D2 activation. J Biol Chem **2003**;278(4):2661-8.

63. Tvorogov D, Carpenter G. EGF-dependent association of phospholipase C-gamma1 with c-Cbl. Exp Cell Res **2002**;277(1):86-94.

64. Miyake T, Parsons SJ. Functional interactions between Choline kinase alpha, epidermal growth factor receptor and c-Src in breast cancer cell proliferation. Oncogene **2012**;31(11):1431-41.

65. Key TJ, Allen NE, Verkasalo PK, Banks E. Energy balance and cancer: the role of sex hormones. Proc Nutr Soc **2001**;60(1):81-9.

66. Cantley LC. The phosphoinositide 3-kinase pathway. Science **2002**;296(5573):1655-7.

67. Takai Y, Sasaki T, Matozaki T. Small GTP-binding proteins. Physiol Rev **2001**;81(1):153-208.

68. Balla T. Phosphoinositides: tiny lipids with giant impact on cell regulation. Physiol Rev **2013**;93(3):1019-137.

69. Nasuhoglu C, Feng S, Mao J, Yamamoto M, Yin HL, Earnest S, Barylko B, Albanesi JP, Hilgemann DW. Nonradioactive analysis of phosphatidylinositides and other anionic phospholipids by anion-exchange high-performance liquid chromatography with suppressed conductivity detection. Anal Biochem **2002**;301(2):243-54.

70. Wenk MR, Lucast L, Di Paolo G, Romanelli AJ, Suchy SF, Nussbaum RL, Cline GW, Shulman GI, McMurray W, De Camilli P. Phosphoinositide profiling in complex lipid mixtures using electrospray ionization mass spectrometry. Nat Biotechnol **2003**;21(7):813-7.

71. Santos CR, Schulze A. Lipid metabolism in cancer. FEBS J **2012**;279(15):2610-23.

72. Hashmi S, Wang Y, Suman DS, Parhar RS, Collison K, Conca W, Al-Mohanna F, Gaugler R. Human cancer: is it linked to dysfunctional lipid metabolism? Biochim Biophys Acta **2014**;1850(2):352-64.

73. Ramirez de Molina A, Gutierrez R, Ramos MA, Silva JM, Silva J, Bonilla F, Sanchez JJ, Lacal JC. Increased choline kinase activity in human breast carcinomas: clinical evidence for a potential novel antitumor strategy. Oncogene **2002**;21(27):4317-22.

74. Daly PF, Cohen JS. Magnetic resonance spectroscopy of tumors and potential in vivo clinical applications: a review. Cancer Res **1989**;49(4):770-9.

75. Negendank W. Studies of human tumors by MRS: a review. NMR Biomed **1992**;5(5):303-24.

76. Yalcin A, Clem B, Makoni S, Clem A, Nelson K, Thornburg J, Siow D, Lane AN, Brock SE, Goswami U, Eaton JW, Telang S, Chesney J. Selective inhibition of choline kinase simultaneously attenuates MAPK and PI3K/AKT signaling. Oncogene **2010**;29(1):139-49.

77. Iorio E, Mezzanzanica D, Alberti P, Spadaro F, Ramoni C, D'Ascenzo S, Millimaggi D, Pavan A, Dolo V, Canevari S, Podo F. Alterations of choline phospholipid metabolism in ovarian tumor progression. Cancer Res **2005**;65(20):9369-76.

78. Cocco L, Follo MY, Manzoli L, Suh PG. Phosphoinositide-specific phospholipase C in health and disease. J Lipid Res **2015**;56(10):1853-60.

79. Hilvo M, Denkert C, Lehtinen L, Muller B, Brockmoller S, Seppanen-Laakso T, Budczies J, Bucher E, Yetukuri L, Castillo S, Berg E, Nygren H, Sysi-Aho M, Griffin JL, Fiehn O, Loibl S, Richter-Ehrenstein C, Radke C, Hyotylainen T, Kallioniemi O, Iljin K, Oresic M. Novel theranostic opportunities offered by characterization of altered membrane lipid metabolism in breast cancer progression. Cancer Res **2011**;71(9):3236-45.

80. Husain Z, Huang Y, Seth P, Sukhatme VP. Tumor-derived lactate modifies antitumor immune response: effect on myeloid-derived suppressor cells and NK cells. J Immunol **2013**;191(3):1486-95.

81. Colegio OR, Chu NQ, Szabo AL, Chu T, Rhebergen AM, Jairam V, Cyrus N, Brokowski CE, Eisenbarth SC, Phillips GM, Cline GW, Phillips AJ, Medzhitov R. Functional polarization of tumour-associated macrophages by tumour-derived lactic acid. Nature **2014**;513(7519):559-63.

82. Ende D, Rutter A, Russell P, Mountford CE. Chemical shift imaging of human colorectal tissue (ex vivo). NMR Biomed **1996**;9(4):179-83.

83. King NJ, Delikatny EJ, Holmes KT. 1H magnetic resonance spectroscopy of primary human and murine cells of the myeloid lineage. Immunomethods **1994**;4(2):188-98.

84. Pearce EL, Pearce EJ. Metabolic pathways in immune cell activation and quiescence. Immunity **2013**;38(4):633-43.

85. Noy R, Pollard JW. Tumor-associated macrophages: from mechanisms to therapy. Immunity **2014**;41(1):49-61.

86. Lauber K, Bohn E, Krober SM, Xiao YJ, Blumenthal SG, Lindemann RK, Marini P, Wiedig C, Zobywalski A, Baksh S, Xu Y, Autenrieth IB, Schulze-Osthoff K, Belka C, Stuhler G, Wesselborg S. Apoptotic cells induce migration of phagocytes via caspase-3-mediated release of a lipid attraction signal. Cell **2003**;113(6):717-30.

87. Gude DR, Alvarez SE, Paugh SW, Mitra P, Yu J, Griffiths R, Barbour SE, Milstien S, Spiegel S. Apoptosis induces expression of sphingosine kinase 1 to release sphingosine-1-phosphate as a "come-and-get-me" signal. FASEB J **2008**;22(8):2629-38.

88. Savill J, Dransfield I, Gregory C, Haslett C. A blast from the past: clearance of apoptotic cells regulates immune responses. Nat Rev Immunol **2002**;2(12):965-75.

89. Ravichandran KS. Find-me and eat-me signals in apoptotic cell clearance: progress and conundrums. J Exp Med **2010**;207(9):1807-17.

90. Edinger AL, Thompson CB. Death by design: apoptosis, necrosis and autophagy. Curr Opin Cell Biol **2004**;16(6):663-9.

91. Viswanathan VS, Ryan MJ, Dhruv HD, Gill S, Eichhoff OM, Seashore-Ludlow B, Kaffenberger SD, Eaton JK, Shimada K, Aguirre AJ, Viswanathan SR, Chattopadhyay S, Tamayo P, Yang WS, Rees MG, Chen S, Boskovic ZV, Javaid S, Huang C, Wu X, Tseng YY, Roider EM, Gao D, Cleary JM, Wolpin BM, Mesirov JP, Haber DA, Engelman JA, Boehm JS, Kotz JD, Hon CS, Chen Y, Hahn WC, Levesque MP, Doench JG, Berens ME, Shamji AF, Clemons PA, Stockwell BR, Schreiber SL. Dependency of a therapy-resistant state of cancer cells on a lipid peroxidase pathway. Nature **2017**;547(7664):453-7.

92. Delikatny EJ, Chawla S, Leung DJ, Poptani H. MR-visible lipids and the tumor microenvironment. NMR Biomed **2011**;24(6):592-611.

93. Milkevitch M, Jeitner TM, Beardsley NJ, Delikatny EJ. Lovastatin enhances phenylbutyrate-induced MR-visible glycerophosphocholine but not apoptosis in DU145 prostate cells. Biochim Biophys Acta **2007**;1771(9):1166-76.

94. Iorio E, Di Vito M, Spadaro F, Ramoni C, Lococo E, Carnevale R, Lenti L, Strom R, Podo F. Triacsin C inhibits the formation of 1H NMR-visible mobile lipids and lipid bodies in HuT 78 apoptotic cells. Biochim Biophys Acta **2003**;1634(1-2):1-14.

95. Miki Y, Mukae S, Murakami M, Ishikawa Y, Ishii T, Ohki H, Matsumoto M, Komiyama K. Butyrate inhibits oral cancer cell proliferation and regulates expression of secretory phospholipase A2-X and COX-2. Anticancer Res **2007**;27(3B):1493-502.

96. Boren J, Brindle KM. Apoptosis-induced mitochondrial dysfunction causes cytoplasmic lipid droplet formation. Cell Death Differ **2012**;19(9):1561-70.

97. Farese RV, Jr., Walther TC. Lipid droplets finally get a little R-E-S-P-E-C-T. Cell **2009**;139(5):855-60.

98. Guo Y, Walther TC, Rao M, Stuurman N, Goshima G, Terayama K, Wong JS, Vale RD, Walter P, Farese RV. Functional genomic screen reveals genes involved in lipid-droplet formation and utilization. Nature **2008**;453(7195):657-61.

99. Morjani H, Aouali N, Belhoussine R, Veldman RJ, Levade T, Manfait M. Elevation of glucosylceramide in multidrug-resistant cancer cells and accumulation in cytoplasmic droplets. Int J Cancer **2001**;94(2):157-65.

100. Bensaad K, Favaro E, Lewis CA, Peck B, Lord S, Collins JM, Pinnick KE, Wigfield S, Buffa FM, Li JL, Zhang Q, Wakelam MJ, Karpe F, Schulze A, Harris AL. Fatty acid uptake and lipid storage induced by HIF-1alpha contribute to cell growth and survival after hypoxia-reoxygenation. Cell Rep **2014**;9(1):349-65.

101. Rysman E, Brusselmans K, Scheys K, Timmermans L, Derua R, Munck S, Van Veldhoven PP, Waltregny D, Daniels VW, Machiels J, Vanderhoydonc F, Smans K, Waelkens E, Verhoeven G, Swinnen JV. De novo lipogenesis protects cancer cells from free radicals and chemotherapeutics by promoting membrane lipid saturation. Cancer Res **2010**;70(20):8117-26.

102. Mukundan L, Odegaard JI, Morel CR, Heredia JE, Mwangi JW, Ricardo-Gonzalez RR, Goh YP, Eagle AR, Dunn SE, Awakuni JU, Nguyen KD, Steinman L, Michie SA, Chawla A. PPAR-delta senses and orchestrates clearance of apoptotic cells to promote tolerance. Nat Med **2009**;15(11):1266-72.

103. Wright LC, Groot Obbink KL, Delikatny EJ, Santangelo RT, Sorrell TC. The origin of ^{1}H NMR-visible triacylglycerol in human neutrophils: high fatty acid environments result in preferential sequestration of palmitic acid into plasma membrane triacylglycerol. European Journal of Biochemistry **2000**;267:68-78.

104. Huang C, Freter C. Lipid metabolism, apoptosis and cancer therapy. Int J Mol Sci **2015**;16(1):924-49.

105. Podo F, Canevari S, Canese R, Pisanu ME, Ricci A, Iorio E. MR evaluation of response to targeted treatment in cancer cells. NMR Biomed **2011**;24(6):648-72.

106. Hakumaki JM, Poptani H, Sandmair AM, Yla-Herttuala S, Kauppinen RA. 1H MRS detects polyunsaturated fatty acid accumulation during gene therapy of glioma: implications for the in vivo detection of apoptosis. Nat Med **1999**;5(11):1323-7.

107. Milkevitch M, Shim H, Pilatus U, Pickup S, Wehrle JP, Samid D, Poptani H, Glickson JD, Delikatny EJ. Increases in NMR-visible lipid and glycerophosphocholine during phenylbutyrate-induced apoptosis in human prostate cancer cells. Biochim Biophys Acta **2005**;1734(1):1-12.

108. Greenhough A, Smartt HJ, Moore AE, Roberts HR, Williams AC, Paraskeva C, Kaidi A. The COX-2/PGE2 pathway: key roles in the hallmarks of cancer and adaptation to the tumour microenvironment. Carcinogenesis **2009**;30(3):377-86.

109. Podo F. Tumour phospholipid metabolism. NMR Biomed **1999**;12(7):413-39.

110. Ackerstaff E, Glunde K, Bhujwalla ZM. Choline phospholipid metabolism: a target in cancer cells? J Cell Biochem **2003**;90(3):525-33.

111. Glunde K, Jie C, Bhujwalla ZM. Molecular causes of the aberrant choline phospholipid metabolism in breast cancer. Cancer Research **2004**;64(12):4270-6.

112. Mawn TM, Popov AV, Beardsley NJ, Stefflova K, Milkevitch M, Zheng G, Delikatny EJ. In Vivo Detection of Phospholipase C by Enzyme-Activated Near-Infrared Probes. Bioconjugate Chem **2011**;22(12):2434-43.

113. Al-Saffar NM, Troy H, Ramirez de Molina A, Jackson LE, Madhu B, Griffiths JR, Leach MO, Workman P, Lacal JC, Judson IR, Chung YL. Noninvasive magnetic resonance spectroscopic pharmacodynamic markers of the choline kinase inhibitor MN58b in human carcinoma models. Cancer Res **2006**;66(1):427-34.

114. Kumar M, Arlauckas SP, Saksena S, Verma G, Ittyerah R, Pickup S, Popov AV, Delikatny EJ, Poptani H. Magnetic resonance spectroscopy for detection of choline kinase inhibition in the treatment of brain tumors. Mol Cancer Ther **2015**;14(4):899-908.

115. van Asten JJ, Vettukattil R, Buckle T, Rottenberg S, van Leeuwen F, Bathen TF, Heerschap A. Increased levels of choline metabolites are an early marker of docetaxel treatment response in BRCA1-mutated mouse mammary tumors: an assessment by ex vivo proton magnetic resonance spectroscopy. J Transl Med **2015**;13:114.

116. Sharma U, Baek HM, Su MY, Jagannathan NR. In vivo 1H MRS in the assessment of the therapeutic response of breast cancer patients. NMR Biomed **2011**;24(6):700-11.

117. Danishad KK, Sharma U, Sah RG, Seenu V, Parshad R, Jagannathan NR. Assessment of therapeutic response of locally advanced breast cancer (LABC) patients undergoing

neoadjuvant chemotherapy (NACT) monitored using sequential magnetic resonance spectroscopic imaging (MRSI). NMR Biomed **2010**;23(3):233-41.

118. Bathen TF, Heldahl MG, Sitter B, Vettukattil R, Bofin A, Lundgren S, Gribbestad IS. In vivo MRS of locally advanced breast cancer: characteristics related to negative or positive choline detection and early monitoring of treatment response. MAGMA **2011**;24(6):347-57.
119. Drisis S, Flamen P, Ignatiadis M, Metens T, Chao SL, Chintinne M, Lemort M. Total choline quantification measured by 1H MR spectroscopy as early predictor of response after neoadjuvant treatment for locally advanced breast cancer: The impact of immunohistochemical status. J Magn Reson Imaging **2018**.
120. Bolan PJ, Kim E, Herman BA, Newstead GM, Rosen MA, Schnall MD, Pisano ED, Weatherall PT, Morris EA, Lehman CD, Garwood M, Nelson MT, Yee D, Polin SM, Esserman LJ, Gatsonis CA, Metzger GJ, Newitt DC, Partridge SC, Hylton NM, Investigators ATtI-. MR spectroscopy of breast cancer for assessing early treatment response: Results from the ACRIN 6657 MRS trial. J Magn Reson Imaging **2017**;46(1):290-302.
121. Viswanath P, Radoul M, Izquierdo-Garcia JL, Ong WQ, Luchman HA, Cairncross JG, Huang B, Pieper RO, Phillips JJ, Ronen SM. 2-Hydroxyglutarate-Mediated Autophagy of the Endoplasmic Reticulum Leads to an Unusual Downregulation of Phospholipid Biosynthesis in Mutant IDH1 Gliomas. Cancer Res **2018**.
122. Cao MD, Cheng M, Rizwan A, Jiang L, Krishnamachary B, Bhujwalla ZM, Bathen TF, Glunde K. Targeting choline phospholipid metabolism: GDPD5 and GDPD6 silencing decrease breast cancer cell proliferation, migration, and invasion. NMR Biomed **2016**;29(8):1098-107.
123. Bharti SK, Mironchik Y, Wildes F, Penet MF, Goggins E, Krishnamachary B, Bhujwalla ZM. Metabolic consequences of HIF silencing in a triple negative human breast cancer xenograft. Oncotarget **2018**;9(20):15326-39.
124. Kuesel AC, Sutherland GR, Halliday W, Smith IC. 1H MRS of high grade astrocytomas: mobile lipid accumulation in necrotic tissue. NMR Biomed **1994**;7(3):149-55.
125. Delikatny EJ, Russell P, Hunter JC, Hancock R, Atkinson KH, van Haaften-Day C, Mountford CE. Proton MR and human cervical neoplasia: ex vivo spectroscopy allows distinction of invasive carcinoma of the cervix from carcinoma in situ and other preinvasive lesions. Radiology **1993**;188(3):791-6.
126. Mountford CE, Grossman G, Reid G, Fox RM. Characterization of transformed cells and tumours by proton nuclear magnetic resonance spectroscopy. Cancer Research **1982**;42:2270-6.
127. Cross KJ, Holmes KT, Mountford CE, Wright PE. Assignment of acyl chain resonances from membranes of mammalian cells by two-dimensional NMR methods. Biochemistry **1984**;23:5895-7.
128. Delgado-Goni T, Julia-Sape M, Candiota AP, Pumarola M, Arus C. Molecular imaging coupled to pattern recognition distinguishes response to temozolomide in preclinical glioblastoma. NMR Biomed **2014**;27(11):1333-45.

129. Liimatainen T, Hakumaki JM, Kauppinen RA, Ala-Korpela M. Monitoring of gliomas in vivo by diffusion MRI and (1)H MRS during gene therapy-induced apoptosis: interrelationships between water diffusion and mobile lipids. NMR Biomed **2009**;22(3):272-9.

130. Chawla S, Krejza J, Vossough A, Zhang Y, Kapoor GS, Wang S, O'Rourke DM, Melhem ER, Poptani H. Differentiation between oligodendroglioma genotypes using dynamic susceptibility contrast perfusion-weighted imaging and proton MR spectroscopy. AJNR Am J Neuroradiol **2013**;34(8):1542-9.

131. Doblas S, He T, Saunders D, Hoyle J, Smith N, Pye Q, Lerner M, Jensen RL, Towner RA. In vivo characterization of several rodent glioma models by 1H MRS. NMR Biomed **2012**;25(4):685-94.

132. Preul MC, Caramanos Z, Collins DL, Villemure JG, Leblanc R, Olivier A, Pokrupa R, Arnold DL. Accurate, noninvasive diagnosis of human brain tumors by using proton magnetic resonance spectroscopy. Nat Med **1996**;2(3):323-5.

133. Astrakas LG, Zurakowski D, Tzika AA, Zarifi MK, Anthony DC, De Girolami U, Tarbell NJ, Black PM. Noninvasive magnetic resonance spectroscopic imaging biomarkers to predict the clinical grade of pediatric brain tumors. Clin Cancer Res **2004**;10(24):8220-8.

134. Wilson M, Cummins CL, Macpherson L, Sun Y, Natarajan K, Grundy RG, Arvanitis TN, Kauppinen RA, Peet AC. Magnetic resonance spectroscopy metabolite profiles predict survival in paediatric brain tumours. Eur J Cancer **2013**;49(2):457-64.

135. Ross BD, Chenevert TL, Kim B, Ben-Yoseph O. Magnetic Resonance Imaging and Spectroscopy: Application to Experimental Neuro-Oncology. Q Magn Reson Biol Med **1994**;1(2):89-106.

136. Liimatainen T, Hakumaki J, Tkac I, Grohn O. Ultra-short echo time spectroscopic imaging in rats: implications for monitoring lipids in glioma gene therapy. NMR Biomed **2006**;19(5):554-9.

137. Liimatainen TJ, Erkkila AT, Valonen P, Vidgren H, Lakso M, Wong G, Grohn OH, Yla-Herttuala S, Hakumaki JM. 1H MR spectroscopic imaging of phospholipase-mediated membrane lipid release in apoptotic rat glioma in vivo. Magn Reson Med **2008**;59(6):1232-8.

138. Hemminki O, Immonen R, Narvainen J, Kipar A, Paasonen J, Jokivarsi KT, Yli-Ollila H, Soininen P, Partanen K, Joensuu T, Parvianen S, Pesonen SK, Koski A, Vaha-Koskela M, Cerullo V, Pesonen S, Grohn OH, Hemminki A. In vivo magnetic resonance imaging and spectroscopy identifies oncolytic adenovirus responders. Int J Cancer **2014**;134(12):2878-90.

139. He Q, Shkarin P, Hooley RJ, Lannin DR, Weinreb JC, Bossuyt VI. In vivo MR spectroscopic imaging of polyunsaturated fatty acids (PUFA) in healthy and cancerous breast tissues by selective multiple-quantum coherence transfer (Sel-MQC): a preliminary study. Magn Reson Med **2007**;58(6):1079-85.

140. Wang AS, Lodi A, Rivera LB, Izquierdo-Garcia JL, Firpo MA, Mulvihill SJ, Tempero MA, Bergers G, Ronen SM. HR-MAS MRS of the pancreas reveals reduced lipid and elevated lactate and taurine associated with early pancreatic cancer. NMR Biomed **2014**;27(11):1361-70.

141. Cho SG, Lee DH, Lee KY, Ji H, Lee KH, Ros PR, Suh CH. Differentiation of chronic focal pancreatitis from pancreatic carcinoma by in vivo proton magnetic resonance spectroscopy. J Comput Assist Tomogr **2005**;29(2):163-9.

142. Erkan M, Hausmann S, Michalski CW, Fingerle AA, Dobritz M, Kleeff J, Friess H. The role of stroma in pancreatic cancer: diagnostic and therapeutic implications. Nat Rev Gastroenterol Hepatol **2012**;9(8):454-67.

143. Ackerstaff E, Gimi B, Artemov D, Bhujwalla ZM. Anti-inflammatory agent indomethacin reduces invasion and alters metabolism in a human breast cancer cell line. Neoplasia **2007**;9(3):222-35.

144. Delikatny EJ, Cooper WA, Brammah S, Sathasivam N, Rideout DC. Nuclear magnetic resonance-visible lipid induced by cationic lipophilic chemotherapeutic agents are accompanied by increased lipid droplet formation and damaged mitochondria. Cancer Research **2002**;62:1394-400.

145. Blankenberg FG, Katsikis PD, Storrs RW, Beaulieu C, Spielman D, Chen JY, Naumovski L, Tait JF. Quantitative analysis of apoptotic cell death using proton nuclear magnetic resonance spectroscopy. Blood **1997**;89(10):3778-86.

146. Iorio E, Di Vito M, Spadaro F, Ramoni C, Lococo E, Carnevale R, Lenti L, Strom R, Podo F. Triacsin C inhibits the formation of 1H NMR-visible mobile lipids and lipid bodies in HuT 78 apoptotic cells. Biochimica et Biophysica Acta **2003**;1634(1-2):1-14.

147. Milkevitch M, Beardsley NJ, Delikatny EJ. Phenylbutyrate induces apoptosis and lipid accumulations via a peroxisome proliferator-activated receptor gamma-dependent pathway. NMR in Biomedicine **2010**;23(5):473-9.

148. Roman SK, Jeitner TM, Hancock R, Cooper WA, Rideout DC, Delikatny EJ. Induction of magnetic resonance-visible lipid in a transformed human breast cell line by tetraphenylphosphonium chloride. International Journal of Cancer **1997**;73:570-9.

149. Mirbahai L, Wilson M, Shaw CS, McConville C, Malcomson RD, Kauppinen RA, Peet AC. Lipid biomarkers of glioma cell growth arrest and cell death detected by 1 H magic angle spinning MRS. NMR Biomed **2012**;25(11):1253-62.

150. Pisanu ME, Ricci A, Paris L, Surrentino E, Liliac L, Bagnoli M, Canevari S, Mezzanzanica D, Podo F, Iorio E, Canese R. Monitoring response to cytostatic cisplatin in a HER2(+) ovary cancer model by MRI and in vitro and in vivo MR spectroscopy. Br J Cancer **2014**;110(3):625-35.

151. Mesti T, Savarin P, Triba MN, Le Moyec L, Ocvirk J, Banissi C, Carpentier AF. Metabolic impact of anti-angiogenic agents on U87 glioma cells. PLoS One **2014**;9(6):e99198.

152. Radoul M, Chaumeil MM, Eriksson P, Wang AS, Phillips JJ, Ronen SM. MR Studies of Glioblastoma Models Treated with Dual PI3K/mTOR Inhibitor and Temozolomide:Metabolic Changes Are Associated with Enhanced Survival. Mol Cancer Ther **2016**;15(5):1113-22.

153. Schmitz JE, Kettunen MI, Hu DE, Brindle KM. 1H MRS-visible lipids accumulate during apoptosis of lymphoma cells in vitro and in vivo. Magn Reson Med **2005**;54(1):43-50.

154. He T, Doblas S, Saunders D, Casteel R, Lerner M, Ritchey JW, Snider T, Floyd RA, Towner RA. Effects of PBN and OKN007 in rodent glioma models assessed by 1H MR spectroscopy. Free Radic Biol Med **2011**;51(2):490-502.

155. Lyng H, Sitter B, Bathen TF, Jensen LR, Sundfor K, Kristensen GB, Gribbestad IS. Metabolic mapping by use of high-resolution magic angle spinning 1H MR spectroscopy for assessment of apoptosis in cervical carcinomas. BMC Cancer **2007**;7:11.

156. Lee SC, Poptani H, Pickup S, Jenkins WT, Kim S, Koch CJ, Delikatny EJ, Glickson JD. Early detection of radiation therapy response in non-Hodgkin's lymphoma xenografts by in vivo 1H magnetic resonance spectroscopy and imaging. NMR Biomed **2010**;23(6):624-32.

157. Lee JS, Orita H, Gabrielson K, Alvey S, Hagemann RL, Kuhajda FP, Gabrielson E, Pomper MG. FDG-PET for pharmacodynamic assessment of the fatty acid synthase inhibitor C75 in an experimental model of lung cancer. Pharm Res **2007**;24(6):1202-7.

158. Sankaranarayanapillai M, Zhang N, Baggerly KA, Gelovani JG. Metabolic shifts induced by fatty acid synthase inhibitor orlistat in non-small cell lung carcinoma cells provide novel pharmacodynamic biomarkers for positron emission tomography and magnetic resonance spectroscopy. Mol Imaging Biol **2013**;15(2):136-47.

159. Beauregard JM, Williams SG, Degrado TR, Roselt P, Hicks RJ. Pilot comparison of F-fluorocholine and F-fluorodeoxyglucose PET/CT with conventional imaging in prostate cancer. J Med Imaging Radiat Oncol **2010**;54(4):325-32.

160. Sollini M, Sghedoni R, Erba PA, Cavuto S, Froio A, De Berti G, Pisanello A, Fraternali A, Iori M, Iaccarino C, Asti M, Filice A, Versari A. Diagnostic performances of [18f]fluorocholine positron emission tomography in brain tumors. Q J Nucl Med Mol Imaging **2015**;62(2):209-19.

161. Reske SN, Moritz S, Kull T. [11C]Choline-PET/CT for outcome prediction of salvage radiotherapy of local relapsing prostate carcinoma. Q J Nucl Med Mol Imaging **2012**;56(5):430-9.

162. Beheshti M, Vali R, Waldenberger P, Fitz F, Nader M, Loidl W, Broinger G, Stoiber F, Foglman I, Langsteger W. Detection of bone metastases in patients with prostate cancer by 18F fluorocholine and 18F fluoride PET-CT: a comparative study. Eur J Nucl Med Mol Imaging **2008**;35(10):1766-74.

163. Kitajima K, Murphy RC, Nathan MA, Froemming AT, Hagen CE, Takahashi N, Kawashima A. Detection of recurrent prostate cancer after radical prostatectomy: comparison of 11C-choline PET/CT with pelvic multiparametric MR imaging with endorectal coil. J Nucl Med **2014**;55(2):223-32.

164. Giovacchini G, Picchio M, Garcia-Parra R, Briganti A, Abdollah F, Gianolli L, Schindler C, Montorsi F, Messa C, Fazio F. 11C-choline PET/CT predicts prostate cancer-specific survival in patients with biochemical failure during androgen-deprivation therapy. J Nucl Med **2014**;55(2):233-41.

165. Rommel D, Bol A, Abarca-Quinones J, Peeters F, Robert A, Labar D, Galant C, Gregoire V, Duprez T. Rodent rhabdomyosarcoma: comparison between total choline concentration at H-MRS and [18F]-fluoromethylcholine uptake at PET using accurate methods for collecting data. Mol Imaging Biol **2010**;12(4):415-23.

166. Challapalli A, Aboagye EO. Positron Emission Tomography Imaging of Tumor Cell Metabolism and Application to Therapy Response Monitoring. Front Oncol **2016**;6:44.

167. Eckelman WC, Babich JW. Synthesis and validation of fatty acid analogs radiolabeled by nonisotopic substitution. J Nucl Cardiol **2007**;14(3 Suppl):S100-9.

168. Pandey MK, Belanger AP, Wang S, DeGrado TR. Structure dependence of long-chain [18F]fluorothia fatty acids as myocardial fatty acid oxidation probes. J Med Chem **2012**;55(23):10674-84.

169. Kataoka K, Nohara R, Hosokawa R, Hirai T, Okuda K, Li-Guang C, Fujibayashi Y, Fujita M, Konishi J, Sasayama S. Myocardial lipid metabolism in compensated and advanced stages of heart failure: evaluation by canine pacing model with BMIPP. J Nucl Med **2001**;42(1):124-9.

170. Tamaki N, Morita K, Kuge Y, Tsukamoto E. The role of fatty acids in cardiac imaging. J Nucl Med **2000**;41(9):1525-34.

171. DeGrado TR, Wang S, Holden JE, Nickles RJ, Taylor M, Stone CK. Synthesis and preliminary evaluation of (18)F-labeled 4-thia palmitate as a PET tracer of myocardial fatty acid oxidation. Nucl Med Biol **2000**;27(3):221-31.

172. DeGrado TR, Kitapci MT, Wang S, Ying J, Lopaschuk GD. Validation of 18F-fluoro-4-thia-palmitate as a PET probe for myocardial fatty acid oxidation: effects of hypoxia and composition of exogenous fatty acids. J Nucl Med **2006**;47(1):173-81.

173. Taylor M, Wallhaus TR, Degrado TR, Russell DC, Stanko P, Nickles RJ, Stone CK. An evaluation of myocardial fatty acid and glucose uptake using PET with [18F]fluoro-6-thia-heptadecanoic acid and [18F]FDG in Patients with Congestive Heart Failure. J Nucl Med **2001**;42(1):55-62.

174. DeGrado TR, Bhattacharyya F, Pandey MK, Belanger AP, Wang S. Synthesis and preliminary evaluation of 18-(18)F-fluoro-4-thia-oleate as a PET probe of fatty acid oxidation. J Nucl Med **2010**;51(8):1310-7.

175. Tu Z, Li S, Sharp TL, Herrero P, Dence CS, Gropler RJ, Mach RH. Synthesis and evaluation of 15-(4-(2-[(1)(8)F]Fluoroethoxy)phenyl)pentadecanoic acid: a potential PET tracer for studying myocardial fatty acid metabolism. Bioconjug Chem **2010**;21(12):2313-9.

176. Maki MT, Haaparanta M, Nuutila P, Oikonen V, Luotolahti M, Eskola O, Knuuti JM. Free fatty acid uptake in the myocardium and skeletal muscle using fluorine-18-fluoro-6-thia-heptadecanoic acid. J Nucl Med **1998**;39(8):1320-7.

177. Zaidi N, Lupien L, Kuemmerle NB, Kinlaw WB, Swinnen JV, Smans K. Lipogenesis and lipolysis: the pathways exploited by the cancer cells to acquire fatty acids. Prog Lipid Res **2013**;52(4):585-9.

178. Camarda R, Zhou AY, Kohnz RA, Balakrishnan S, Mahieu C, Anderton B, Eyob H, Kajimura S, Tward A, Krings G, Nomura DK, Goga A. Inhibition of fatty acid oxidation as a therapy for MYC-overexpressing triple-negative breast cancer. Nat Med **2016**;22(4):427-32.

179. Han Q, Cao Y, Gathaiya NW, Kemp BJ, Jensen MD. Free fatty acid flux measured using [1-(11)C]palmitate positron emission tomography and [U-(13)C]palmitate in humans. Am J Physiol Endocrinol Metab **2017**:ajpendo002842017.

180. Christensen NL, Jakobsen S, Schacht AC, Munk OL, Alstrup AKO, Tolbod LP, Harms HJ, Nielsen S, Gormsen LC. Whole-Body Biodistribution, Dosimetry, and Metabolite Correction of [(11)C]Palmitate: A PET Tracer for Imaging of Fatty Acid Metabolism. Mol Imaging **2017**;16:1536012117734485.

181. Vavere AL, Kridel SJ, Wheeler FB, Lewis JS. 1-11C-acetate as a PET radiopharmaceutical for imaging fatty acid synthase expression in prostate cancer. J Nucl Med **2008**;49(2):327-34.

182. Oyama N, Akino H, Kanamaru H, Suzuki Y, Muramoto S, Yonekura Y, Sadato N, Yamamoto K, Okada K. 11C-acetate PET imaging of prostate cancer. J Nucl Med **2002**;43(2):181-6.

183. Mena E, Turkbey B, Mani H, Adler S, Valera VA, Bernardo M, Shah V, Pohida T, McKinney Y, Kwarteng G, Daar D, Lindenberg ML, Eclarinal P, Wade R, Linehan WM, Merino MJ, Pinto PA, Choyke PL, Kurdziel KA. 11C-Acetate PET/CT in localized prostate cancer: a study with MRI and histopathologic correlation. J Nucl Med **2012**;53(4):538-45.

184. Wachter S, Tomek S, Kurtaran A, Wachter-Gerstner N, Djavan B, Becherer A, Mitterhauser M, Dobrozemsky G, Li S, Potter R, Dudczak R, Kletter K. 11C-acetate positron emission tomography imaging and image fusion with computed tomography and magnetic resonance imaging in patients with recurrent prostate cancer. J Clin Oncol **2006**;24(16):2513-9.

185. Haseebuddin M, Dehdashti F, Siegel BA, Liu J, Roth EB, Nepple KG, Siegel CL, Fischer KC, Kibel AS, Andriole GL, Miller TR. 11C-acetate PET/CT before radical prostatectomy: nodal staging and treatment failure prediction. J Nucl Med **2013**;54(5):699-706.

186. Snyder F, Wood R. Alkyl and alk-1-enyl ethers of glycerol in lipids from normal and neoplastic human tissues. Cancer Res **1969**;29(1):251-7.

187. Meyer KL, Schwendner SW, Counsell RE. Potential tumor or organ-imaging agents. 30. Radioiodinated phospholipid ethers. J Med Chem **1989**;32(9):2142-7.

188. Rampy MA, Pinchuk AN, Weichert JP, Skinner RW, Fisher SJ, Wahl RL, Gross MD, Counsell RE. Synthesis and biological evaluation of radioiodinated phospholipid ether stereoisomers. J Med Chem **1995**;38(16):3156-62.

189. Weichert JP, Clark PA, Kandela IK, Vaccaro AM, Clarke W, Longino MA, Pinchuk AN, Farhoud M, Swanson KI, Floberg JM, Grudzinski J, Titz B, Traynor AM, Chen HE, Hall LT, Pazoles CJ, Pickhardt PJ, Kuo JS. Alkylphosphocholine analogs for broad-spectrum cancer imaging and therapy. Sci Transl Med **2014**;6(240):240ra75.

190. Gode D, Volmer DA. Lipid imaging by mass spectrometry - a review. Analyst **2013**;138(5):1289-315.

191. Yalcin EB, de la Monte SM. Review of matrix-assisted laser desorption ionization-imaging mass spectrometry for lipid biochemical histopathology. J Histochem Cytochem **2015**;63(10):762-71.

192. Chughtai K, Jiang L, Greenwood TR, Glunde K, Heeren RM. Mass spectrometry images acylcarnitines, phosphatidylcholines, and sphingomyelin in MDA-MB-231 breast tumor models. J Lipid Res **2013**;54(2):333-44.

193. Fernandez R, Garate J, Lage S, Teres S, Higuera M, Bestard-Escalas J, Lopez DH, Guardiola-Serrano F, Escriba PV, Barcelo-Coblijn G, Fernandez JA. Identification of Biomarkers of Necrosis in Xenografts Using Imaging Mass Spectrometry. J Am Soc Mass Spectrom **2016**;27(2):244-54.

194. Northen TR, Yanes O, Northen MT, Marrinucci D, Uritboonthai W, Apon J, Golledge SL, Nordstrom A, Siuzdak G. Clathrate nanostructures for mass spectrometry. Nature **2007**;449(7165):1033-6.

195. Vidova V, Novak P, Strohalm M, Pol J, Havlicek V, Volny M. Laser desorption-ionization of lipid transfers: tissue mass spectrometry imaging without MALDI matrix. Anal Chem **2010**;82(12):4994-7.

196. Sturm RM, Greer T, Chen R, Hensen B, Li L. Comparison of NIMS and MALDI platforms for neuropeptide and lipid mass spectrometric imaging in C. borealis brain tissue. Anal Methods **2013**;5(6):1623-8.

197. Mao X, He J, Li T, Lu Z, Sun J, Meng Y, Abliz Z, Chen J. Application of imaging mass spectrometry for the molecular diagnosis of human breast tumors. Sci Rep **2016**;6:21043.

198. Ide Y, Waki M, Hayasaka T, Nishio T, Morita Y, Tanaka H, Sasaki T, Koizumi K, Matsunuma R, Hosokawa Y, Ogura H, Shiiya N, Setou M. Human breast cancer tissues contain abundant phosphatidylcholine(36ratio1) with high stearoyl-CoA desaturase-1 expression. PLoS One **2013**;8(4):e61204.

199. Guenther S, Muirhead LJ, Speller AV, Golf O, Strittmatter N, Ramakrishnan R, Goldin RD, Jones E, Veselkov K, Nicholson J, Darzi A, Takats Z. Spatially resolved metabolic phenotyping of breast cancer by desorption electrospray ionization mass spectrometry. Cancer Res **2015**;75(9):1828-37.

200. Uehara T, Kikuchi H, Miyazaki S, Iino I, Setoguchi T, Hiramatsu Y, Ohta M, Kamiya K, Morita Y, Tanaka H, Baba S, Hayasaka T, Setou M, Konno H. Overexpression of Lysophosphatidylcholine Acyltransferase 1 and Concomitant Lipid Alterations in Gastric Cancer. Ann Surg Oncol **2016**;23 Suppl 2:206-13.

201. Jones EE, Powers TW, Neely BA, Cazares LH, Troyer DA, Parker AS, Drake RR. MALDI imaging mass spectrometry profiling of proteins and lipids in clear cell renal cell carcinoma. Proteomics **2014**;14(7-8):924-35.

202. Wei Y, Chen L, Zhou W, Chingin K, Ouyang Y, Zhu T, Wen H, Ding J, Xu J, Chen H. Tissue spray ionization mass spectrometry for rapid recognition of human lung squamous cell carcinoma. Sci Rep **2015**;5:10077.

203. Mirnezami R, Spagou K, Vorkas PA, Lewis MR, Kinross J, Want E, Shion H, Goldin RD, Darzi A, Takats Z, Holmes E, Cloarec O, Nicholson JK. Chemical mapping of the colorectal cancer microenvironment via MALDI imaging mass spectrometry (MALDI-MSI) reveals novel cancer-associated field effects. Mol Oncol **2014**;8(1):39-49.

204. Kurabe N, Hayasaka T, Ogawa M, Masaki N, Ide Y, Waki M, Nakamura T, Kurachi K, Kahyo T, Shinmura K, Midorikawa Y, Sugiyama Y, Setou M, Sugimura H. Accumulated phosphatidylcholine (16:0/16:1) in human colorectal cancer; possible involvement of LPCAT4. Cancer Sci **2013**;104(10):1295-302.

205. Kawashima M, Iwamoto N, Kawaguchi-Sakita N, Sugimoto M, Ueno T, Mikami Y, Terasawa K, Sato TA, Tanaka K, Shimizu K, Toi M. High-resolution imaging mass

spectrometry reveals detailed spatial distribution of phosphatidylinositols in human breast cancer. Cancer Sci **2013**;104(10):1372-9.

206. Goto T, Terada N, Inoue T, Nakayama K, Okada Y, Yoshikawa T, Miyazaki Y, Uegaki M, Sumiyoshi S, Kobayashi T, Kamba T, Yoshimura K, Ogawa O. The expression profile of phosphatidylinositol in high spatial resolution imaging mass spectrometry as a potential biomarker for prostate cancer. PLoS One **2014**;9(2):e90242.

207. Goto T, Terada N, Inoue T, Kobayashi T, Nakayama K, Okada Y, Yoshikawa T, Miyazaki Y, Uegaki M, Utsunomiya N, Makino Y, Sumiyoshi S, Yamasaki T, Kamba T, Ogawa O. Decreased expression of lysophosphatidylcholine (16:0/OH) in high resolution imaging mass spectrometry independently predicts biochemical recurrence after surgical treatment for prostate cancer. Prostate **2015**;75(16):1821-30.

208. Amstalden van Hove ER, Blackwell TR, Klinkert I, Eijkel GB, Heeren RM, Glunde K. Multimodal mass spectrometric imaging of small molecules reveals distinct spatio-molecular signatures in differentially metastatic breast tumor models. Cancer Res **2010**;70(22):9012-21.

209. Jiang L, Chughtai K, Purvine SO, Bhujwalla ZM, Raman V, Pasa-Tolic L, Heeren RM, Glunde K. MALDI-Mass Spectrometric Imaging Revealing Hypoxia-Driven Lipids and Proteins in a Breast Tumor Model. Anal Chem **2015**;87(12):5947-56.

210. Marien E, Meister M, Muley T, Gomez Del Pulgar T, Derua R, Spraggins JM, Van de Plas R, Vanderhoydonc F, Machiels J, Binda MM, Dehairs J, Willette Brown J, Hu Y, Dienemann H, Thomas M, Schnabel PA, Caprioli RM, Lacal JC, Waelkens E, Swinnen JV. Phospholipid profiling identifies acyl chain elongation as a ubiquitous trait and potential target for the treatment of lung squamous cell carcinoma. Oncotarget **2016**;7(11):12582-97.

211. Jelonek K, Pietrowska M, Ros M, Zagdanski A, Suchwalko A, Polanska J, Marczyk M, Rutkowski T, Skladowski K, Clench MR, Widlak P. Radiation-induced changes in serum lipidome of head and neck cancer patients. Int J Mol Sci **2014**;15(4):6609-24.

212. Woo HK, Northen TR, Yanes O, Siuzdak G. Nanostructure-initiator mass spectrometry: a protocol for preparing and applying NIMS surfaces for high-sensitivity mass analysis. Nat Protoc **2008**;3(8):1341-9.

213. O'Brien PJ, Lee M, Spilker ME, Zhang CC, Yan Z, Nichols TC, Li W, Johnson CH, Patti GJ, Siuzdak G. Monitoring metabolic responses to chemotherapy in single cells and tumors using nanostructure-initiator mass spectrometry (NIMS) imaging. Cancer Metab **2013**;1(1):4.

214. Park HM, Russo KA, Karateev G, Park M, Dubikovskaya E, Kriegsfeld LJ, Stahl A. A System for In Vivo Imaging of Hepatic Free Fatty Acid Uptake. Gastroenterology **2016**;152(1):78-81.

215. Thorek D, Robertson R, Bacchus WA, Hahn J, Rothberg J, Beattie BJ, Grimm J. Cerenkov imaging - a new modality for molecular imaging. Am J Nucl Med Mol Imaging **2012**;2(2):163-73.

216. Thorek DL, Ogirala A, Beattie BJ, Grimm J. Quantitative imaging of disease signatures through radioactive decay signal conversion. Nat Med **2013**;19(10):1345-50.

217. Czupryna J, Kachur AV, Blankemeyer E, Popov AV, Arroyo AD, Karp JS, Delikatny EJ. Cerenkov-specific contrast agents for detection of pH in vivo. J Nucl Med **2015**;56(3):483-8.

218. Yodh, A., Chance B. Spectroscopy and Imaging with Diffusing Light Physics Today **1995**;48(3):34.

219. Jia Y, Bailey ST, Hwang TS, McClintic SM, Gao SS, Pennesi ME, Flaxel CJ, Lauer AK, Wilson DJ, Hornegger J, Fujimoto JG, Huang D. Quantitative optical coherence tomography angiography of vascular abnormalities in the living human eye. Proc Natl Acad Sci U S A **2015**;112(18):E2395-402.

220. Shemonski ND, South FA, Liu YZ, Adie SG, Carney PS, Boppart SA. Computational high-resolution optical imaging of the living human retina. Nat Photonics **2015**;9:440-3.

221. Spaide RF, Klancnik JM, Jr., Cooney MJ. Retinal vascular layers imaged by fluorescein angiography and optical coherence tomography angiography. JAMA Ophthalmol **2015**;133(1):45-50.

222. Ughi GJ, Gora MJ, Swager AF, Soomro A, Grant C, Tiernan A, Rosenberg M, Sauk JS, Nishioka NS, Tearney GJ. Automated segmentation and characterization of esophageal wall in vivo by tethered capsule optical coherence tomography endomicroscopy. Biomed Opt Express **2016**;7(2):409-19.

223. Bouma BE, Tearney GJ, Compton CC, Nishioka NS. High-resolution imaging of the human esophagus and stomach in vivo using optical coherence tomography. Gastrointest Endosc **2000**;51(4 Pt 1):467-74.

224. Jang IK, Bouma BE, Kang DH, Park SJ, Park SW, Seung KB, Choi KB, Shishkov M, Schlendorf K, Pomerantsev E, Houser SL, Aretz HT, Tearney GJ. Visualization of coronary atherosclerotic plaques in patients using optical coherence tomography: comparison with intravascular ultrasound. J Am Coll Cardiol **2002**;39(4):604-9.

225. Prabhu D, Mehanna E, Gargesha M, Wen D, Brandt E, van Ditzhuijzen NS, Chamie D, Yamamoto H, Fujino Y, Farmazilian A, Patel J, Costa M, Bezerra HG, Wilson DL. 3D registration of intravascular optical coherence tomography and cryo-image volumes for microscopic-resolution validation. Proc SPIE Int Soc Opt Eng **2016**;9788.

226. Jiang JX, Keating JJ, Jesus EM, Judy RP, Madajewski B, Venegas O, Okusanya OT, Singhal S. Optimization of the enhanced permeability and retention effect for near-infrared imaging of solid tumors with indocyanine green. Am J Nucl Med Mol Imaging **2015**;5(4):390-400.

227. Vinegoni C, Botnaru I, Aikawa E, Calfon MA, Iwamoto Y, Folco EJ, Ntziachristos V, Weissleder R, Libby P, Jaffer FA. Indocyanine green enables near-infrared fluorescence imaging of lipid-rich, inflamed atherosclerotic plaques. Sci Transl Med **2011**;3(84):84ra45.

228. Weissleder R, Nahrendorf M, Pittet MJ. Imaging macrophages with nanoparticles. Nat Mater **2014**;13(2):125-38.

229. Leimgruber A, Berger C, Cortez-Retamozo V, Etzrodt M, Newton AP, Waterman P, Figueiredo JL, Kohler RH, Elpek N, Mempel TR, Swirski FK, Nahrendorf M, Weissleder R, Pittet MJ. Behavior of endogenous tumor-associated macrophages assessed in vivo using a functionalized nanoparticle. Neoplasia **2009**;11(5):459-68, 2 p following 68.

230. Shao H, Yoon TJ, Liong M, Weissleder R, Lee H. Magnetic nanoparticles for biomedical NMR-based diagnostics. Beilstein J Nanotechnol **2010**;1:142-54.
231. Villa AM, Caporizzo E, Papagni A, Miozzo L, Del Buttero P, Grilli MD, Amboldi N, Fazio F, Doglia SM, Giglioni B. Choline and phosphatidylcholine fluorescent derivatives localization in carcinoma cells studied by laser scanning confocal fluorescence microscopy. Eur J Cancer **2005**;41(10):1453-9.
232. Thumser AE, Storch J. Characterization of a BODIPY-labeled fluorescent fatty acid analogue. Binding to fatty acid-binding proteins, intracellular localization, and metabolism. Mol Cell Biochem **2007**;299(1-2):67-73.
233. Korb ML, Warram JM, Grudzinski J, Weichert J, Jeffery J, Rosenthal EL. Breast cancer imaging using the near-infrared fluorescent agent, CLR1502. Mol Imaging **2014**;13.
234. Arlauckas SP, Popov AV, Delikatny EJ. Direct Inhibition of Choline Kinase by a Near-Infrared Fluorescent Carbocyanine. Molecular Cancer Therapeutics **2014**;13(9):2149-58.
235. Vinegoni C, Dubach JM, Thurber GM, Miller MA, Mazitschek R, Weissleder R. Advances in measuring single-cell pharmacology in vivo. Drug Discov Today **2015**;20(9):1087-92.
236. Arlauckas SP, Kumar M, Popov AV, Poptani H, Delikatny EJ. Near infrared fluorescent imaging of choline kinase alpha expression and inhibition in breast tumors. Oncotarget **2017**;8(10):16518-30.
237. Yoon Y, Lee PJ, Kurilova S, Cho W. In situ quantitative imaging of cellular lipids using molecular sensors. Nat Chem **2011**;3(11):868-74.
238. Di Paolo G, De Camilli P. Phosphoinositides in cell regulation and membrane dynamics. Nature **2006**;443(7112):651-7.
239. Verderame MF. pp60v-src transformation of rat cells but not chicken cells strongly correlates with low-affinity phosphopeptide binding by the SH2 domain. Mol Biol Cell **1997**;8(5):843-54.
240. Caers J, Peymen K, Suetens N, Temmerman L, Janssen T, Schoofs L, Beets I. Characterization of G protein-coupled receptors by a fluorescence-based calcium mobilization assay. J Vis Exp **2014**(89):e51516.
241. Bazzi MD, Nelsestuen GL. Association of protein kinase C with phospholipid vesicles. Biochemistry **1987**;26(1):115-22.
242. Peddie CJ, Blight K, Wilson E, Melia C, Marrison J, Carzaniga R, Domart MC, O'Toole P, Larijani B, Collinson LM. Correlative and integrated light and electron microscopy of in-resin GFP fluorescence, used to localise diacylglycerol in mammalian cells. Ultramicroscopy **2014**;143:3-14.
243. Sato M, Ueda Y, Umezawa Y. Imaging diacylglycerol dynamics at organelle membranes. Nat Methods **2006**;3(10):797-9.
244. Farber SA, Pack M, Ho SY, Johnson ID, Wagner DS, Dosch R, Mullins MC, Hendrickson HS, Hendrickson EK, Halpern ME. Genetic analysis of digestive physiology using fluorescent phospholipid reporters. Science **2001**;292(5520):1385-8.

245. Hama K, Provost E, Baranowski TC, Rubinstein AL, Anderson JL, Leach SD, Farber SA. In vivo imaging of zebrafish digestive organ function using multiple quenched fluorescent reporters. Am J Physiol Gastrointest Liver Physiol **2009**;296(2):G445-53.

246. Hendrickson HS, Hendrickson EK, Johnson ID, Farber SA. Intramolecularly quenched BODIPY-labeled phospholipid analogs in phospholipase A(2) and platelet-activating factor acetylhydrolase assays and in vivo fluorescence imaging. Anal Biochem **1999**;276(1):27-35.

247. Fraher D, Sanigorski A, Mellett NA, Meikle PJ, Sinclair AJ, Gibert Y. Zebrafish Embryonic Lipidomic Analysis Reveals that the Yolk Cell Is Metabolically Active in Processing Lipid. Cell Rep **2016**;14(6):1317-29.

248. Popov AV, Mawn TM, Kim S, Zheng G, Delikatny EJ. Design and synthesis of phospholipase C and A2-activatable near-infrared fluorescent smart probes. Bioconjug Chem **2010**;21(10):1724-7.

249. Nakanishi M, Rosenberg DW. Multifaceted roles of PGE2 in inflammation and cancer. Semin Immunopathol **2013**;35(2):123-37.

250. Huang Z, Laliberte F, Tremblay NM, Weech PK, Street IP. A continuous fluorescence-based assay for the human high-molecular-weight cytosolic phospholipase A2. Anal Biochem **1994**;222(1):110-5.

251. Zeng W, Wang X, Xu P, Liu G, Eden HS, Chen X. Molecular imaging of apoptosis: from micro to macro. Theranostics **2015**;5(6):559-82.

252. Zhao M, Beauregard DA, Loizou L, Davletov B, Brindle KM. Non-invasive detection of apoptosis using magnetic resonance imaging and a targeted contrast agent. Nat Med **2001**;7(11):1241-4.

253. Rice DR, Clear KJ, Smith BD. Imaging and therapeutic applications of zinc(ii)-dipicolylamine molecular probes for anionic biomembranes. Chem Commun (Camb) **2016**;52(57):8787-801.

254. Koulov AV, Stucker KA, Lakshmi C, Robinson JP, Smith BD. Detection of apoptotic cells using a synthetic fluorescent sensor for membrane surfaces that contain phosphatidylserine. Cell Death Differ **2003**;10(12):1357-9.

255. Neves AA, Krishnan AS, Kettunen MI, Hu DE, Backer MM, Davletov B, Brindle KM. A paramagnetic nanoprobe to detect tumor cell death using magnetic resonance imaging. Nano Lett **2007**;7(5):1419-23.

256. Jung HI, Kettunen MI, Davletov B, Brindle KM. Detection of apoptosis using the C2A domain of synaptotagmin I. Bioconjug Chem **2004**;15(5):983-7.

257. Surman AJ, Bonnet CS, Lowe MP, Kenny GD, Bell JD, Toth E, Vilar R. A Pyrophosphate-Responsive Gadolinium(III) MRI Contrast Agent. Chem - Eur J **2011**;17(1):223-30, S/1-S/16.

258. Fang W, Wang F, Ji S, Zhu X, Meier HT, Hellman RS, Brindle KM, Davletov B, Zhao M. SPECT imaging of myocardial infarction using 99mTc-labeled C2A domain of synaptotagmin I in a porcine ischemia-reperfusion model. Nucl Med Biol **2007**;34(8):917-23.

259. Niu G, Chen X. Apoptosis imaging: beyond annexin V. J Nucl Med **2010**;51(11):1659-62.

260. Alam IS, Neves AA, Witney TH, Boren J, Brindle KM. Comparison of the C2A domain of synaptotagmin-I and annexin-V as probes for detecting cell death. Bioconjug Chem **2010**;21(5):884-91.

Figure Legends

Figure 1: Lipid metabolism pathways in the cell. Glucose transported into the cell is metabolized to pyruvate via the glycolytic pathway, and can be fed into the tricarboxylic acid (TCA) cycle for ATP production in the mitochondria. Citrate from the TCA cycle or from exogenous sources is converted to Acetyl-CoA in the cytoplasm and can be used for cholesterol or fatty acid (e.g. palmitate) biosynthesis. Cholesterol produced in this fashion can be used to synthesize membranes or be incorporated into sterols. Fatty acids can be desaturated or extended and then incorporated into triglycerides or incorporated into phospholipids via the Kennedy Pathway. Cholesterol and triglycerides fatty acids can also be taken up through specific transport mechanisms. The resulting lipid droplets, shown in the inset, contain fatty acids stored in phospholipid and fatty acid form that can be mobilized by phospholipases and lipases, respectively. Beta-oxidation (β-Ox) of free fatty acids from lipid droplets can be triggered to meet energy needs. In place of the third acyl group ($Acyl_3$) attached to the glycerol moiety of triacylglycerides (orange oval), phospholipids have a phosphorylated polar head group (yellow sphere) that confers water solubility and creates organized bi-layer and micelle structures. Phospholipases can also elicit 2^{nd} messenger signaling cascades by releasing bioactive fatty acids (e.g. sphingolipids, eicosanoids) and/or polar head groups in response to growth or stress cues. External cell signaling cues can also be transmitted by lipids in the case of isoprenylation and subsequent transport of small GTPases to dock with G protein-coupled receptors (GPCRs) on the cell surface.

Figure 2: Major lipid metabolic pathways altered in cancer cells. Metabolic reprogramming during malignant transformation mimics autonomous growth signaling in unicellular organisms. Common oncogenes in the PI3K/Akt/MTOR pathway, are often mutated

or upregulated due to their presence downstream of external growth factors and their ability to re-route cellular carbon sources toward fatty acid utilization as an energy source. Cancer cells can also supply the TCA cycle from glucose via aberrant glycolysis and from glutamine via IDH mutations, although the contributions of these pathways differ greatly depending on the energy needs of the cell. The transcription factor Myc promotes many malignant processes in cancer cells because it is a master regulator capable of triggering survival pathways in response to hypoxia and nutrient deprivation. Hypoxic conditions are a factor in many solid tumors and influence the local tumor microenvironment by dampening the immune response and activating hypoxia-inducible factor-1α (HIF1α), which among other things, initiates the regulatory function of sterol regulatory element binding protein 1 (SREBP-1) on fatty acid synthesis. Free fatty acids such as palmitate are used as energy sources or converted to bioactive eicosanoids to dampen the immune response and stabilize the ER stress that can result from saturated fatty acid accumulation.

Figure 3: Changes in lipid metabolism in response to oncolytic viral treatment of Syrian hamster carcinomas. The oncolytic viral treatment induces coagulative necrosis, which is seen as hypo-intense areas within the tumor on T_2-weighted MR image. *In vivo* MRS from the voxel (overlaid on the image) is shown on the right demonstrating resonances from unsaturated fatty acids, taurine and choline. No changes in PUFA resonances were observed in coagulative necrosis resulting from oncolytic viral treatment. Reprinted with permission from (138).

Figure 4. A) Confocal micrographs of SKOV3.ip cells treated for 48 h with cisplatin (CDDP) show increased lipid droplets as measured by Nile red staining, compared to untreated

controls (CTRL). Fixed cells were counterstained with phalloidin 488 for actin (green) and DAPI for nuclei (blue). Scale bar represents 23.8 μm. (B) ^{1}H NMR spectra of intact SKOV3.ip cells treated with 5 mM CDDP for 48 h (red) show increases in mobile lipids compared with untreated control cells (black). Labeled lipid resonances include: methine protons at 5.3 ppm (-CH=CH-); fatty chain methylene group at 1.3 ppm (-$(CH2)_n$)- ; methyl group at 0.9 ppm (-CH_3) ; and total choline (tCho) at 3.2 ppm (-N.$(CH_3)_3$). Reprinted with permission from (150).

Figure 5: Increased lipids in response to choline kinase inhibition as an alternate therapy for the treatment of gliomas. *In vivo* MRS from an untreated F98 rat glioma (bottom spectrum) and after 5 days of treatment with a choline kinase inhibitor, MN58b (top spectrum). Increased mono-unsaturated lipid peaks (1.3 ppm) are evident with treatment. In addition, a significant increase in the poly-unsaturated fatty acids (PUFA, 2.8 ppm), indicating apoptotic cell death. As expected, a decrease in the total choline (tCho) peak was also observed in response to choline kinase inhibition. The MR image demonstrates placement of the voxel for MRS studies. Reprinted with permission from (114).

Figure 6: Single voxel ^{1}H MR spectra from a GL261 tumor implanted into a mouse brain. Treatment with three cycles of temozolomide led to significant (*) increases in mobile lipid:Cre and tCho:Cre resonances at 28 days post inoculation (left) compared to spectra acquired before treatment (tight). Labeled resonances: Cho (choline: 3.2 ppm, Cre (creatine): 3.3 ppm, MLs (mobile lipid methylenes): 1.3 ppm, PUFAs: 2.8 ppm. Reprinted with permission from (128).

Figure 7: Chemical structure of the common PET tracers used for detection of lipid metabolism. The radioactive isotope is denoted in red.

Figure 8: MALDI-MSI images and corresponding H&E sections from human colorectal tumors (A-C) and adjacent tumor free regions (D-F). A selective projection of *m/z* 478.3 onto MALDI-MSI images reveals elevations in 1-palmitoyl-lysophosphatidylcholine in cancer-containing areas compared to the non-tumor bearing tissue sections. Elevations in *m/z* 504.3, representing 1-oleoyl-lysophosphatidylcholine, were also observed in this study. Reprinted with permission from (203).

Figure 9: *In vivo* NIR fluorescence imaging of phospholipase activity using the PC-PLC activatable probe Pyro-PL-BHQ in DU145 prostate tumor xenografts. Each mouse received 80 nmol *i.v.* of (A) Pyro-PtdEtn, a permanently fluorescent analog used as a control, (B) Pyro-PtdEtn-BHQ or (C) Pyro-PtdEtn-BHQ plus pre- and post- injections of the PC-PLC inhibitor D609. The fluorescence intensity from Pyro-PL-BHQ activation peaked at 6-7 h, and was inhibited by D609 treatment. Fluorescence persisted for up to 31 h in tumor tissue (T) excised from mice when compared to muscle (M) control. Reprinted with permission from (112).

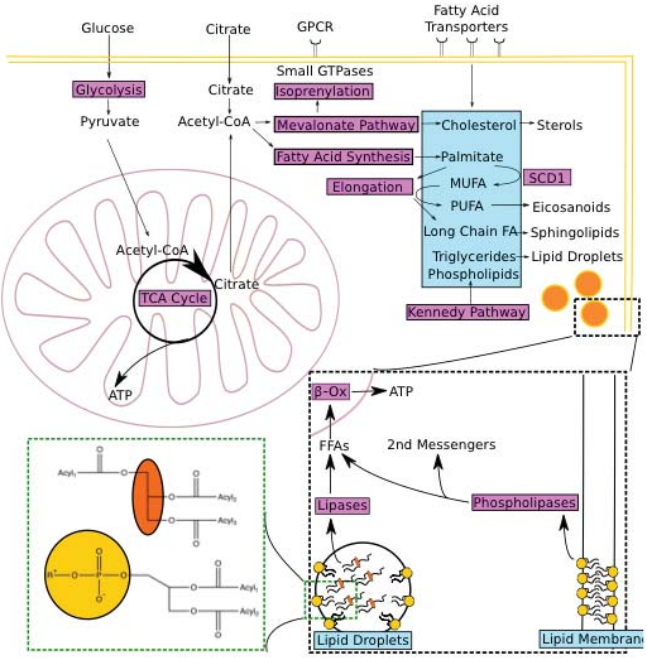

Figure 1

Figure 1: Lipid metabolism pathways in the cell. Glucose transported into the cell is metabolized to pyruvate via the glycolytic pathway, and can be fed into the tricarboxylic acid (TCA) cycle for ATP production in the mitochondria. Citrate from the TCA cycle or from exogenous sources is converted to Acetyl-CoA in the cytoplasm and can be used for cholesterol or fatty acid (e.g. palmitate) biosynthesis. Cholesterol produced in this fashion can be used to synthesize membranes or be incorporated into sterols. Fatty acids can be desaturated or extended and then incorporated into triglycerides or incorporated into phospholipids via the Kennedy Pathway. Cholesterol and triglycerides fatty acids can also be taken up through specific transport mechanisms. The resulting lipid droplets, shown in the inset, contain fatty acids stored in phospholipid and fatty acid form that can be mobilized by phospholipases and lipases, respectively. Beta-oxidation (β-Ox) of free fatty acids from lipid droplets can be triggered to meet energy needs. In place of the third acyl group (Acyl3) attached to the glycerol moiety of triacylglycerides (orange oval), phospholipids have a phosphorylated polar head group (yellow sphere) that confers water solubility and creates organized bi-layer and micelle structures. Phospholipases can also elicit 2nd messenger signaling cascades by releasing bioactive fatty acids (e.g. sphingolipids, eicosanoids) and/or polar head groups in response to growth or stress cues. External cell signaling cues can also be transmitted by lipids in the case of isoprenylation and subsequent transport of small GTPases to dock with G protein-coupled receptors (GPCRs) on the cell surface.

279x209mm (72 x 72 DPI)

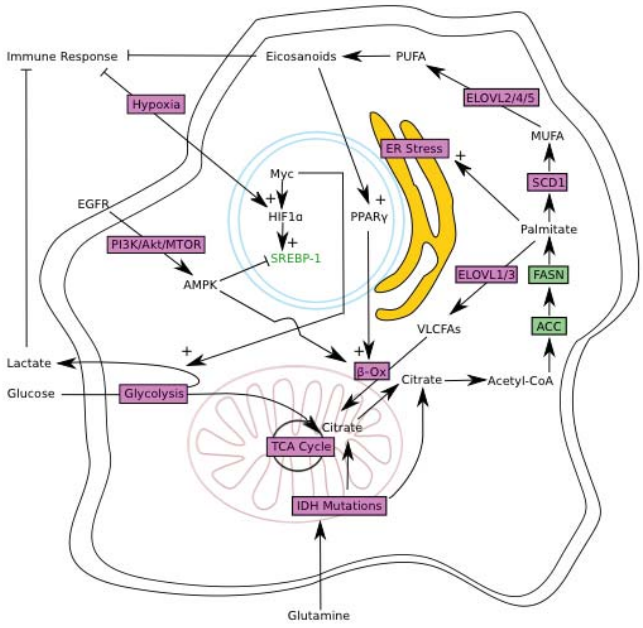

Figure 2

Figure 2: Major lipid metabolic pathways altered in cancer cells. Metabolic reprogramming during malignant transformation mimics autonomous growth signaling in unicellular organisms. Common oncogenes in the PI3K/Akt/MTOR pathway, are often mutated or upregulated due to their presence downstream of external growth factors and their ability to re-route cellular carbon sources toward fatty acid utilization as an energy source. Cancer cells can also supply the TCA cycle from glucose via aberrant glycolysis and from glutamine via IDH mutations, although the contributions of these pathways differ greatly depending on the energy needs of the cell. The transcription factor Myc promotes many malignant processes in cancer cells because it is a master regulator capable of triggering survival pathways in response to hypoxia and nutrient deprivation. Hypoxic conditions are a factor in many solid tumors and influence the local tumor microenvironment by dampening the immune response and activating hypoxia-inducible factor-1α (HIF1α), which among other things, initiates the regulatory function of sterol regulatory element binding protein 1 (SREBP-1) on fatty acid synthesis. Free fatty acids such as palmitate are used as energy sources or converted to bioactive eicosanoids to dampen the immune response and stabilize the ER stress that can result from saturated fatty acid accumulation.

279x209mm (72 x 72 DPI)

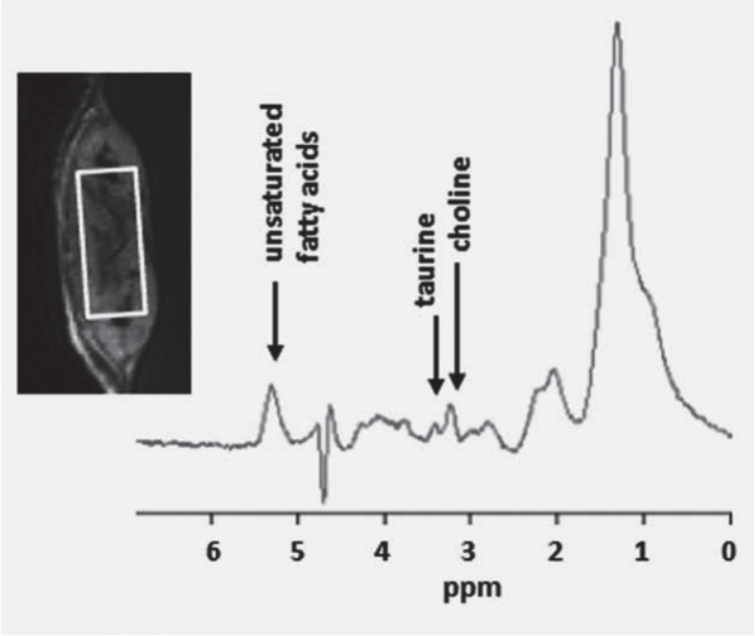

Figure 3

Figure 3: Changes in lipid metabolism in response to oncolytic viral treatment of Syrian hamster carcinomas. The oncolytic viral treatment induces coagulative necrosis, which is seen as hypo-intense areas within the tumor on T2-weighted MR image. In vivo MRS from the voxel (overlaid on the image) is shown on the right demonstrating resonances from unsaturated fatty acids, taurine and choline. Unlike the increased PUFA resonances observed during apoptosis (Figure 3), no No changes in PUFA resonances were observed in coagulative necrosis resulting from oncolytic viral treatment. Reprinted with permission from (138).

279x209mm (72 x 72 DPI)

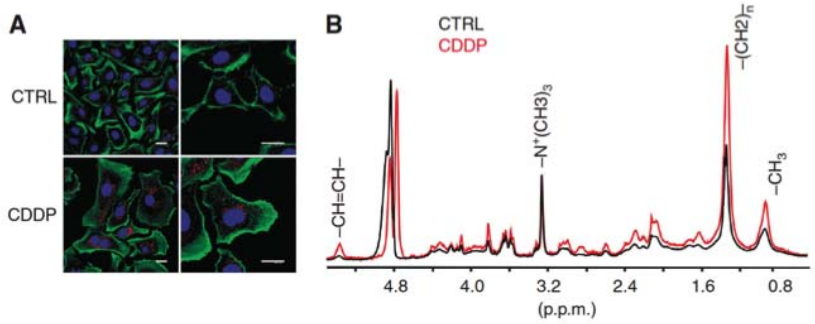

Figure 4

Figure 4. A) Confocal micrographs of SKOV3.ip cells treated for 48 h with cisplatin (CDDP) show increased lipid droplets as measured by Nile red staining, compared to untreated controls (CTRL). Fixed cells were counterstained with phalloidin 488 for actin (green) and DAPI for nuclei (blue). Scale bar represents 23.8 μm. (B) 1H NMR spectra of intact SKOV3.ip cells treated with 5 mM CDDP for 48 h (red) show increases in mobile lipids compared with untreated control cells (black). Labeled lipid resonances include: methine protons at 5.3 ppm (-CH=CH-); fatty chain methylene group at 1.3 ppm (-(CH2)n)- ; methyl group at 0.9 ppm (-CH3) ; and total choline (tCho) at 3.2 ppm (-N.(CH3)3). Reprinted with permission from (150).

279x209mm (72 x 72 DPI)

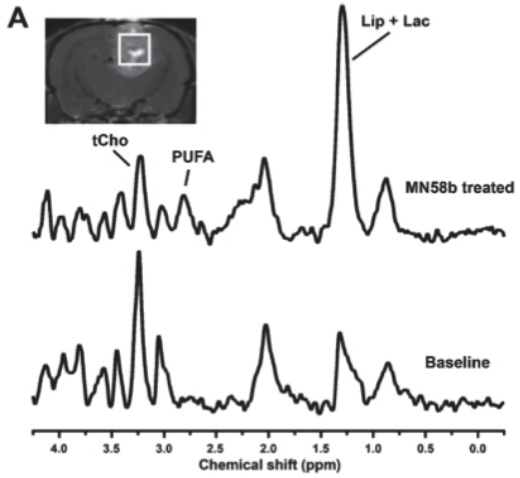

Figure 5

Figure 5: Increased lipids in response to choline kinase inhibition as an alternate therapy for the treatment of gliomas. In vivo MRS from an untreated F98 rat glioma (bottom spectrum) and after 5 days of treatment with a choline kinase inhibitor, MN58b (top spectrum). Increased mono-unsaturated lipid peaks (1.3 ppm) are evident with treatment. In addition, a significant increase in the poly-unsaturated fatty acids (PUFA, 2.8 ppm), indicating apoptotic cell death. As expected, a decrease in the total choline (tCho) peak was also observed in response to choline kinase inhibition. The MR image demonstrates placement of the voxel for MRS studies. Reprinted with permission from (114).

279x209mm (72 x 72 DPI)

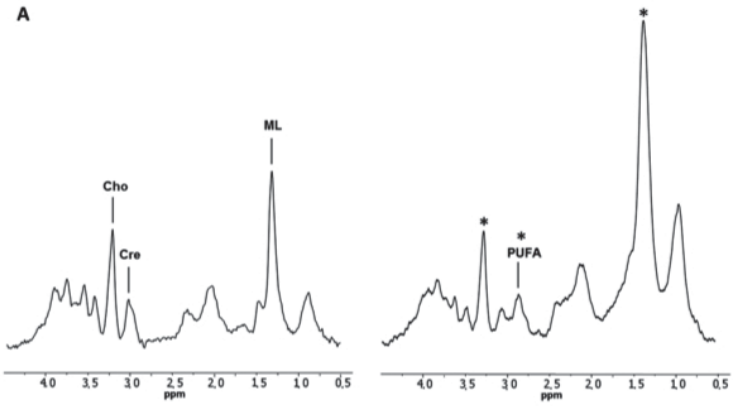

Figure 6

Figure 6: Single voxel 1H MR spectra from a GL261 tumor implanted into a mouse brain. Treatment with three cycles of temozolomide led to significant (*) increases in mobile lipid:Cre and tCho:Cre resonances at 28 days post inoculation (left) compared to spectra acquired before treatment (tight). Labeled resonances: Cho (choline: 3.2 ppm, Cre (creatine): 3.3 ppm, MLs (mobile lipid methylenes): 1.3 ppm, PUFAs: 2.8 ppm. Reprinted with permission from (128).

279x209mm (72 x 72 DPI)

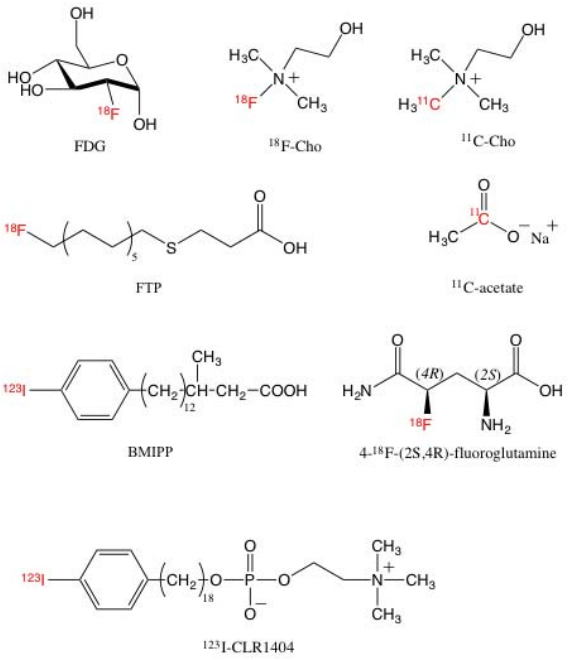

Figure 7

Figure 7: Chemical structure of the common PET tracers used for detection of lipid metabolism. The radioactive isotope is denoted in red.

279x209mm (72 x 72 DPI)

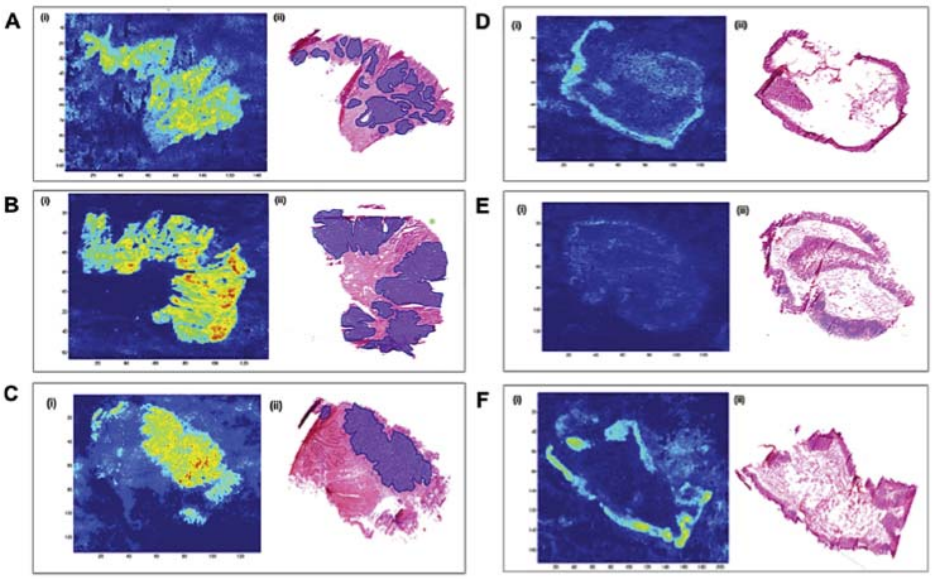

Figure 8

Figure 8: MALDI-MSI images and corresponding H&E sections from human colorectal tumors (A-C) and adjacent tumor free regions (D-F). A selective projection of m/z 478.3 onto MALDI-MSI images reveals elevations in 1-palmitoyl-lysophosphatidylcholine in cancer-containing areas compared to the non-tumor bearing tissue sections. Elevations in m/z 504.3, representing 1-oleoyl-lysophosphatidylcholine, were also observed in this study. Reprinted with permission from (203).

279x209mm (72 x 72 DPI)

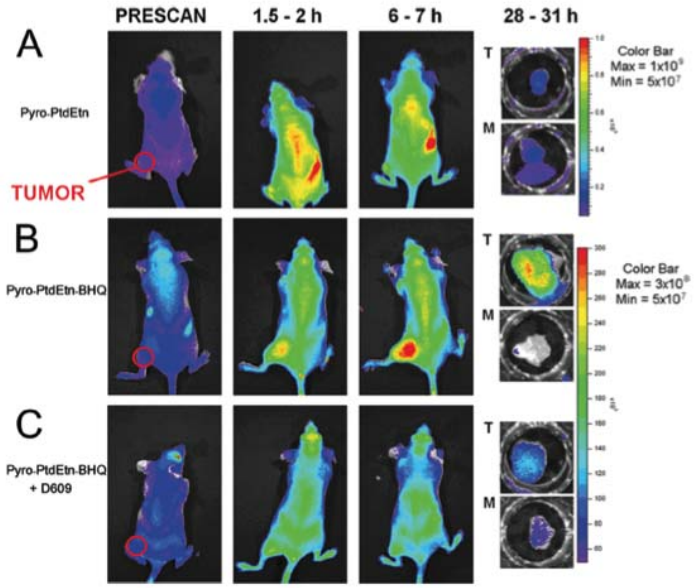

Figure 9

Figure 9: In vivo NIR fluorescence imaging of phospholipase activity using the PC-PLC activatable probe Pyro-PL-BHQ in DU145 prostate tumor xenografts. Each mouse received 80 nmol i.v. of (A) Pyro-PtdEtn, a permanently fluorescent analog used as a control, (B) Pyro-PtdEtn-BHQ or (C) Pyro-PtdEtn-BHQ plus pre- and post- injections of the PC-PLC inhibitor D609. The fluorescence intensity from Pyro-PL-BHQ activation peaked at 6-7 h, and was inhibited by D609 treatment. Fluorescence persisted for up to 31 h in tumor tissue (T) excised from mice when compared to muscle (M) control. Reprinted with permission from (112).

279x209mm (72 x 72 DPI)

Graphical Abstract:Imaging of Cancer Lipid Metabolism in Response to Therapy

Sean Arlauckas, Elizabeth A. Browning, Harish Poptani, E. James Delikatny

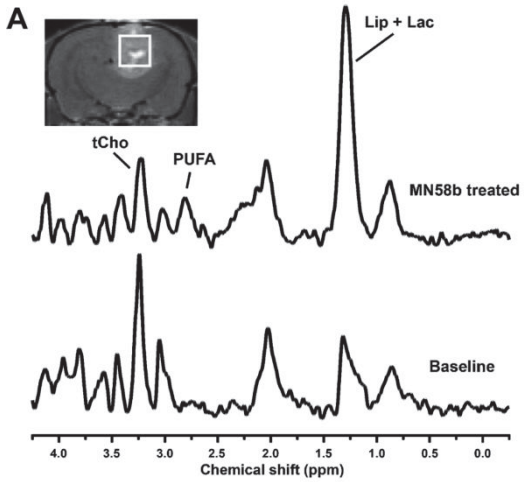

Abstract

Lipids play a critical role in biological systems ranging from structural integrity to signaling, energy, defense and communication. This article reviews lipids and lipid metabolic pathways altered in cancer development and their changes in response to therapy that are amenable for study by imaging. We focus first on MR spectroscopy, which was instrumental in defining the field of lipid imaging (Figure) and still plays a major role, followed by complementary molecular imaging methods including PET, mass spectroscopic imaging and optical imaging.